

**CD8 T cell responses during primary and secondary  
influenza infection - Role of MHC-I expression on  
non-immune cells**

**Dissertation**

zur

Erlangung des Doktorgrades (Dr. rer. nat.)

der

Mathematisch-Naturwissenschaftlichen Fakultät

der

Rheinischen Friedrich-Wilhelms-Universität Bonn

vorgelegt von

**Salvador Vento Asturias**

aus

Barcelona, Spanien

Bonn November 2020

Angefertigt mit Genehmigung der Mathematisch-Naturwissenschaftlichen Fakultät der  
Rheinischen Friedrich-Wilhelms-Universität Bonn

1. Gutachter: Herr Prof. Dr. Natalio Garbi

2. Gutachter: Herr Prof. Dr. Joachim L. Schultze

Tag der Promotion: 04 Juni 2021

Erscheinungsjahr: 2021

# Table of Contents

<b>1. ABSTRACT</b> .....	<b>1</b>
<b>2. INTRODUCTION</b> .....	<b>2</b>
2.1. LUNG ANATOMY .....	2
2.2. INFLUENZA VIRUS.....	3
2.2.1. <i>Influenza virus infection</i> .....	4
2.2.2. <i>Mutations and vaccines</i> .....	4
2.3. NON-IMMUNE RESPONSE TO INFLUENZA .....	5
2.4. IMMUNE RESPONSE TO INFLUENZA .....	7
2.4.1. <i>Innate response</i> .....	7
2.4.2. <i>Adaptive response</i> .....	9
2.4.3. <i>Immune pathology</i> .....	15
2.4.4. <i>Animal models</i> .....	15
<b>3. AIM OF THE STUDY</b> .....	<b>17</b>
<b>4. MATERIALS AND METHODS</b> .....	<b>18</b>
4.1. MATERIALS.....	18
4.1.1. <i>Equipment</i> .....	18
4.1.2. <i>Reagents</i> .....	19
4.1.3. <i>Buffers</i> .....	21
4.1.4. <i>Consumables</i> .....	22
4.1.5. <i>Antibodies</i> .....	23
4.1.6. <i>Infectious agents</i> .....	24
4.1.7. <i>Mouse lines</i> .....	25
4.2. METHODS.....	26
4.2.1. <i>Intratracheal infection</i> .....	26
4.2.2. <i>Cell depletion</i> .....	26
4.2.3. <i>Generation of bone marrow chimeras</i> .....	26
4.2.4. <i>In vivo differential labelling (IDEAL)</i> .....	27
4.2.5. <i>Isolation of primary cells</i> .....	28
4.2.6. <i>Adoptive CD8 T cell transfer</i> .....	29
4.2.7. <i>Flow cytometry</i> .....	30
4.2.8. <i>Assessment of TCR affinity</i> .....	30
4.2.9. <i>Confocal Microscopy</i> .....	31
4.2.10. <i>Cytotoxicity assays</i> .....	32
4.2.11. <i>Quantification of influenza viral titers</i> .....	33
4.2.12. <i>Gene expression analysis</i> .....	34
4.2.13. <i>Statistical analysis</i> .....	36
<b>5. RESULTS</b> .....	<b>37</b>
5.1. CD8 T CELL MIGRATION AND KILLING CAPACITY IN THE LUNG ENVIRONMENT.....	37
5.1.1. <i>Development of a flow cytometric method to accurately quantify immune cell infiltration in specific lung compartments</i> .....	37
5.1.2. <i>Activated CTLs are not imprinted to specifically migrate into a unique lung compartment</i> 42	
5.1.3. <i>Interstitial and BAS CTLs show similar transcriptomic profiles</i> .....	45
5.1.4. <i>Influenza-specific CTLs show similar killing capacity regardless of their location</i> .....	48
5.2. CD8 T CELL PROTECTION DURING PRIMARY AND SECONDARY VIRAL INFECTION.....	53
5.2.1. <i>CTLs do not alter the course of disease in primary influenza infection</i> .....	53
5.2.2. <i>Memory CD8 T cells are protective during secondary influenza infection</i> .....	59
5.2.3. <i>Memory CTLs quickly upregulate CD69 and migrate into the BAS upon secondary challenge</i> 61	

5.2.4.	<i>Lack of MHC-I in non-immune cells promotes CD8 T cell-mediated protection during secondary influenza infection</i> .....	63
5.2.5.	<i>Dendritic cells are key for memory CD8 T cell-mediated protection against influenza.</i>	72
<b>6.</b>	<b>DISCUSSION</b> .....	<b>77</b>
<b>7.</b>	<b>BIBLIOGRAPHY</b> .....	<b>83</b>
<b>8.</b>	<b>ABBREVIATIONS</b> .....	<b>108</b>
<b>9.</b>	<b>APPENDIX</b> .....	<b>110</b>
<b>10.</b>	<b>PUBLICATIONS</b> .....	<b>113</b>
<b>11.</b>	<b>ACKNOWLEDGMENTS</b> .....	<b>114</b>

# 1. Abstract

Influenza infection results in strong immune responses in the lung usually leading to clearance of infection and, in some cases, immune pathology with varying degrees of prognosis. CD8 T cells are believed to be one of the key players to resolve primary and secondary viral infections by directly eliminating infected cells. During this study I aimed at elucidating how CD8 T cells infiltrate the infected lung and contribute to the clearance of viral infection. With an initial focus on acute influenza infections, I devised a novel flow cytometric method, which I termed IDEAL, to accurately analyze immune cell positioning in the lung via flow cytometry, and used it to identify CTL differences at a genomic, function and migration levels depending on their anatomical location. Despite identifying minor transcriptomic differences between CTLs present in the interstitial and bronchoalveolar compartments, they did not effectively translate into functional differences regarding their cytotoxic capacity or ability to home to a specific lung compartment. Furthermore, using CD8 T cell depletion protocols and adoptive transfers of flu-specific effector CTLs into naïve mice prior or during infection, I found CD8 T cells to be dispensable during acute influenza infection but pivotal to a quick and efficient recovery following a secondary challenge with a heterotypic flu strain. I then continued to investigate how memory CD8 T cells conferred protection against a secondary influenza challenge by studying the necessity of MHC-I/peptide-TCR interactions between infected epithelial cells and CD8 T cells by means of bone marrow chimeras. Influenza-specific CD8 T cells conferred significantly better protection when TCR recognition of infected epithelium was prevented. Furthermore, I studied the importance of dendritic cells in the re-activation of memory CD8 T cells and could show how DCs are key for effector CD8 T cell function and viral clearance. In summary, the results presented here show that (1) CD8 T cells located at different pulmonary compartments have apparently similar phenotype and function within the infected lung, (2) they are, however, dispensable to overcome acute influenza infections but (3) are key during a secondary flu challenge. Finally, (4) during secondary infection I have proven how killing of epithelial cells is rather detrimental for recovery from infection and how memory CD8 T cells require DCs to confer protection.

## 2. Introduction

### 2.1. Lung anatomy

The human lung is composed of 5 lobes, inhaling an average of 10.000L of air per day<sup>1</sup>. An extensive network of arteries, veins and capillaries (ca. 3000km)<sup>2</sup> as well as bronchiole branches (ca. 2400km)<sup>2</sup> and alveoli (ca. 500million)<sup>3</sup> provide optimal conditions for gas exchange. To accommodate such structure and function, the lung is divided into 3 anatomical compartments. Firstly, the bronchoalveolar space (BAS) comprises the luminal side of the alveoli, bronchi and bronchiole and is delimited by a thin layer of epithelial cells(EpC). The BAS is the contact site with inhaled air and, as a result, is highly exposed to potentially harmful particles and pathogens. The lung interstitium is found below the epithelial layer delimiting the BAS, comprising the space between the alveolar basal membrane and the vascular basal membrane both included. The interstitium is mainly formed by elastin, collagen<sup>4</sup>, stromal cells and immune cells<sup>5</sup>. Finally, the vascular compartment is composed of venules, arterioles and capillaries and its function is to distribute blood throughout the lung to facilitate immune surveillance and gas exchange<sup>6</sup>.

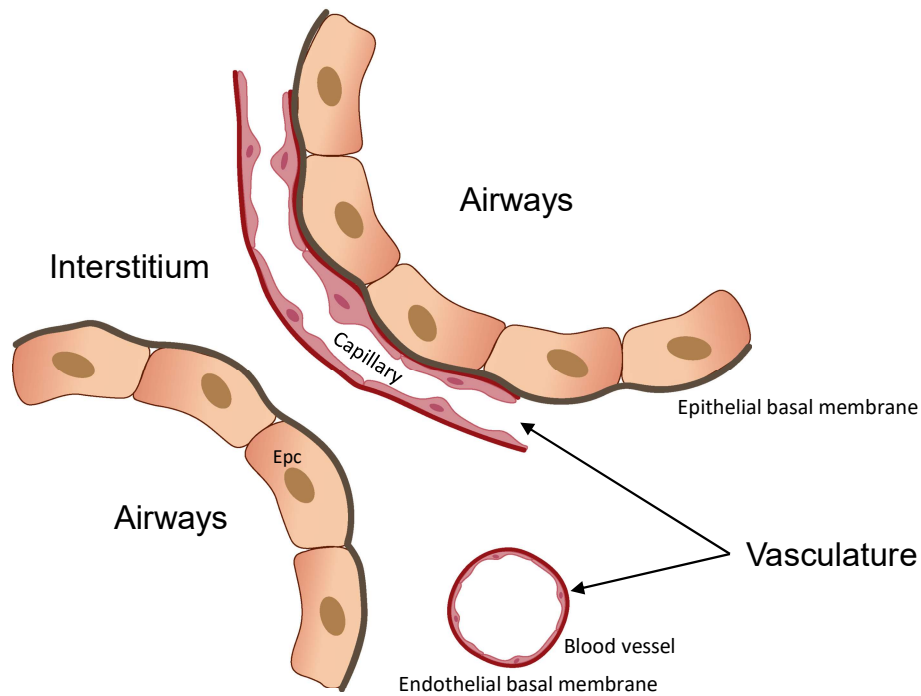


**Figure 1. Main anatomical lung compartments. (A)** The vasculature, interstitium and airways are the three main compartments of the lung. The airway is formed by the continuous network of bronchi, bronchioles and alveolar lumen through which air flows. The vasculature is formed by larger blood vessels (arterioles and venules) and smaller capillaries running along the alveoli to maximize gas exchange. The interstitium is formed by all structures providing support to the vasculature and BAS, typically collagen, elastin and muscle cells.

## 2.2. Influenza virus

Annually, influenza infects an average of 5-15% of the world population, resulting in around 500.000 deaths globally per year<sup>7</sup>. Influenza viruses belong to the family of *Orthomyxoviridae*. These enveloped viruses have segmented negative-strand RNA and are first classified according to the serotype of its nucleoprotein (NP) resulting in influenza A, B or C. Further classification within those influenza strains is provided by the serotype of surface proteins hemagglutinin (HA) and neuraminidase (NA)<sup>8</sup> of which currently, 18 different HA and 11 different NA serological subtypes have been identified. Influenza viruses differ on pathogenicity and host range<sup>9</sup>. While Influenza B and C are found almost exclusively in humans, influenza A can infect a wide array of animals such as humans, swine and birds, among others. The wider host possibility renders influenza A the most dangerous of the 3 types as birds or swine can serve as viral reservoirs<sup>10</sup>.

### **2.2.1. Influenza virus infection**

Once influenza enters the host, it attaches to epithelial cells by binding to sialic acid on their surface with its HA protein<sup>11,12</sup>. Sialic acid is linked with carbohydrates within the glycoproteins, and two of those linkages,  $\alpha(2,3)$  and  $\alpha(2,6)$  provide a binding site for HA<sup>13,14</sup>. Different HA proteins have different specificities against those linkages, and different species have different expression distribution of those linkages, which in turn leads to different viral hosts. While humans show abundance of sialic acid  $\alpha(2,6)$  linkage in the lungs<sup>15</sup>, birds have high expression of sialic acid  $\alpha(2,3)$  in the intestine, which explains why influenza infections in humans are pulmonary while they can be enteric for birds. In addition, pigs have shown to express both linkages in the respiratory tract, which makes them a perfect host for human or avian influenza to mix and become more virulent while jumping species<sup>14,16</sup>.

Once the HA protein is bound to the sialic acid, a process of receptor-mediated endocytosis is initiated. The virus enters the host in an endosome with a low pH, allowing the viral and endosomal membranes to fuse. The acidic environment leads to an open M2 ion channel that results in an acidified viral core<sup>17</sup>. This acidic environment leads to a release of the viral ribonucleoproteins (vRNPs) into the cytoplasm after which they translocate into the nucleus via the cellular nuclear import machinery of the cell<sup>17</sup>.

Finally, once translocated into the nucleus, the virus genome undergoes transcription and replication. vRNPs are then exported through a mechanism not yet well understood. It has been hypothesized that negative sense vRNPs bind the M1 and nuclear export protein (NEP) proteins of the virus which in turn binds CRM1 effectively resulting in the export of the vRNPs from the nucleus<sup>18-20</sup>. New influenza virions are then assembled in the cytosol and expelled from the host by budding the plasma membrane<sup>13</sup>.

### **2.2.2. Mutations and vaccines**

Influenza viruses have high mutation rates suggested to be in the range of  $1-8 \times 10^{-3}$  substitutions per site per year<sup>21</sup> resulting from a lack of proofreading activity in their RNA polymerase complex<sup>22</sup>. Influenza can escape the immune response generated from previous influenza infections or vaccinations by means of antigen shift or antigen



drift<sup>23</sup>. Antigen shift consists in the recombination of HA genes from different influenza A strains and results in a new influenza subtype. This type of recombination only occurs in influenza A viruses due to the wider array of potential hosts, resulting in reassortments of human influenza with influenza from other hosts such as avian flu as in the 2009 influenza pandemic. Antigenic drift, on the other hand, are point mutations in genes encoding for HA and NA proteins, as in the 1918 Spanish flu epidemic<sup>24</sup>. Since surface proteins HA and NA are the most affected by those mutations, previously generated antibodies against a previous infection are quickly rendered obsolete.

As opposed to antibodies, CD8 T cells can also target NP derived antigen. The lower rate of mutations in NP proteins renders CD8 T cells potential candidates for universal vaccines<sup>25</sup>. In addition, CD8 T cells cross-react to the main A, B and C influenza viruses by targeting conserved peptides across different strains<sup>26</sup>. However, lower rate mutations in NP may indicate that CTL responses are not protective against influenza and thus there is no selection pressure. The search for a universal vaccine for influenza is a big challenge due to the high mutation rate in HA and NA, the main targets for antibody responses. However, other influenza proteins do not show such high polymorphisms, likely due to a loss of viral fitness. As most of those proteins are internal (NP, PA, M1, M2, etc) Ab cannot target them. On the other hand, CD8 T cells can target those more conserved viral peptides presented by the major histocompatibility complex I (MHC-I), hence, putting CD8 T cells at the center of research strategies to develop a universal vaccine based on CD8 T cell function rather than antibodies. CD8 T cells targeting membrane matrix protein (M2e)<sup>27,28</sup> or more conserved regions of HA and CD8 T cells<sup>29</sup> are some of the current candidates under preclinical or clinical trials<sup>30</sup>.

### **2.3. Non-immune response to influenza**

The large surface area needed for an optimal gas exchange in the lung, results in constant exposure to pathogens and harmful substances. As a result, a battery of physical, chemical and immunological mechanisms provide the first layers of defense. Mucus secretion by goblet cells along bronchial surfaces can trap foreign bodies and together with the ciliated epithelium provide the first line of defense by and, through ciliary beating movement (muco-ciliary clearance), expel them out of the system<sup>31</sup>. Furthermore, a layer of surfactant, composed mainly of lipids and proteins, provides

surface tension and protection over the luminal side of the alveolar epithelium<sup>32</sup>. Surfactant proteins such as SP-A and SP-D, secreted by type II alveolar epithelial cells, bind viral HA thus preventing viral entry into cells<sup>33–35</sup>. In addition, SP-A and SP-D have been shown to promote neutrophil phagocytosis and viral particle binding<sup>36</sup>. Finally, club epithelial cells secrete antimicrobial peptides such as MUC5AC, which serve as a decoy for HA proteins as they present the  $\alpha(2,3)$  and thus provide a binding site for influenza<sup>37 38</sup>

#### 2.3.1.1. Epithelial response

Once influenza virus circumvents the first defense mechanisms, epithelial cells start a response against the virus. Sensing of influenza virus in epithelial cells is mediated by pattern recognition receptors (PRR) which can recognize viral RNA. Some of the key PRR are Toll like receptor 3 (TLR3), RIG-I and MDA5 which expression increases upon viral infection<sup>39,40</sup>. RIG-I and MDA-5 interact with the adaptor mitochondrial anti-viral signaling (MAVS) which in turn activates IFN responses as well as the inflammasome<sup>41–43</sup>. Furthermore, NOD like receptor 3 (NLRP3) binds apoptosis-associated speck-like protein containing a CARD (ASC), which leads to the activation of pro-caspase 1 into its cleaved form<sup>44</sup>. In its active form, Caspase-1 has been shown to aid in the maturation of IL-1 $\beta$  and IL-18 into active cytokines as well as pyroptosis<sup>45</sup>.

Upon viral sensing, IFN responses induce expression of an array of interferon stimulated genes (ISG) which are key to activate the innate and adaptive immune response<sup>46</sup>. In addition, type III IFN have been shown to be the dominant response in the airway epithelium<sup>47,48,48–50</sup> as they generate antiviral responses with little damage to the host<sup>51</sup>. Type I IFN responses impair viral replication through myxovirus resistance 1 (MX1), interferon induced transmembrane (IFITM) and IFN-induced protein with tetratricopeptide repeats (IFIT) families<sup>52</sup>. MX1 is localized in the nucleus and blocks primary transcription of influenza vRNA<sup>53,54</sup>. IFITM leads to a blockade of cytosolic entry<sup>55,56</sup> and IFIT result in inhibited translation of viral RNA<sup>57,58</sup>. On the other hand, an overresponse of IFN-I have also been shown to generate severe immunopathology<sup>59,60</sup>

Epithelial cells generate a quick response, and as a result of the IFN induced genes, cytokines and chemokines such as CXCL10, TGF- $\beta$ , TNF- $\alpha$ , IL-6, IL-8, CCL2, and IL-1 $\beta$  are produced within the first 24h of influenza infection<sup>61–63</sup>. These cytokines and chemokines are key for the early stages of the immune response. For instance, IL-1 $\beta$  promotes cytokine and chemokine expression on other cells as well as adhesion molecule expression, hence, enhancing immune cell recruitment<sup>64,65</sup>. On the other hand, CCL2 and CXCL10 act as chemoattractant for monocytes and T cells respectively. In addition, epithelial cells have also been shown to secrete cathelicidin LL37, which has been shown to improve disease outcome ( lower mortality, morbidity and viral titers) when administered to mice<sup>66,67</sup>

## **2.4. Immune response to influenza**

### **2.4.1. Innate response**

Innate immune responses are characterized by being the first responders of the immune system as they respond within hours of primary infection and develop quickly during the first days of infection. Innate cells are then key in containing infections and triggering the adaptive immune response for further protection<sup>46</sup>.

#### **2.4.1.1. Alveolar macrophages**

Alveolar macrophages (AlvM) are resident in the alveolar lumen and can be found in a ratio of around 1 AlvM per 3 alveoli<sup>68–70</sup>. AlvMs are varied in function and are key to lung homeostasis, clearance of surfactant and cell debris, pathogen recognition, initiation and resolution of lung inflammation, and repair of damaged tissue<sup>69</sup>. In steady state, AlvMs have high phagocytic activity, low levels of inflammatory cytokines and modulate inflammation and adaptive immunity<sup>68</sup>.

AlvMs are generally not infected by influenza virus, however, they play an important role in the secretion of chemokines and cytokines such as TNF- $\alpha$ , IL-1, IL-6 and IL-8 which in turn drive neutrophil, monocyte and NK cells infiltration into the airways<sup>71,72</sup>. In further stages of the immune response, AlvM play an important role eliminating antibody-opsonized infected cells and viruses<sup>73</sup>. Furthermore, they can present antigen with low efficiency by phagocytosis of infected material<sup>68</sup>

#### 2.4.1.2. Neutrophils

During steady state conditions, most of the neutrophils are found in the circulation. However, it has been shown that circulating neutrophils get retained in the lung microvasculature while maintaining a dynamic equilibrium with the circulation pool<sup>74,75</sup>. The mechanisms of neutrophil retention in the lung microvasculature are still poorly understood, some have shown that physical conditions such as capillary vessel size, hemodynamics and time needed for neutrophils to adapt their shape do play a role.<sup>76-78</sup> In addition, interactions between neutrophils and the endothelial layer has also been shown to play a major role in retention<sup>76,79,80</sup>.

Neutrophils are amongst the first immune cell to infiltrate the lungs once influenza has infected the host<sup>81</sup>. The initial response in the lung by the non-immune cells as well as AlVM triggers the migration of neutrophils into the infected lung via secretion of TNF- $\alpha$ , IL-1b, IL-6, CXCL1 and CXCL2<sup>82</sup>. In addition, it was recently shown that neutrophils use the CXCR4/CXCL12 axis to migrate into the lung and potentially providing a path for other immune cells to infiltrate the lung<sup>83</sup>. Neutrophils responses have been shown to be both, protective<sup>84</sup> and to contribute to disease severity<sup>85</sup>, largely depending on the virulence of the infection. Neutrophils protection is conferred by phagocytosis of apoptotic or dying cells since they are, as AlVM, not usually infected by the virus. On the other hand, neutrophils can contribute to tissue damage by means of neutrophil extracellular traps and generation of free radicals such as ROS and NOS<sup>85-87</sup>.

#### 2.4.1.3. Monocytes

Monocytes are recruited into the lungs upon influenza infection following upon CCL2, CCL3 and CCL5 produced by AlVM and epithelial cells. While transendothelial migration is dependent on interactions between ICAM-1/ $\beta$ 2 integrin and VCAM-1/ $\beta$ 1 integrin, transepithelial migration mainly requires the CCL2/CCR2 axis. Due to the inflammatory environment in the lung, monocytes are driven into differentiation into macrophages and dendritic cells (DCs), resulting in a key role for phagocytosis of infected/dead material and priming of the adaptive immune system.

#### 2.4.1.4. DC activation and lymph node homing

DCs are myeloid cells distributed through all organs. Albeit being rare cells, their strategic positioning in organs prone to pathogen encounters renders them pivotal to the adaptive immune response. As specialized antigen presenting cells (APC), DCs are crucial for naive T cell activation in the SLO<sup>88</sup> and reactivation of memory T cells<sup>89</sup>. The uptake of material from dying cells triggers a variety of PRRs which lead to DC activation<sup>90</sup>. Activated DCs upregulate CCR7, which is a key mediator for trafficking through the lymphatic system into the lymph nodes. DC positioning into the T cell zone is mediated by CCR7 ligands CCL19 and 21 which are expressed by fibroblastic reticular cells in the T cell zone<sup>91-94</sup>. In the T cell zone, DCs cross-present antigens in the context of MHC-I or MHC-II to activate CD8 or CD4 T cells, respectively.

#### **2.4.2. Adaptive response**

Homing of DCs into the lymph nodes triggers the activation cascade of the adaptive immune response. The different members of the adaptive immune response work in unison to control and clear influenza infection in the lung epithelium. CD8 T cells, also known as cytotoxic T lymphocytes (CTLs), migrate into infected tissues 5 to 7 days after infection and through cytolytic pathways kill influenza infected cells. In contrast, CD4 T cells act as helper cells and provide further signals for other cells to perform their effector function such as B cell class switch<sup>95</sup>. B cells contribute by producing neutralizing antibodies against key epitopes for viral function.

The coordination between CD8 and CD4 T cells together with B cell responses is key to an effective adaptive response. CD8 T cell contribution has been studied with mice lacking functional MHC-I, showing delayed clearance of influenza<sup>96,97</sup> and impaired survival in highly virulent infections. Although this data indicates CTLs have a significant impact on viral clearance, they are not the sole contributors to clearing the virus as it has been shown CD4 T cells can clear the infection when CD8 T cells are depleted or lacking<sup>98,99</sup>. Furthermore, depletion of both cell types results in host death as the virus cannot be cleared<sup>100,101</sup>. Previous studies suggest a combination of at least 2 of the adaptive immune cell types is necessary to overcome infection as depletion of one of the cell population can be compensated by the other remaining cell types<sup>98</sup>.

#### 2.4.2.1. T cell priming

T cells need a variety of signals to become optimally activated to subsequently proliferate and differentiate into effector T cells. DCs presenting influenza antigens on MHC molecules in the T cell zone of the lung-draining mediastinal LN are central in this process. To recognize a widespread range of pathogens it is estimated humans harbor around  $10^8$  unique TCRs<sup>102</sup>. Due to the high diversity of TCRs, there is a low frequency of antigen-specific T cells (1 in  $10^6$  naïve CD8 T cells specific for a given epitope)<sup>102,103</sup>. Naïve T cells express CD62L which allows them to be in constant circulation between the blood and secondary lymphoid organs (SLO). Upon entering the lymph nodes, T cells are continuously scanning DCs via the TCR-MHC axis. The constant scanning of DCs by naive T cells in secondary lymphoid organs (SLO) increases the probability of otherwise rare encounters between those flu-specific T cells and those few DCs presenting flu antigens at the early stages of the infection<sup>104,105</sup>. Antigen presentation on MHC-I may happen either by classical or cross-presentation of influenza antigens. During classical MHC-I presentation, DCs themselves become infected and present viral peptide antigens on their surface in complex with MHC-I molecules following the classical cytosolic route<sup>106,107</sup>. On the other hand, cross-presentation happens when DCs phagocytose infected cells and present the viral antigens contained in the infected material in complex with MHC-I molecules<sup>108</sup>. Precise details of MHC-I cross-presentation are still unclear. Both an endosomal-autonomous pathway<sup>109</sup> and endosomal-cytosolic pathway<sup>110</sup> have been described<sup>111</sup>. In any case, cross-presentation is believed to be of utmost importance during influenza infections<sup>112</sup> because the virus primarily infects epithelial cells<sup>113</sup>. Therefore, DCs are believed to obtain viral antigens through phagocytosis of infected epithelium in order to activate a protective CD8 T cell response<sup>112</sup>. MHC-II presentation, as MHC-I cross-presentation, occurs when infected material is phagocytosed by DCs. However, in the case of MHC-II presentation, influenza-derived peptide fragments are loaded onto MHC-II molecules in the endolysosomal compartment<sup>114</sup>.

Engagement of TCR with cognate peptide on the DCs MHC triggers TCR signaling, leading to proliferation. T cell frequencies for influenza epitopes range from 1:600 to 1:1400 during steady state, however, during influenza infection T cell expansion brings the frequencies in the mediastinal lymph node (mLN) up to a 1,5% for a given epitope

during primary responses and 17% during secondary responses<sup>115</sup>. As the first step on the T cell response, this mechanism of T cell activation constitutes signal 1<sup>116</sup>.

DCs express an array of costimulatory molecules such as CD40, CD80 and CD86, which provide pro-survival signals by engaging with CD40L and CD28 on the proliferating T cells<sup>117</sup>. In addition, DCs further modulate T cell responses to avoid excessive activation by producing co-inhibitory signals which interact with CTLA-4 on activated T cells<sup>118,119</sup>. These co-stimulatory signals lead to survival via a cascade of intracellular signaling. Activated tyrosine kinase LCK results in CD3 phosphorylation which then binds activated  $\zeta$  chain-associated protein kinase 70 (ZAP-70). ZAP-70 initiates a series of events leading to activation of diverse transcription factors such as activator protein (AP-1), nuclear factor kappa-light-chain-enhancer of activated B cells (NF- $\kappa$ B) and nuclear factor of activated T cells (NF-AT). As a result, T cell gene expression is modified in pro of T cell survival<sup>120</sup>. This signaling cascade constitutes signal 2.

Finally, T cell differentiation occurs when signal 3 is provided. Depending on the cytokine profile resulting from the initial response to the pathogen we can differentiate between type 1, 2 and 3 responses. Type 1 responses are driven by production of IFN $\gamma$  (primarily by lymphoid cells)<sup>121,122</sup> and IL-12 (primarily by macrophages and DCs) which result in activation of the transcription factor T-bet and the generation of CD4 th1 cells and CTLs. Type 2 responses are characterized by IL-4 and IL-2 cytokine signature and resulting in the activation of the transcription factor GATA3 which lead to a CD4 th2 response. Finally, a IL-21, IL-6, IL-23 and TGF- $\beta$  cytokine profile leads to ROR $\gamma$ T activation and a CD4 TH17 type 3 response<sup>123</sup>. As type 1 responses are usually triggered in bacterial and viral infections, during influenza infection we find a type 1 response profile<sup>124</sup>.

#### 2.4.2.2. T cell migration and effector response

Proliferating T cells in the SLO downregulate CD62L and S1P1, thus, allowing CTLs to exit the lymph nodes and enter systemic circulation<sup>125</sup>. To perform their effector protective function in the influenza infected lung, activated T cells need to transmigrate from the blood to the site of infection in the lung. For this, endothelial cells become

activated by pro-inflammatory cytokines such as TNF $\alpha$  and IFN $\gamma$  that are released at the site of infection and result in upregulation of adhesion molecules such as ICAM-1<sup>126–128</sup>. This leads to the tethering of activated LFA-1<sup>+</sup> influenza-specific T cells into the endothelium and initiates their transmigration following chemokines cues released at the site of infection such as CXCL9, CXCL10<sup>129</sup>, CCL17 and CCL22<sup>130</sup>.

CD8 T cell responses peak between 6-9 days after infection. CTLs, provide protection by eliminating infected cells<sup>25</sup>. This cytolytic activity by CTLs is highly specific as killing of infected cells will only occur upon specific TCR recognition of specific MHC-I peptide complex on the infected cell<sup>131</sup>. Effector CTLs kill infected cells using a variety of mechanisms. There are 3 main mechanisms CTLs use to induce apoptosis in infected cells, perforin/granzyme<sup>132</sup>, TRAIL<sup>133</sup> and FAS ligand<sup>134</sup>. Granzymes released upon TCR engagement penetrate target cells through pores on their membrane formed by perforin<sup>132,135</sup>. Once granzymes enter the cytosol it induces apoptosis via procaspase 3 and Bid<sup>136,137</sup>. TRAIL, expressed on CD8 T cells, binds TRAIL-R1 or TRAIL-R2 on infected cells which triggers a signaling cascade resulting in caspase 8 activation and leading to apoptosis through downstream caspases<sup>133,138</sup>. FAS ligand on CTLs binds FAS expressed on infected cells and leads to apoptosis using the same caspase 8 signaling as TRAIL<sup>134,139,140</sup>.

Independently of the mechanism utilized, killing of infected cells results in (1) inhibition of viral replication resulting in lower viral counts and (2) accessibility of protective antibodies to the released influenza viruses for neutralization.

#### 2.4.2.3. Generation of memory T cells

Following the peak of T cell response and pathogen clearance, the antigen-specific T cell compartment undergoes significant contraction following death of about 90-95% of the Ag-specific T cells by apoptosis<sup>141,142</sup>. The remaining Ag-specific T cell compartment is comprised of memory T cells, constituting a heterogeneous pool of T cells from a transcriptional<sup>143,144</sup>, epigenetic<sup>144</sup> and functional<sup>145,146</sup> perspectives. Memory T cells can be divided into central memory T cells (T<sub>CM</sub>), effector memory T cells (T<sub>EM</sub>) and tissue resident memory T cells (T<sub>RM</sub>). A defining characteristic of T<sub>CM</sub> is their expression of CCR7 and CD62L, which allows them to transmigrate through the HEVs and recirculate between bloodstream, secondary lymphoid organs and the



lymphatic system following CCL19/21 cues similarly to naive cells<sup>116,147</sup>. Upon activation  $T_{CM}$  proliferate and differentiate into  $T_{EM}$ , serving as precursors of  $T_{EM}$ . On the other hand,  $T_{EM}$  do not express CCR7 but express  $\beta_1$  and  $\beta_2$  integrins and are primarily in bloodstream or reside in nonlymphoid tissues.  $T_{EM}$  are specialized to quickly migrate to inflamed tissues, mature into effector T cells and, depending on their previous th signature they will secrete IFN- $\gamma$ , IL-4 or IL-5 early upon restimulation<sup>147,148</sup>. Finally,  $T_{RM}$ , as the name indicates, are a subset of memory T cells that do not recirculate but reside in nonlymphoid organs<sup>147,149</sup>.  $T_{RM}$  have been described in most organs studies albeit in different frequencies, including skin<sup>150,151</sup>, lung<sup>152–154</sup>, vaginal mucosa<sup>155,156</sup>, brain<sup>157</sup> and intestine<sup>158,159</sup>.  $T_{RM}$  are characterized by having low expression of CCR7 and high CD103 which binds E-cadherin<sup>160</sup>, a highly expressed molecule on the surface of epithelial cells. It is believed that CD103 retains  $T_{RM}$  close to epithelial cells in NLO<sup>146,149,155</sup>. In addition,  $T_{RM}$  have reduced S1PR expression to further promote retention in tissue<sup>161</sup>. Furthermore, it has recently been shown that upon restimulation  $T_{RM}$  show plasticity towards  $T_{EM}$  and  $T_{CM}$  and undergo retrograde migration into the circulation while keeping biased homing potential to their original site<sup>162</sup>.

Different models have been described for the generation of memory T cells. In a linear model effector T cells differentiate into memory T cells at the contraction phase<sup>141,163</sup>. CTLs then acquire a resting state while retaining the ability to quickly produce IFN $\gamma$  and TNF $\alpha$ . Memory CTLs in the linear model can then reacquire cytotoxic activity upon antigen exposure<sup>164,165</sup>. More recently, a model of asymmetric has been described. In the asymmetric model, activated effector T cells give rise to a heterogeneous population and generate memory T cells early in the response<sup>163,166,167</sup>. It is however not clear if both models of memory T cell differentiation are mutually exclusive or occur simultaneously<sup>163</sup>.

Once generated, in a process dependent on IL-15 and IL-7<sup>168</sup>, T cell memory is maintained homeostatically in absence of antigen during long periods of time<sup>169</sup> of up to 15 years<sup>170</sup> by slow rate division, thus, keeping the memory pool relatively stable. Upon infection,  $T_{RM}$  at the site of pathogen entry become the first responders amongst the memory T cell pool, quickly acquiring effector functions<sup>146,149,171,172</sup> to confer protection<sup>173,174</sup>. In parallel, antigen travels into the draining LN either directly or via migrating DCs which leads to  $T_{CM}$  activation and further differentiation into  $T_{EM}$ .  $T_{EM}$

are then able to migrate into infected lung providing a second wave of memory T cell effectors<sup>149</sup>.

#### 2.4.2.4. B cell response

B cells are the producers of antibodies against viral epitopes. B cells recognize antigen via the B cell receptor(BCR) which can engage free antigen or antigen presented by DCs<sup>175</sup>. Activated B cells relocate to the edge of the lymphoid follicle where they interact with previously activated antigen-specific CD4 helper T cells through CD40-CD40L. Activated CD4 T cells provide help to B cells by recognizing antigen on B cells by means of MHC-II and help trigger B cells to proliferate further. Initially plasmablasts produce a first wave of IgM antibodies around day 5 after infection which provide certain protection but do not have high specificity. In parallel, activated B cells together with CD4 follicular T helper cells (Tfh) migrate into the follicle and form germinal centers<sup>176,177</sup>. Germinal centers are conformed mainly by B cells but house a Tfh population of up to 10% which provide help to B cells. B cells in the germinal center undergo strong proliferation and somatic hypermutation. During somatic hypermutation, B cells introduce mutations that change the amino acids in the immunoglobulin, thus, creating different clones with different antigen affinity. In next step, during affinity maturation B cells with high antigen affinity are selected for survival for a more specific antibody response. Cytokines produced by Tfh upon MHC-II engagement in the germinal centers induce B cells to antibody class switch. Tfh secrete IL-4, IFN- $\gamma$  and TGF- $\beta$  which induce IgG1/IgE, IgG3/IgG2a and IgG2b/IgA antibody responses respectively<sup>178,179</sup>.

During influenza infection, due to the easier access to HA most of the antibody response is directed against this antigen. However, antibodies can also be found in lower quantities for NA and internal proteins. Early in the response IgM antibodies offer early protection albeit at a lower affinity. Upon B cell activation and maturation, B cells produce IgG1 and to a lower extent IgG2 antibodies against influenza<sup>10,180</sup>. In addition, IgA antibodies against influenza have been detected on mucosal surfaces. Despite the strong B cell response against influenza, the fact that most of the antibodies are targeting HA, a protein very susceptible to antigen drift, renders these responses potentially ineffective against secondary infections by other influenza strains<sup>180</sup>.

### **2.4.3. Immune pathology**

Influenza infections can be damaging by either killing epithelial cells and thus favoring super infections or by promoting an overt immune response that results in damage not only to infected cells but also healthy cells. An overreaction of the immune system can result in excessive infiltration of neutrophils, macrophages and T cells ultimately resulting in impaired survival due to bystander killing of essential pulmonary cells<sup>60,181</sup>. Neutrophils further contribute to immune pathology by the generation of extracellular traps<sup>85,105,182</sup>. Furthermore, excessive recognition of epithelial cells expressing influenza HA by CD8 T cells results in the direct or indirect killing of large numbers of epithelial cells which results in severe immunopathology<sup>183</sup>.

It is therefore of high interest to determine the mechanisms by which immune cells migrate and protect the host against influenza. It would then be conceivable develop mechanisms that regulate the immune response and optimize viral clearance while preserving tissue integrity.

### **2.4.4. Animal models**

Research on human samples has become more valuable with the advent of transcriptomics and specially single-cell mRNAseq. The development of a wide array of new techniques has opened the scope of the BAL and sputum samples from infected patients to decipher valuable immune pathways during acute and fatal disease outcomes. However, the use of animals from early to advanced stages of research has been key to develop the necessary knowledge to develop novel therapies and vaccines for a wide variety of pathogens and diseases<sup>184</sup>.

A diversity of animal models have been used for research within the last decades<sup>185</sup>. The choice of one animal model over another is not a trivial decision. For influenza research, it is important that the animal is susceptible to influenza infections and viral replication as well as provide with measurable signs of disease. Some of the most used models are mice and ferrets<sup>185–187</sup>.

Mice are, for a variety of reasons, the most used animals within the research world. The mouse model provides an excellent system for early stages of research as they are easily genetically modified, providing key tools to study host responses to

infection<sup>188</sup>. In addition, their small size, husbandry requirements and low cost, together with a wide range of specific reagents offer a robust system. However, mice susceptibility to influenza infection is strain dependent, that is, it varies depending on mouse and viral strain. Mice strains such as BALB/c and C57BL/6J have been the most used for type-1 immunity research<sup>187</sup>. The wide array of modified systems on the C57BL/6J background has made this one of the most popular strains for immunology research. Due to influenza infection being dependent on strain, some influenza viruses have been adapted to the mouse model for research purposes. Influenza A A/PR/8/1934(H1N1) was adapted from the 1934 human virus while A/X-31 (H3N2) was genetically engineered to carry HA and NA from A/Hong Kong/1/1968 in A/PR/8/1934(H1N1) background. Disease in mice typically results in weight loss, ruffled fur, huddling and lethargy<sup>185</sup>. On severe infections, mice show signs of lung lesions and edema and might result in death. Unlike humans, mice do not develop fever and the focus of infections is on lower airways instead of the upper airways found in humans<sup>185</sup>.

Ferrets are an alternative to mice for influenza infections. Ferrets provide an excellent model as they closely mimic infection in humans because ferrets are naturally susceptible to human influenza without adaptation and show a mainly upper respiratory tract infection. Another advantage over the mouse model is the route of infection. Whereas mice need to be experimentally infected via the intranasal or intratracheal routes, ferrets can be infected by cohabitation, which closely resembles the situation in humans<sup>186</sup>. In addition, ferrets show similar symptoms to humans, fever, lethargy and nasal congestion. Due to the similar symptomatology to humans, ferrets are commonly used for testing antiviral drugs ameliorating the disease outcome. However, and unlike mouse models, their size, husbandry, costs and lack of immunological reagents are seen as a drawback of this model<sup>185,186</sup>.

Other animals have been used for influenza research, such as, guinea pigs and cotton rat among others. However, the characteristics of mice and ferrets make them the primary choice for influenza research<sup>185</sup>.

### **3. Aim of the study**

Albeit the extensive research on influenza infections in the lung, many questions remain unanswered such as the role of CD8 T cell in general during infection and the specific contributions of CD8 T cells located at different pulmonary compartments. Upon infection, immune cells migrate into the lung environment and distribute throughout the different compartments (interstitium, bronchoalveolar space and vasculature). However, understanding the importance of immune cell localization for immunity against invading pathogens has been hampered because of lack of a method to precisely determine cell positioning in the lung.

Using a mouse model for pulmonary influenza infection, the present study aims at (1) characterizing compartment-specific phenotype and function of influenza-specific CD8 T cells, (2) determining the extent to which CD8 T cell positioning in the lung affects disease outcome during primary and secondary infections, (3) identifying the role of MHC-I interactions between influenza-specific memory CTLs and EpCs and (4) determining the role of dendritic cells on memory CD8 T cell re-activation during a secondary flu challenge.

Answering these questions is fundamental for elucidating how anti-flu CTL responses are orchestrated and for the development of novel vaccination strategies aimed at generating a universal flu vaccine by targeting the memory T cell pool.

## 4. Materials and methods

### 4.1. Materials

#### 4.1.1. Equipment

<b>Instruments</b>	<b>Company</b>
710 confocal microscope	Carl Zeiss Microscopy, Jena, Germany
Biobeam2000	MCP-STs, Braunschweig, Germany
Centrifuge 5810 R	Eppendorf, Hamburg, Germany
FACS Aria III	Becton, Dickinson and Company, Franklin Lakes, NJ, USA
FACS Canto II	Becton, Dickinson and Company, Franklin Lakes, NJ, USA
Fluovac system	Harvard Apparatus, Cambridge, MA, USA
Heracell 240 incubator	Thermo Fisher Scientific, Waltham, MA, USA
Julabo TW8 waterbath	Julabo, Seelbach, Germany
LSR Fortessa	Becton, Dickinson and Company, Franklin Lakes, NJ, USA
Minivent mechanical ventilator	Harvard Apparatus, Cambridge, MA, USA
nCounter sprint instrument	Nanostring Technologies, Seattle, WA, USA
Perfect spin 24 table-top centrifuge	Peqlab, Erlangen, Germany
Rodent laryngoscope Model LS-2-M	Penn Century, Wyndmoor, PA, USA
SW41 Rotor	Beckman Coulter, Brea, CA, USA
VT1000S vibrating-blade microtome	Leica Biosystems, Nußloch, Germany

#### 4.1.2. Reagents

Reagent	Manufacturer
100xMEM vitamins solution	Sigma-Aldrich, St. Louis, MO, USA
2-mercaptoethanol	Sigma-Aldrich, St. Louis, MO, USA
50xMEM amino acids solution	Sigma-Aldrich, St. Louis, MO, USA
Agarose, Low Melting Point, Analytical Grade	Promega, Madison, WI, USA
NP366-374 (ASNENMETM) peptide	Xaia Custom Peptides, Göteborg, Sweden
Bovine serum albumin fraction V (BSA)	Roth, Karlsruhe, Germany
Carboxyfluorescein succinimidyl ester (CFSE)	Molecular Probes, Leiden, The Netherlands
CD8a (Ly-2) MicroBeads, mouse	Miltenyi Biotech, Bergisch Gladbach, Germany
Cell Proliferation Dye eFluor® 670	eBioscience, San Diego, CA, USA
Collagenase type IV	Sigma-Aldrich, St. Louis, MO, USA
Crystal violet	Sigma-Aldrich, St. Louis, MO, USA
Dextramer H2-D <sup>b</sup> /ASNENMETM (NP366-374) APC/PE	Immudex, Copenhagen, Denmark
Diphtheria toxin	Sigma-Aldrich, St. Louis, MO, USA
DNase I	Sigma-Aldrich, St. Louis, MO, USA
Dulbecco's Modified Eagle's Medium (DMEM)	Sigma-Aldrich, St. Louis, MO, USA
Ethylene diamine tetraacetic acid (EDTA)	Merck, Darmstadt, Germany
Fetal calf serum (FCS)	Life Technologies, Carlsbad, CA, USA
Fixable Viability Dye eFluor™ 780	eBioscience, San Diego, CA, USA
Fixation/Permeabilization solution	Becton, Dickinson and Company, Franklin Lakes, NJ, USA
Fluoromount G	Southern Biotech, Birmingham, AL, USA
Golgi plug	Becton, Dickinson and Company, Franklin Lakes, NJ, USA

Golgi stop	Becton, Dickinson and Company, Franklin Lakes, NJ, USA
Hoechst 33528	Sigma-Aldrich, St. Louis, MO, USA
Human poly-immunoglobulin	CSL Behring, King of Prussia, PA, USA
Isoflurane	AbbVie, North Chicago, IL, USA
L-Glutamine	PAA, Cölbe, Germany
Minimum Essential Medium (MEM)	Sigma-Aldrich, St. Louis, MO, USA
NaN <sub>3</sub>	Sigma-Aldrich, St. Louis, MO, USA
nCounter Mouse Inflammation Gene Expression CodeSet	Nanostring Technologies, Seattle, WA, USA
Penicillin/Streptomycin	Merck, Darmstadt, Germany
Phorbol 12-myristate 13-acetate (PMA)	Sigma-Aldrich, St. Louis, MO, USA
Phosphate buffered saline (PBS)	Life Technologies, Carlsbad, CA, USA
Propidium iodide	Sigma-Aldrich, St. Louis, MO, USA
RPMI 1640 medium	Invitrogen, Darmstadt, Germany
Sodium bicarbonate solution	Sigma-Aldrich, St. Louis, MO, USA
TPCK trypsin	Sigma-Aldrich, St. Louis, MO, USA



### 4.1.3. Buffers

Buffer	Ingredients
Buffer RLT	RNAeasy lysis buffer, Qiagen, Hilden, Germany
Culture buffer	DMEM, 10% (v/v) FCS, 5% (v/v) L-Glutamine, 5% (v/v) penicillin/streptavidin
Digestion buffer	PBS, 3% (v/v) FCS, 1mg/ml Collagenase IV, 50U/ml DNase I
FACS blocking buffer	PBS, 3% (v/v) FCS, 0.1% (v/v) NaN <sub>3</sub> , 15 mg/ml human poly-Ig
FACS buffer	PBS, 3% (v/v) FCS, 0.1% (v/v) NaN <sub>3</sub>
Full medium	RPMI 1640 medium, 10% (v/v) FCS, 1% (v/v) L-Glutamine, 1% (v/v) penicillin/streptavidin, 0.05mM 2-mercaptoethanol
MACS buffer	PBS, 3% (v/v) FCS, 2mM EDTA
PCR mix	For 1x sample: H <sub>2</sub> O(calculated depending on number of primers), PCR buffer 8.5 µl, MgCl <sub>2</sub> 7 µl, dNTPs 7 µl, primers 0.05 µl each and Taq polymerase 0.6 µl (Total volume must add up to 70 µl)
RBC lysis buffer	500µl H <sub>2</sub> O, 150mM NH <sub>4</sub> CL, 10mM KHCO <sub>3</sub> and 0.1mM EDTA
Stopping buffer	PBS, 10% (v/v) FCS
Viral infection buffer	MEM, 0.3% (v/v) BSA fraction V, 1µl/ml TPCK trypsin

#### 4.1.4. Consumables

<b>Consumable</b>	<b>Manufacturer</b>
LS Cell separation columns	Miltenyi Biotech, Bergisch Gladbach, Germany
Micro-haematocrit capillary	Sigma-Aldrich, St. Louis, MO, USA
15-50ml Conical centrifuge tubes	Corning Incorporated, Corning, NY, USA
Polyethylene tubing, diameter 0.58 mm	Intramedic, Neu-Isenburg, Germany
0.5, 1.5 safe-lock microcentrifuge tubes	Eppendorf, Hamburg, Germany
5ml Polystyrene tubes	Sarstedt, Nümbrecht, Germany
6 well plate	TPP, Trasadingen, Switzerland
12 well plate	TPP, Trasadingen, Switzerland
Hypodermic needle 22G x 1"	BBraun Melsungen, Melsungen, Germany
Indwelling cannula 22G x 1"	BBraun Melsungen, Melsungen, Germany
96 well U-bottom plate	TPP, Trasadingen, Switzerland
96 well V-bottom plate	TPP, Trasadingen, Switzerland
Cell strainer 100 µm	Corning Incorporated, Corning, NY, USA
Tissue culture flask 25, 75, 150 cm <sup>2</sup>	TPP, Trasadingen, Switzerland

#### 4.1.5. Antibodies

##### 4.1.5.1. Antibodies for flow cytometry and confocal microscopy

All antibodies were specific against mouse antigens.

<b>Antigen</b>	<b>Clone</b>	<b>Manufacturer</b>
CD103	2E7	BioLegend, San Diego, CA, USA
CD11b	M1/70	BioLegend, San Diego, CA, USA
CD11c	N418	BioLegend, San Diego, CA, USA
CD8 $\alpha$	53-6.7	BioLegend, San Diego, CA, USA
CD4	GK1.5	BioLegend, San Diego, CA, USA
CD44	IM7	BioLegend, San Diego, CA, USA
CD45.1	A20	BioLegend, San Diego, CA, USA
CD45.2	104	BioLegend, San Diego, CA, USA
CD64	X54-5/7.1	BioLegend, San Diego, CA, USA
CD69	H1.2F3	BioLegend, San Diego, CA, USA
F4/80	BM8	BioLegend, San Diego, CA, USA
I-A/I-E	M5/114.15.2	BioLegend, San Diego, CA, USA
Ly6c	HK1.4	BioLegend, San Diego, CA, USA
Ly6G	RB6-8C5	BioLegend, San Diego, CA, USA
Siglec-F	E50-2440	eBioscience, San Diego, CA, USA
CD8 $\beta$	53-5.8	BioLegend, San Diego, CA, USA
CD90.2	30-H12	BioLegend, San Diego, CA, USA
CD90.1	OX-7	BioLegend, San Diego, CA, USA
CD19	4G7	BioLegend, San Diego, CA, USA
IFN $\gamma$	DB-1	BioLegend, San Diego, CA, USA

#### 4.1.5.2. Depleting antibodies

$\alpha$ -CD4	GK1.5	Bioxcell, West Lebanon, NH, USA
$\alpha$ -CD8	YTS169.4	Bioxcell, West Lebanon, NH, USA
$\alpha$ -NK	PK136	Bioxcell, West Lebanon, NH, USA
rat IgG2b isotype control	LTF-2	Bioxcell, West Lebanon, NH, USA
mouse IgG2a isotype control	C1.18.4	Bioxcell, West Lebanon, NH, USA

#### 4.1.6. Infectious agents

<b>Virus strain</b>	<b>Name</b>	<b>Modifications</b>
IFV A/PR/8/1934(H1N1)	PR8	Adapted to mice by serial <i>in vivo</i> infections <sup>189</sup>
IFV A/WSN/33OVAI	WSN-OVAI	Genetically engineered influenza virus containing the CD8 T cell epitope OVA 257-264 epitope <sup>190</sup>
IFV A/X-31	X-31	Carries surface proteins from A/Hong Kong/1/1968 influenza and the six internal genes from PR8 <sup>191</sup>

#### 4.1.7. Mouse lines

All animals were on a C57BL/6J background and were housed in a specific pathogen-free (SPF) environment, as defined by FELASA guidelines, in the House for Experimental Therapy (HET) of the Medical Faculty of the University of Bonn according to German and institutional regulations. Mice were weaned 21 days after birth and experiments started when mice were between 8 and 12 weeks of age.

Below is a list of mice used for this work.

Mouse line	Official name	Description
B6	C57BL/6J	Wild type (WT) mice of H2-K <sup>b</sup> background
CD45.1 <sup>192</sup>	C57BL/6-Tg(TcraTcrb)1100Mjb/J	Expression of pan-leukocyte CD45.1 congenic marker
OT-I <sup>193</sup>	B6.SJL- <i>Ptprc</i> <sup>a</sup> <i>Peprc</i> <sup>b</sup> /BoyJ	Expression of transgenic T cell receptor recognizing OVA <sub>257-264</sub> in the context of H2-K <sup>b</sup>
<i>Cxcr3</i> <sup>-/-194</sup>	B6.129P2- <i>Cxcr3tm1Dgen</i> /J	Deficient for <i>Cxcr3</i> gene
Thy1.1 <sup>195</sup>	B6.PL-Thy1a/CyJ	Expression of the T cell specific Thy1.1 congenic marker
<i>β2m</i> <sup>-/-196</sup>	B6.129-B2m <sup>tm1Jae</sup> N12	Deficient for β <sub>2</sub> -microglobulin; Residual expression of MHC-I at the surface and 99% reduction of CD8 conventional T cells
CD11c.DOG <sup>197</sup>	B6.Cg-Tg(Itgax-DTR/OVA/EGFP)1Gjh/Crl	BAC transgenic mice expressing human DTR and ovalbumin 140-386 under the CD11c promoter. No expression of functional eGFP.
<i>TdTomato</i> <sup>198</sup>	tdTomato	Ubiquitous expression of TdTomato.

Mouse line	Description
<i>Cxcr3</i> <sup>-/-</sup> x OT-I	OT-I transgenic TCR mice deficient for <i>Cxcr3</i> gene
CD45.1 x B6	Expression of pan-leukocyte markers CD45.1 and CD45.2

## 4.2. Methods

### 4.2.1. Intratracheal infection

Mice were intratracheally infected as previously described<sup>199</sup>. In brief, mice were anesthetized with 2% isoflurane/O<sub>2</sub>(v/v) using a Fluovac system and subsequently intubated with a 22G x 1" cannula through the oral cavity using a small animal laryngoscope. 50µl of the infectious solution was administered through the cannula using a mechanically-assisted mouse ventilator (Minivent) set at 250 strokes/min and 250µl tidal volume. Following administration, mice were actively ventilated for further 60s for pulmonary distribution of the viral particles before returning them into their cage.

### 4.2.2. Cell depletion

#### 4.2.2.1. Depletion by antibody

Depletion of CD4 T cells, CD8 T cells and NK cells *in vivo* was performed by i.p. administration of 150µl PBS containing 300µg of αCD4 antibody (GK1.5), αCD8α antibody (YTS169.4) or αNK1.1 antibody (PK136)<sup>200</sup>. To deplete cells for longer than 3 days, mice received further injections every 4 days. Control mice received the same dose of isotype control (Rat IgG2b (CD4 and CD8) and mouse IgG2a (NK1.1) respectively).

#### 4.2.2.2. Depletion by Diphtheria toxin

CD11c.DOG mice received 8ng/g body weight diphtheria toxin (DT) i.p. in 200µl of PBS on 2 consecutive days as previously described<sup>197</sup>.

### 4.2.3. Generation of bone marrow chimeras

To generate bone marrow chimeras (BMx), recipient mice were first depleted of NK cells via i.p. administration of 300µg of anti-NK1.1 antibody (clone: PK136) in 200µl PBS in order to avoid rejection of donor  $\beta_2m^{-/-}$  cells by recipient NK cells<sup>201</sup>. 1 day later,

recipient mice underwent full-body irradiation with 1 Gy in a Biobeam2000. Next day  $1 \times 10^6$  RBC-lysed donor bone marrow cells collected from femur and tibia were i.v. transferred in 100  $\mu$ l PBS into each recipient mice. Chimerism in the T cell, B cell, and neutrophil compartments was assessed in blood at 8 and 12 weeks after irradiation using flow cytometry. BMx were used for experiments at 90 days after reconstitution.

#### **4.2.4. *In vivo* differential labelling (IDEAL)**

I developed a fluorescence-based method to precisely discriminate cells that are in the different lung compartments (vasculature lumen, parenchyma and BAS) called differential *in vivo* labelling (IDEAL). This method is based on the i.v. administration of a CD45.2 FITC antibody to mark cells in the blood vascular lumen, and of CD45.2 AF647 antibody i.t. to mark cells in the BAS. For this, mice were anesthetized i.p. with Rompun (10mg/kg) and Ketamine (80mg/kg) and injected i.v. with 200 $\mu$ l PBS containing 5 $\mu$ g of fluorochrome-labeled antibody as previously described<sup>202</sup>. After exactly 5 min, heparinized blood was taken from the lower aorta/vena cava to serve as a positive control for i.v. labelling. To eliminate excess of i.v. administered antibody from the lung circulation, mice were perfused (0,73ml/min) through the right ventricle with PBS for 5 minutes with perfusate eliminated through the lower aorta/vena cava. Cells located in the BAS were then stained by administering 1ml PBS containing 5 $\mu$ g of fluorochrome-labeled antibody intratracheally as indicated in section 4.2.3.3 and incubated for 5 minutes. The antibody solution was then aspirated off and the BAS washed 3 times with 1ml PBS/2mM EDTA to remove excess of antibody. All BALF washes were pooled in 50ml i.c. PBS to stop further staining. BAL and PBL samples were used as an internal control to confirm staining of cells located in the respective compartments.

Cells were stained *ex vivo* with an anti-CD45 antibody labelled with a different fluorochrome. Leukocytes in the lumen of blood vessels were identified as CD45<sup>+</sup> CD45.2 FITC<sup>+</sup> CD45.2 AF647<sup>-</sup>; interstitial leukocytes as CD45<sup>+</sup> CD45.2 FITC<sup>-</sup> CD45.2 AF647<sup>-</sup>, and leukocytes in the BAS as CD45<sup>+</sup> CD45.2 FITC<sup>-</sup> CD45.2 AF647<sup>+</sup>.

Differential *in vivo* labelling was used in sections 4.2.9, 4.2.10 and 4.2.11.

## 4.2.5. Isolation of primary cells

### 4.2.5.1. Bronchoalveolar lavage

BALF was taken as previously described<sup>199</sup>. Briefly, mice were killed by i.p. administration of 200µl PBS containing 200mg/kg body weight of Ketamin and the tracheas were exposed by removing skin, and muscles around the neck area. Tracheas were cannulated with a polyethylene tubing (0.58mm in diameter, ca. 2cm length) fitted into a 1 ml syringe equipped with a 22G needle taking care of not reaching the carina. Bronchoalveolar lavage (BAL) was performed by washing 3 times with 1ml PBS containing 2mM EDTA at room temperature (RT). Collected BALF was then centrifuged at 1200rpm for 10 minutes at 4°C, resuspended in the desired medium and shortly kept at 4 °C until further use. Most of the cellularity was recovered in the first two washes. Less than approximately 1 % of the total cellularity was recovered in subsequent washes (data not shown).

### 4.2.5.2. Lung

Lung single-cell suspensions were performed as previously described<sup>199</sup>. Briefly, mice were killed by i.p. administration of 200µl PBS containing 200mg/kg body weight of Ketamin followed by exsanguination by cutting the lower aorta/vena cava. Lungs were dissected out taking care of not collecting the mediastinal LNs. Dissected lungs were injected with 1ml of digestion buffer and subsequently disrupted using forceps as previously described. Disrupted tissue was incubated for 30 minutes in a water bath at 37°C and pipetted every 10 minutes to ensure proper tissue digestion. Upon digestion, cell suspensions were filtered through a 100µm cell strainer and centrifuged at 1200rpm for 10 minutes at 4°C and washed with ice-cold PBS twice before resuspending in the desired medium. Cell suspensions were shortly kept on ice until further use.



#### 4.2.5.3. Spleen and Lymph nodes

Dissected spleen and mediastinal lymph nodes were collected in 2 ml ice-cold PBS and passed through a 100µm cell strainer. Cell suspensions were centrifuged at 1200rpm for 10 minutes at 4°C and resuspended in the desired medium. If required, spleen cell suspensions were filtered again through a cell strainer. Samples were shortly kept at 4°C until further use.

#### 4.2.5.4. Peripheral blood

Peripheral blood was collected from the lower aorta/vena cava using heparinized capillaries and placed in 1.5ml microcentrifuge tubes. Heparinized blood was lysed with 1ml RBC lysis buffer for 7 minutes at RT, centrifuged in a 24 table-top centrifuge at 4500rpm for 4 minutes at 4°C. Cells were washed twice with 1ml ice-cold PBS, resuspended in the desired medium, and kept on ice until further use.

#### 4.2.5.5. Cell counting

Ten microliters of a cell suspension in 0.2% Trypan Blue was counted in a Neubauer chamber as indicated by manufacturer.

### **4.2.6. Adoptive CD8 T cell transfer**

CD8 T cells were positively isolated by MACS using Miltenyi's CD8 microbeads following manufacturer's protocol. Briefly, spleen cell suspensions were incubated with MACS Buffer containing CD8 microbeads for 15 minutes on ice. Samples were washed with MACS Buffer, resuspended in 2ml MACS Buffer and passed through a pre-washed LS column on a MidiMACS magnet. Columns were then washed 3 times with MACS Buffer and the CD8 T cell-enriched fraction recovered by plunging MACS buffer into the column away from the magnet. Cells were washed twice with i.c. MACS Buffer and resuspended in ice-cold PBS.  $5 \times 10^4$  to  $5 \times 10^5$  CD8 T cells were injected into the mouse tail vein in 200µl of PBS. A purity of 85% live CD8 T cells was generally achieved (not shown).

## **4.2.7. Flow cytometry**

### **4.2.7.1. Staining of surface antigen**

Up to  $2 \times 10^6$  cells per well were surfaced stained in 96-U-bottom plates in 50  $\mu$ l of FACS blocking buffer containing saturating amounts of fluorochrome-labelled antibodies. After 20min on ice, cells were washed twice with FACS Buffer before being resuspended in 200  $\mu$ l FACS Buffer containing either 250ng/ml propidium iodide (PI) or 100ng/ml Hoechst 33258 as viability dyes. In some experiments, cells were incubated with 2.5  $\mu$ l of K<sup>b</sup>/ SIINFEKL-dextramer in 50  $\mu$ l PBS containing 5% FCS during 20min at 4°C before staining with surface antigens.

### **4.2.7.2. Staining of intracellular antigen**

Following surface antigen staining, cells were stained with PBS containing Fixable Viability Dye eFluor 780. Cells were then fixed by BD Biosciences Fixation/permeabilization buffer for 30 minutes on ice. Cells were subsequently washed twice in PBS and stained in 50  $\mu$ l of Fix/perm including saturated amounts of fluorochrome-labelled antibodies targeting intracellular antigen during 45 minutes on ice. Finally, cells were washed 3 times in Fix/Perm buffer and resuspended in 100  $\mu$ l of FACS Buffer.

Cells were acquired on a FACS Canto II or LSR Fortessa using FACSDiva version 8.0 and analyzed using FlowJo v10.

## **4.2.8. Assessment of TCR affinity**

### **4.2.8.1. Dextramer binding decay**

Cells isolated from spleen and mLN were pooled per group at a concentration of  $2 \times 10^6$  cells per ml and  $5 \times 10^5$  cells plated in each well of 96-U well plates. Following surface staining, decreasing amounts of dextramer were used, starting at 2,5  $\mu$ l of dextramer and performing  $\frac{1}{2}$  dilutions until  $2,4 \times 10^{-3}$ . Column 12 was a blank control. After 20 minutes incubation on ice, cells were washed in ice-cold FACS buffer and resuspended

in 150µl ice-cold FACS buffer containing Hoechst viability dye. Cells were acquired immediately by flow cytometry to minimize detachment of the bound dextramers.

#### 4.2.8.2. IFN $\gamma$ production after peptide restimulation

Cells isolated from spleen and mLN were pooled in full medium and adjusted at  $2 \times 10^6$  cells/ml.  $5 \times 10^5$  cells were then plated into each well of 96-U well plates. 200µl of full medium containing Golgi Plug (Brefeldin A) and Golgi stop (Monesin) were added to each well at a final dilution of 1/500 and 1/750 respectively. Finally, 40µl of serially-diluted influenza virus-derived CTL epitopes<sup>204</sup> in full medium were added to the cultures to reach a total volume of 200µl per well. Cells were then spun at 1000rpm for 2 minutes and incubated for 5h at 37°C in a humidified 5% CO<sub>2</sub> incubator. Cells were then washed twice in PBS and stained for viability, surface antigens and intracellular IFN $\gamma$  as indicated in 4.2.5.

#### **4.2.9. Confocal Microscopy**

Vibratome lung slices were analyzed by confocal microscopy as previously described<sup>199</sup>. Briefly, mice were killed by i.p. administration of 200µl PBS containing 200mg/kg body weight of Ketamin and the tracheas intubated as indicated in section 4.2.3.3. Following exposure of the lungs by opening the thoracic cavity, lungs were immediately filled with 1 ml 2% low melting point agarose at 37°C. Lungs were kept in the inspiration phase, removed and placed in ice-cold PBS on ice for a maximum of 1h. Selected lung lobes were embedded in 4% low-melting agarose and cut in 150µm slices using a vibratome set at 5.5mm/s and a vibrating frequency of 100Hz. Unfixed slices were mounted on glass slides with PBS containing 0.5µg/ml DAPI, covered with a coverslip and sealed with nail polish. Mounted slides were kept in the fridge until analysis by confocal microscopy within 5h. Images were acquired with Zeiss Zen Black edition and analyzed with Imaris v.7 software.

## 4.2.10. Cytotoxicity assays

### 4.2.10.1. In vitro quantification of antigen-specific CD8 T cell cytotoxicity

The influenza-specific cytolytic capacity of CTLs located in each of the different lung compartments was quantified using an *ex vivo* cytotoxicity assay in which effector CTLs (E) recovered from different compartments were mixed with peptide-pulsed target splenocytes (T).

To obtain effector CTLs, naïve B6 received  $5 \times 10^3$  CD45.1 OT-I *i.v.* one day before *i.t.* infection with  $2.75 \times 10^5$  p.f.u. A/WSN/33 (WSN)-OVAI influenza virus. *In vivo* differential labelling using anti-CD45.2 antibodies was performed as described in section 4.2.4. Lungs were then harvested and single-cell suspensions obtained as described in section 4.2.5.2. Cell suspension was stained with CD45 and CD8 antibodies and viable OT-I CTLs from each lung compartment were recovered by flow cytometric sorting using a FACS Aria III. Sorted CTLs (purity ca. 98% not shown) were resuspended at  $2 \times 10^5$  cells/ml in full medium.

Target cells comprised of naïve splenocytes that were pulsed for 15 minutes at 37°C with 1µM of SIINFEKL peptide. Pulsed target cells were then labeled with 1.5µM CFSE or eFluor647 cell dye for 15 minutes at RT (Fluorochrome<sup>hi</sup>). Control splenocytes that were not peptide-pulsed were labeled with 0.075µM CFSE or eFluor647 (Fluorochrome<sup>lo</sup>), respectively. Staining of targets was stopped by adding ice-cold PBS containing 10% FCS and washed twice in ice cold PBS. Control and target cells were then mixed at a 1:1 ratio. Effector cells were titrated in a 96-well V-plate along a constant number of  $2 \times 10^4$  target cells per well to achieve the required E:T ratio (from 0.03125 to 2 effectors per target). After 5h incubation at 37°C in a humidified 5% CO<sub>2</sub> incubator, cells were resuspended in FACS buffer containing PI for viability. The K<sup>b</sup>/SIINFEKL-specific cytotoxic capacity was calculated as follows by gating on live PI<sup>-</sup> target cells:

$$100 - \left( \frac{100 \times \left( \frac{\% \text{Fluorochrome high}}{\% \text{Fluorochrome low}} \right) \text{with } T}{\left( \frac{\% \text{Fluorochrome high}}{\% \text{Fluorochrome low}} \right) \text{without } T} \right)$$

#### 4.2.10.2. In vivo of antigen-specific CD8 T cell cytotoxicity

*In vivo* antigen-specific CTL assay was performed to assess the cytolytic capacity of antigen-specific CD8 T cells following as previously described<sup>205</sup>. Effector mice were naïve B6 that received  $5 \times 10^3$  CD45.1 OT-I i.v. one day before i.t. infection with  $2.75 \times 10^5$  p.f.u. A/WSN/33 (WSN)-OVAI influenza virus. Target cells comprised of naïve splenocytes pulsed for 15 minutes at 37°C with 1µM of the peptide of interest, either SIINFEKL or NP366-374 peptide. Target splenocytes were then labeled with 1µM CFSE or eFluor647 cell dye for 15 minutes at RT (Fluorochrome<sup>hi</sup>). Control splenocytes not pulsed with peptide were labeled with 0.1µM CFSE or eFluor647 cell dye (Fluorochrome<sup>lo</sup>). Staining was stopped by adding PBS containing 10% FCS and washed twice in ice cold DPBS. Control and target cells were then mixed 1:1. To quantify the kill in the mLN and spleen effector mice received a total of  $2 \times 10^7$  cells i.v.. On the other hand, to quantify the kill in the BAS, effector mice received  $1.2 \times 10^6$  cells i.t.. 4h later mLN, spleen, skin-draining Lymph nodes and BAL were sampled, and targets analyzed by flow cytometry. Antigen-specific CTL cytolytic activity was calculated as following:

$$100 - \left( \frac{100 \times \left( \frac{\%Fluorochrome\ high}{\%Fluorochrome\ low} \right)_{infected}}{\left( \frac{\%Fluorochrome\ high}{\%Fluorochrome\ low} \right)_{not\ infected}} \right)$$

#### 4.2.11. **Quantification of influenza viral titers**

Influenza viral titers were measured by a standard plaque assay as previously described<sup>206</sup>. MDCK cells from ATCC (Manassas, VA, USA) were grown in DMEM containing 10%FCS, 5% L-Glutamine and 5% penicillin/streptavidin to 90% confluency. Cells were then trypsinized and different cell concentrations plated in triplicate in 6- or 12- well plates. Plates that reached a confluency of about 90% 24h later were chosen for infection with lung homogenates from infected mice.

Upon collection, lungs were snap frozen and placed in 2ml tubes containing ceramic bead and then homogenized using a tissue homogenizer. 1ml lung homogenates were first diluted 1:5000 and then 4 successive 1/10 dilutions in MEM containing 0.3% BSA fraction V and 1µl/ml TPCK trypsin. MDCK cells were washed in PBS and then infected by incubating with 250µl or 500µl of the lung homogenate in

12- or 6-well plates, respectively, for 1h at 37°C and 5% CO<sub>2</sub>. Plates carefully rocked every 20 minutes. After incubation, plates were carefully washed twice with PBS. Wells were then carefully covered with 0.3% agarose in MEM-BSA-TPCK pre-warmed at 37°C. Plates were left at room temperature for 10 minutes to allow for the agarose to solidify and then carefully moved into a humidified incubator at 37°C and 5% CO<sub>2</sub>. When plaques became evident by microscopy (2-3 days post infection), cells were fixed by adding 1 or 2 ml 4% PFA on top of the agarose overlay for 1h at room temperature. Plates were then gently washed under running tap water to remove the agarose overlay and stained in 0.5% crystal violet solution for 15-20 minutes. After intensive washing in running tap water, plates were left to dry over 24h and plaques counted by naked eye or with the help of a dissecting microscope. To calculate PFU per milliliter (PFU/ml), the following equation was used:

$$\text{PFU/ml} = \frac{\text{Average \# of plaques}}{\text{Dilution Factor} * \text{volume of diluted virus added to the well}}$$

#### **4.2.12. Gene expression analysis**

##### **4.2.12.1. Single-cell RT-PCR**

5x10<sup>3</sup> CD8 OT-I T cells were transferred i.v. into naïve B6 mice and 1 day later 2.75x10<sup>5</sup> PFU WSN-S8L were administered i.t.. Mice were then sampled at day 6 post infection and lung cell suspensions were prepared as indicated in 4.2.2 and from this point onwards, kept on ice at all times and processed as quickly as possible. Single CD8 T cells from each lung compartment were sorted as indicated in 4.2.10.1 into 0,5ml PCR strips containing 5 µl of PBS and kept in dry ice until stored at -80°C. Cells were then lysed in the PCR thermocycler by exposing them to 65°C for 2 minutes moving them to ice as soon as possible. Immediately after lysis, 10 µl of RT mix was added to each tube. RT was performed by a cycle of 37°C for 60 min, followed by 3 min at 90°C and maintenance at 10°C. Samples were then stored at -80°C until further use. A 1<sup>st</sup> multiplex PCR was then performed by adding the desired primers in PCR mix. The amount of water was adjusted depending on the number of primers, having a final volume of 85µl. The PCR cycle was as follows:

1st PCR program		
95°C	10 min	Hold
94°C	45 sec	15x
60°C	1 min.	
72°C	1 min 30 sec	
72°C	10 min.	Hold

For the final qualitative PCR, a PCR with the respective primers was performed per each gene of interest. Each qualitative PCR followed the following cycle:

2nd PCR program		
95°C	10 min	Hold
94°C	30 sec	2x
70°C	45 sec	
72 °C	1 min	
94°C	30 sec	2x
66°C	45 sec	
72°C	1 min	
94°C	30 sec	2x
62°C	45 sec	
72°C	1 min	
94°C	30 sec	48x
60°C	45 sec	
72°C	1 min	
72°C	10 min.	Hold

#### 4.2.12.2. Gene expression analysis

5x10<sup>3</sup> CD8 OT-I T cells were transferred i.v. into naïve B6 mice and 1 day later 2.75x10<sup>5</sup> PFU WSN-S8L were administered i.t.. Mice were then sampled at day 6 post infection. 5x10<sup>4</sup> CD8 OT-I T cells from each lung compartment were sorted as indicated in 4.2.10.1 and lysed by vortexing in 150 µl RLT buffer for 1 min followed by centrifugation at 5000rpm in a perfect spin 24 table-top centrifuge for 1 min to recover all material to bottom of tube. Cell lysates were then analyzed as per manufacturer's protocol using an nCounter Mouse Inflammation Gene Expression CodeSet. Analysis was done using nSolver Analysis Software (Nanostring). A cutoff of 100 counts was used as per manufacturer's suggestion and the following housekeeping genes were used as controls: Alas1, Eef1g, G6pdx, Gapdh, Gusb, Hprt, Oaz1, Polr1b, Polr2a, Ppia, Rpl19, Sdha, Tbp, Tubb5.

#### **4.2.13. Statistical analysis**

Raw data was processed using Office Excel v14.0 (Microsoft) and statistical significance was investigated in Prism v7 (GraphPad). Two-tailed unpaired Student's *t*-test was used to compare two groups. To compare three or more groups, one-way ANOVA with a Bonferroni post-test was used. Statistical significance was set at  $P < 0.05$ .



## 5. Results

The role of the exact CD8 T cell positioning in the lung for protection against infection with influenza or other viruses is unresolved. In addition, there is still a lack of knowledge on the mechanisms driving CD8 T cells into the lung environment upon infection as well as the exact way CTLs confer protection. Knowing the mechanisms driving CTL positioning into the lung environment and the mechanisms that are used would open the possibilities of modulating them to further protect the host or reduce immunopathology.

### 5.1. CD8 T cell migration and killing capacity in the lung environment

#### 5.1.1. Development of a flow cytometric method to accurately quantify immune cell infiltration in specific lung compartments

Upon inflammation, Immune cells migrate from the blood into different anatomical compartments of the lung -interstitium and BAS. It is currently unknown whether immune cells at different locations have different phenotype and function, and whether they have differential roles in viral clearance. In the lung, immune cells transmigrate from the vasculature into the interstitium and some of them will further translocate through the epithelial cell layer into the BAS. Most influenza strains only infect bronchiolar and alveolar epithelial cells, hence, for immune cells to directly interact with infected epithelial cells they need to either reach the BAS or, at least, cross the basal membrane separating endothelial from epithelial cells (Figure 1).

To investigate the role of immune cell positioning within the different lung compartments, it is necessary to unambiguously identify the precise location of immune cells within the inflamed lung. The standard method (here referred to as “classic method”) for sampling immune cells in different lung compartments does not allow the study of immune cell positioning and is based on 3 steps (Figure 2A): , (1) mice undergo intracardial perfusion to eliminate immune cells in the circulation; (2) bronchoalveolar lavage is performed to collect immune cells present in the BAS; (3) finally, the post-perfusion, post-BAL lung is taken as a source of interstitial immune cells (i.e. extravascular cells not present in the BAS). The accuracy of this protocol is

based on two assumptions: first, i.v. perfusion removes all intravascular immune cells and, second, that BAL recovers all immune cells located in the BAS. However, a significant fraction of intravascular immune cells remain even after prolonged perfusion of the steady-state lung<sup>153</sup>. It is likely that this is even more pronounced during inflammation, when perfusion is less efficient. In addition, a significant fraction of alveolar macrophages (a type of macrophages only present in the alveolar lumen) is commonly found within the post-perfused, post-BAL lung sample, demonstrating that BAL is inefficient in the recovery of immune cells from the lung airways. As a result, immune cells recovered from the post-perfused, post-BAL lung contain a mixture of cells contained in the intravascular, interstitial and bronchoalveolar compartments.

To overcome the limitations of the classic method, I developed a method called *in vivo* differential labelling (IDEAL) consisting of intravascular staining of leukocytes as previously described<sup>153</sup> and, in addition, intra-tracheal staining of leukocytes to effectively mark all leukocytes within the BAS (Figure 2B). By using IDEAL, all AlvM remaining in the post-perfused, post-BAL lung were indeed identified as cells in the BAS (Figure 2C and D). However, using the classical method, about 90% of total AMs were present in the post-perfused, post-BAL lung as interstitial cells (Figure 2 C and D). These results demonstrate that the classic method is not suitable to differentiate cells between the lung interstitium and the BAS and that the IDEAL method here describe is able to do so.

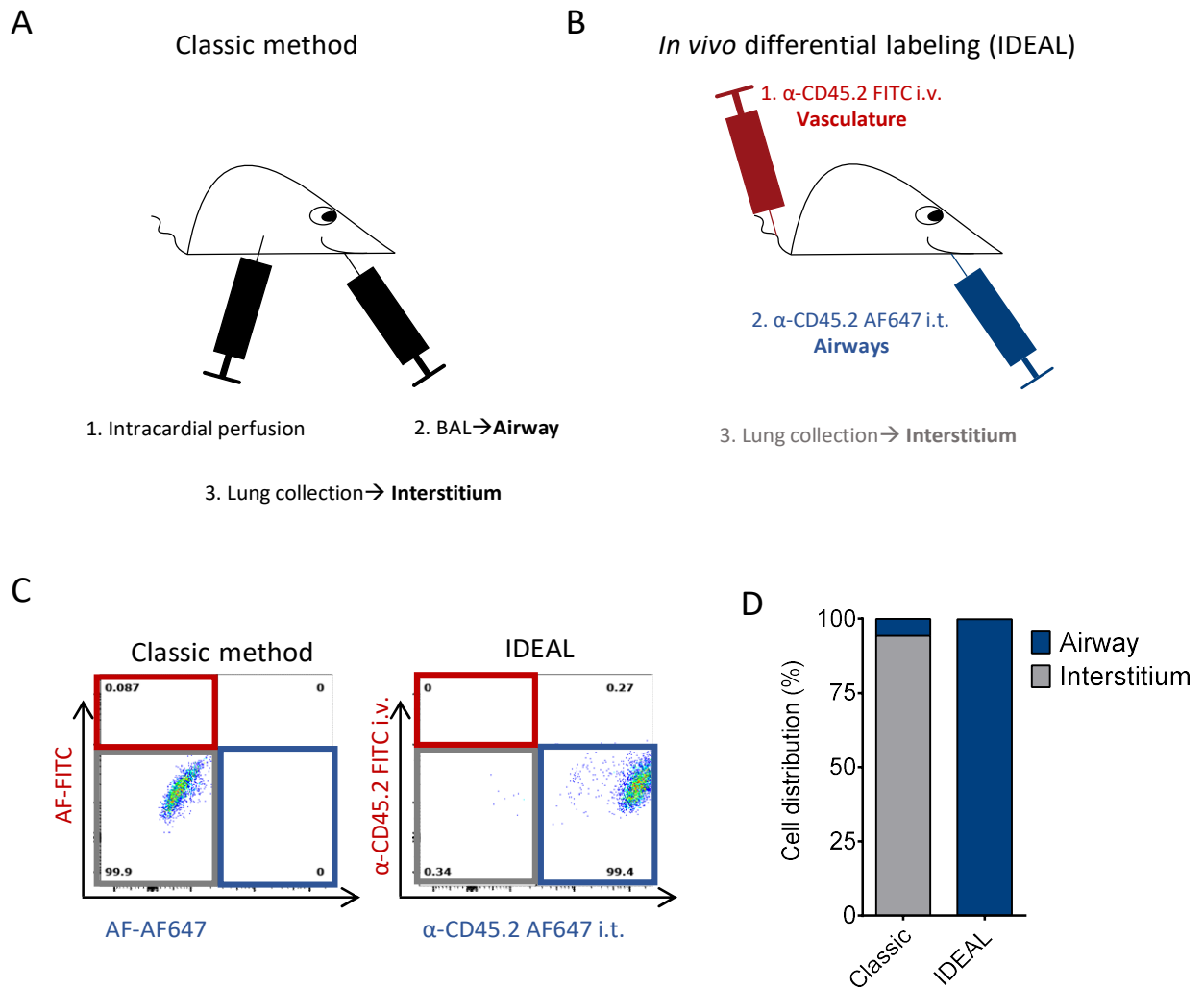


**Figure 2. Differential labeling (IDEAL) allows for accurate analysis of immune cell localization within the lung environment. (A)** Illustration depicting the classic method of lung analysis. In brief, (1) mice undergo intracardial perfusion to eliminate cells present within the vasculature. (2) Bronchoalveolar lavage is performed through a tracheotomy to collect cells within the BAS. (3) Lungs are collected and digested to isolate interstitial cells. **(B)** Illustration depicting the differential labeling protocol of lung analysis. In brief, (1)  $\alpha$ -CD45.2-FITC is administered through the tail vein to mark all cells in the vasculature. Mice vasculature is then perfused to eliminate excess of intravascular antibody. (2)  $\alpha$ -CD45.2-AF647 is then administered intratracheally. BAL is then conducted to wash excess antibody in the airways. (3) Finally, lungs are sampled. **(C)** Representative dot-plots of AlV<sub>M</sub> in the post-perfused, post-BAL lung sample in the steady state after classic method sampling (Left panel) and differential labelling (right panel). **(D)** Alveolar macrophage distribution as analyzed by classic method (Left column) or differential labeling (right column). To quantify airway AMs, counts obtained from lung and from BAL were added. Note that the classic method does not use anti-CD45 antibodies i.v. or i.t.. AF, autofluorescence. Shown are results from a representative of at least 5 independent experiments with 3 mice per group.

I employed the IDEAL method to quantify immune cell subpopulations at the different lung compartments during the acute phase of influenza infection. CD8 T cells are important players during immune responses against viral pathogens. Mice were infected i.t. with  $5 \times 10^3$  PFU of influenza PR8 and sampled at the peak of CTL response (day 7 post infection) (Figure 3A). CD8 T cells in the three different lung compartments could be clearly detected during influenza infection. (Figure 3B). About half of the CD8 T cells localized within the lung interstitium (Figure 3C). The remaining half distributed similarly between the vasculature lumen and the airways (Figure 3C). Only activated or memory CTLs can transmigrate into inflamed organs. Using IDEAL, I could clearly demonstrate that basically all CD8 T cells within the interstitium and airways were CD44<sup>hi</sup>, while CTLs in the vascular compartment were either CD44<sup>-low</sup> (likely naïve) or CD44<sup>hi</sup> (Figure 3D). Of note, CD44<sup>-lo</sup> CD8 T cells would be wrongly identified using the classic method as being interstitial cells.

Neutrophils mediate rapid defence against invading microorganisms but they may also induce significant immunopathology in the lung during influenza infection<sup>207</sup>. Surprisingly, most of the neutrophils located intravascularly, while only around 30% of them transmigrated into the lung tissue (Figure 3D and F).

These results demonstrate that the IDEAL protocol is a robust method for precisely identifying and quantifying immune cells at different lung compartments in the steady state and during infection, opening the opportunity to investigate the relevance of T cell localization in the lung to clear influenza infection.

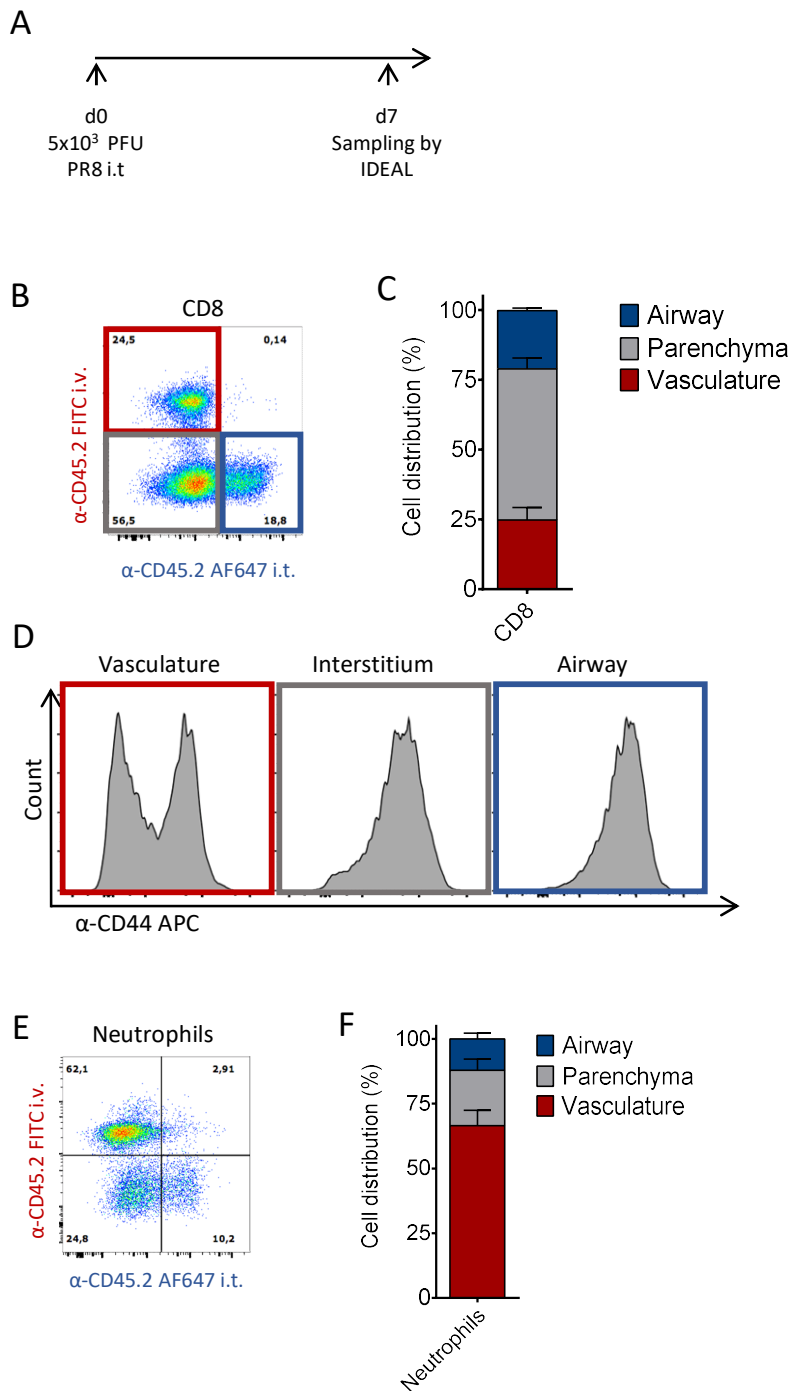


**Figure 3. IDEAL protocol shows that only activated CD8 T cells egress into the lung while neutrophils are mostly present within the vasculature during influenza infection. (A)** Illustration depicting experimental setup **(B)** Representative flow cytometry dot-plot of CD8 T cell distribution in lung sample as analyzed by IDEAL. **(C)** Quantification of CD8 T cell distribution in the infected lung. **(D)** CD44 expression in CD8 T cells at different lung locations. **(E)** Representative flow cytometry dot-plot of neutrophil distribution in influenza-infected lungs. **(F)** Quantification of Neutrophil distribution in the infected lung. Shown are results from a representative of at least 5 independent experiments with 3 mice per group.

### **5.1.2. Activated CTLs are not imprinted to specifically migrate into a unique lung compartment**

It is established the CTLs migrate into the different lung compartments (Figure 3A)<sup>208</sup>. However, the mechanisms driving retention of CTLs into the interstitium or further migration into the BAS remain unclear. Cxcr3 expression on CD8 T cells promotes egression from the vasculature into the influenza-infected lung<sup>209</sup>. However, Cxcr3 was not required for further migration into the BAS.

Two working models may explain migration of CD8 T cells within the infected lung. In one model, upon egression from the vasculature, the same CD8 T cell may indistinctively migrate between the thin alveolar interstitium and the alveolar space following chemokine cues. Alternatively, different cues may preferentially position some CTLs in the interstitial space while others further migrate into the BAS depending on the receptors they express. To investigate whether different CD8 T cells preferentially migrate to specific lung compartments, I performed serial transfers of influenza-specific CD8 T cells combined with IDEAL to precisely identify their location. Naive tdTomato<sup>+</sup> OT-I CD8 T cells were initially transferred into mice that were subsequently infected with WSN-S8L (Figure 4A). Seven days later, effector OT-I CTLs isolated from each lung compartment (intravascular, interstitial and in the airway lumen as identified by IDEAL) (Figure 4B) were re-transferred at equal ratios into WSN-S8L-infected mice (Figure 4C). The precise location 5h after re-transfer was then identified by a second round of IDEAL using a different set of fluorochromes (Figure 4C). By comparing the origin of the transferred cells (first IDEAL staining) and the destination of the re-transferred cells (second IDEAL staining), I could quantify whether cells originated from a specific compartment were more likely to migrate to that compartment, indicating preferential migration, or not.

The re-transferred CTLs showed a similar pattern of migration into the three different lung compartments independently of the compartment from which they originated before re-transfer (Figure 4E and F). Independently of whether CTLs originated from the vascular lumen, interstitium or airways, they migrated to those three compartments upon retransfer with similar frequencies. The results indicate that different CTLs do not have a preferential migration into the compartments studied here, and suggest that

they follow adhesion and chemotactic cues to indistinctively locate into the lung interstitium or BAS. Further experiments are required to investigate whether the BAS is inherently the final destination of CTLs in the influenza-infected lung, or whether specific niches retain CTLs in either compartment.

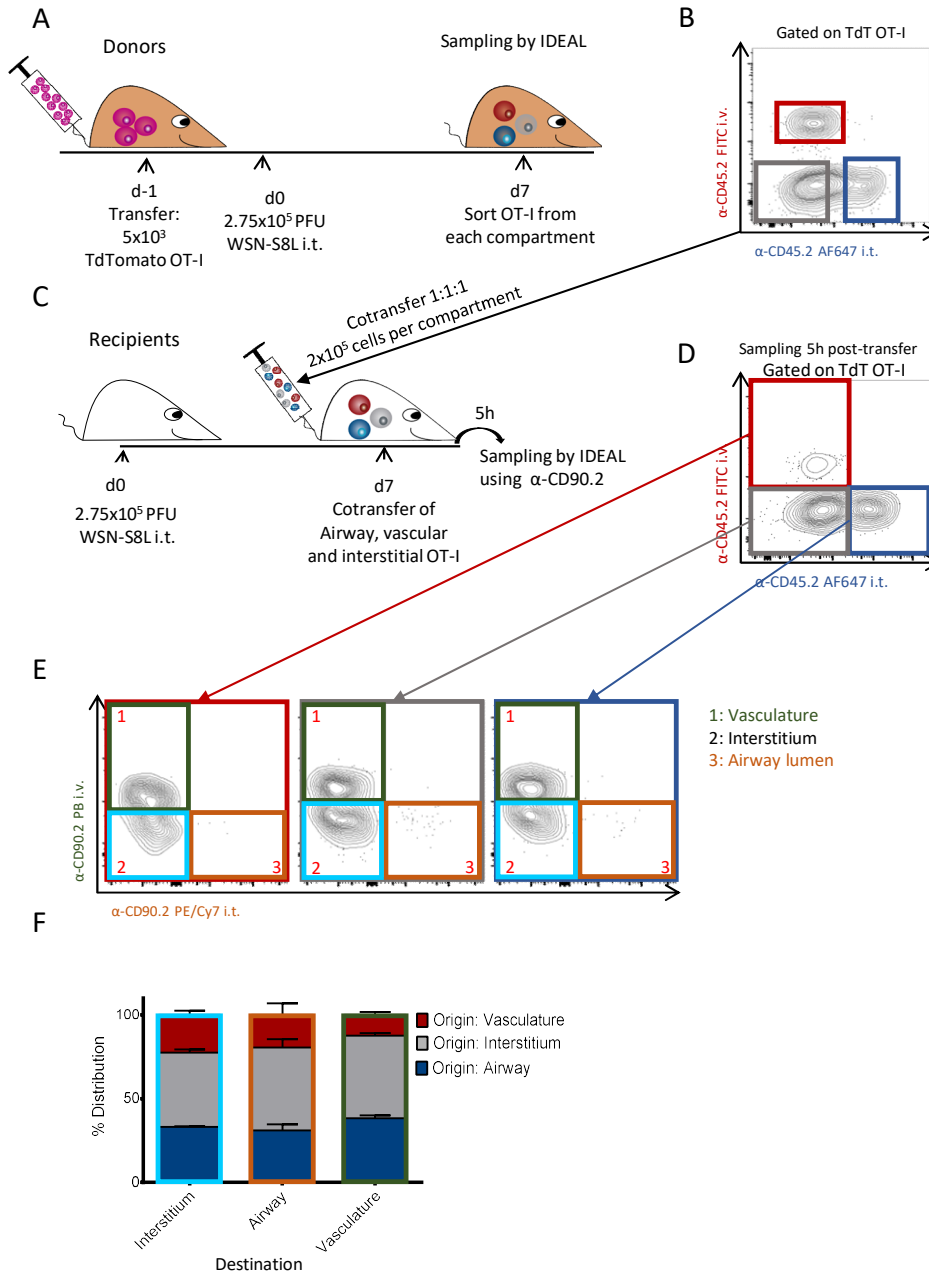


**Figure 4. Activated antigen specific CD8 T cells freely distribute through lung compartments.** (A) Illustration depicting experimental setup of *in vivo* activation of naive OT-I T cells. (B) Flow cytometry dot plot with gates set up for FACS sorting of TdTomato<sup>+</sup> OT-I CD8 T cells present in the vascular lumen (red gate), interstitium (grey gate) and airway lumen (blue gate). (C) Illustration depicting experimental setup of recipient mice co-transferred with cells from (B). 5 hours post transfer, mice were sampled by IDEAL with  $\alpha$ -CD90.2 PB i.v. and  $\alpha$ -CD90.2 PE/Cy7. (D) Representative flow cytometry dot-plot showing origin (Vasculature (red), interstitium (grey) and airway (blue)) of recovered TdTomato<sup>+</sup> OT-I cells in the lung of recipient mice 5 h after cotransfer. Note that most of the re-transferred cells egressed from the vasculature. (E) Representative flow cytometry dot-plots indicating the location of the re-transferred OT-I CD8 T cells that were originally sorted from the intra-vascular lumen (left panel), interstitium (Middle panel) or airway lumen (Right panel). (F) Final distribution of cells from Vasculature (red), interstitium (grey) and airway (blue) of recovered TdTomato<sup>+</sup> OT-I cells in the lung of recipient mice 5 h after cotransfer. Shown are results from a representative of at least 2 independent experiments with 4 mice per group.



### 5.1.3. Interstitial and BAS CTLs show similar transcriptomic profiles

As demonstrated in Section 1.3, activated CTLs do not show preferential migration into a specific pulmonary compartment in the influenza-infected lung. Nevertheless, compartment-specific cues may induce defined transcriptional and functional CTL signatures. To investigate effects of potential compartment-specific cues on CTL cell function, I analyzed mRNA expression of candidate genes in bulk and single OT-I CD8 T cells sorted from each compartment (Figure 5A). Naïve OT-I T cells from spleen were isolated from TdTomato<sup>+</sup> mice and subsequently transferred  $5 \times 10^3$  cells into naïve BL6 mice i.v. 1 day later mice were infected with  $2.75 \times 10^5$  PFU WSN-S8L i.t.. 6 days after infection, lungs from infected mice were sampled by IDEAL and OT-I T cells were sorted from each lung compartment for either bulk or single cell analysis. Bulk analysis was performed with the Nanostring system (Immunology panel for mice) by analyzing a total of 576 genes included in the nCounter Mouse Inflammation Gene Expression CodeSet (Appendix 1). Of those, 258 were expressed above the detection threshold and 33 of those showed significant differences between BAS and interstitium when comparing expression ratios (Figure 5B). As expected, most differences were found between the vascular compartment and either interstitium or BAS (Figure 5B). Our results confirm previous findings that circulating CD8 T cells undergo transcriptional reprogramming once infiltrating the inflamed lung<sup>210</sup>.

Regarding transcriptional differences between CTLs that infiltrated the lung, 33 genes showed statistically significant differences between OT-I CD8 T cells located in the interstitium and BAS (Figure 5B). Higher expression of genes such as *Ifng*, *Prf1* and *Gzmb* suggest a higher antiviral activity by CTLs present in the BAS compared to that of the interstitial CD8 T cells. Although significant, the differences found on the 33 genes are minimal and may not reflect differential protein expression. Consistent with my previous results showing no differential migration between interstitial and BAS CTLs, there were no differences in the mRNA expression for chemokine receptors *cxcr3*, *ccr5* and *cxcr6* between BAS and interstitium. These results show that bulk analysis of antigen specific CTLs in the BAS and interstitium results in minimal differences between BAS and interstitium.

Despite the fact that bulk gene expression analysis did not show differences between CTLs in different lung locations, we hypothesized that single-cell analysis may identify specific CTL populations in those locations. To investigate this, I performed multiplex

single-cell RT-PCR. This technique offers the possibility to analyze whether or not a specific single cell expresses or not the genes of interest, however, it cannot quantify the level of expression. I used multiplex single-cell RT-PCR to quantify the percentage of cells expressing selected genes that are highly relevant for effector CD8 T cell differentiation, migration and function (*Ccr4*, *Ccr5*, *Ccl3*, *Ccl4*, *Ifny*, *Perf*, *Gzmb*, *T-bet*, *Eomes*, *IL-7R*, *Klrg1*, *Blimp-1* and *CD3e*). Most of the cells investigated (higher than 95%) were positive for *Cd3e*, confirming high purity of the sorted populations (Figure 5C). Most genes analyzed with multiplex single-cell RT-PCR were also above background on Nanostring analysis (*Ccr4*, *Ccr5*, *Ccl3*, *Ccl4*, *Ifny*, *Perf*, *Gzmb*, *Eomes*, *IL-7R* and *CD3e*), showing similar results between the two assays. There were no statistically significant differences in the percentage of cells expressing the selected genes that were located in the interstitium or BAS (Fig. 5C). Some genes, like *Gzmb*, were expressed by all CTLs independently of their location, while others, such as *Tbet* and *Klrg1* were expressed by less than 8% of the cells located in the lung interstitium or BAS. There were, however, statistically significant differences between influenza-specific CTLs that had or had not egressed from circulation. *Ccl3* was upregulated in a significant fraction of CTLs that had transmigrated, whereas *Eomes* followed the opposite pattern (Figure 5C). Some genes showed very homogenous expression, *GzmB* was expressed on most cells of each compartment while *Blimp1*, *Klrg1* or *Tbet* were not expressed on most of the cells. On the other hand, heterogeneous expression was found on *IL-7R*, *Eomes* or *Ccl4*. This could be explained by the fact that all sorted cells were antigen-specific, it is possible those cells were on their way into the lung tissue. Therefore, single-cell RT-PCR showed no apparent differences in gene expression between BAS and interstitial CTLs.

Taken together, these results indicate that the location of CTLs in the interstitium or BAS of influenza-infected mice does not result in general differences in gene expression.

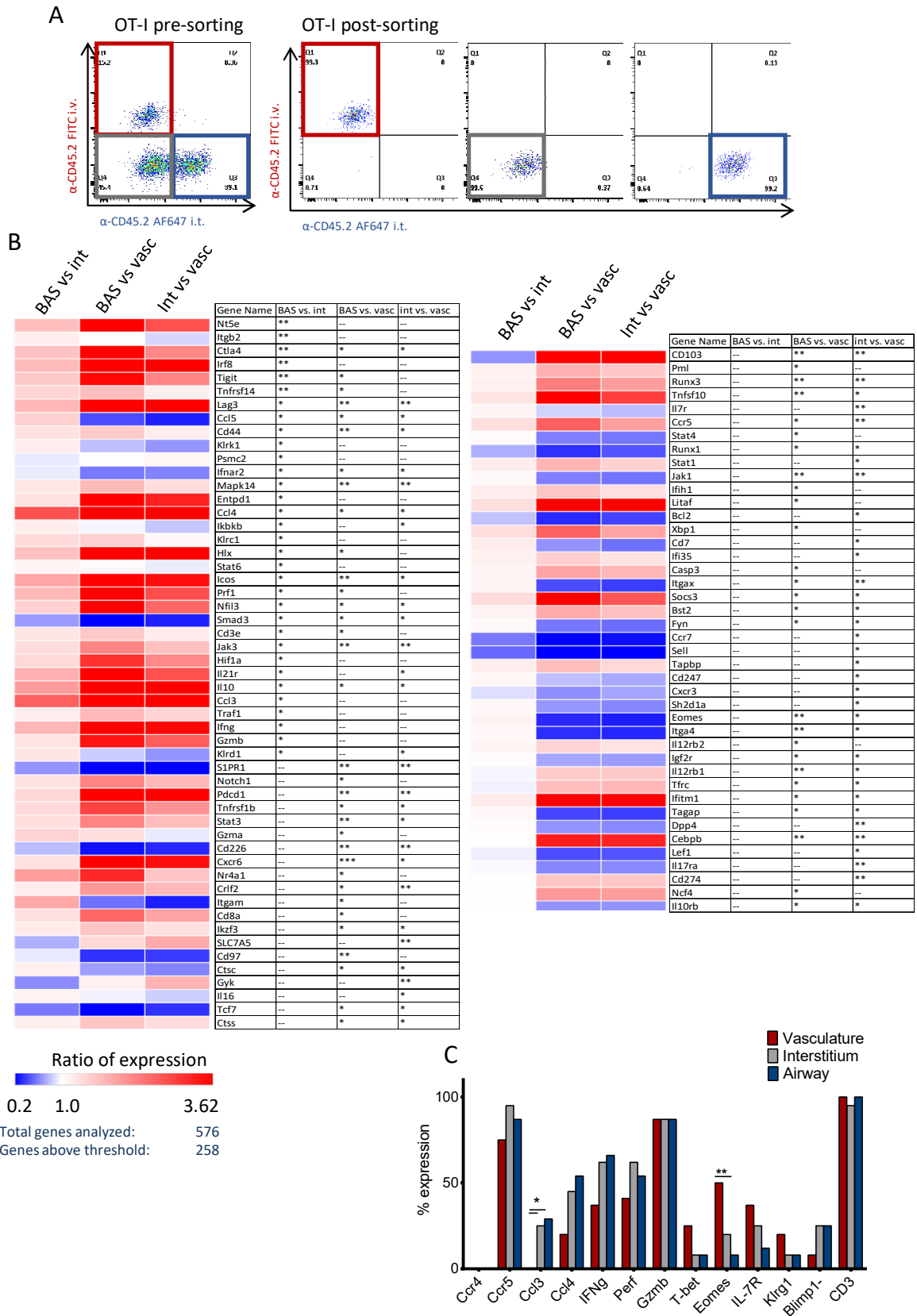


**Figure 5. Genomic analysis shows significant differences between vasculature and interstitium or BAS.**  $5 \times 10^3$  CD8 OT-I T cells were transferred i.v. into naïve B6 mice and 1 day later  $2.75 \times 10^5$  PFU WSN-S8L were administered i.t.. Mice were sampled per differential labeling at day 6 post infection and OT-I cells were sorted from each lung compartment

(Vasculature, Interstitium and Airways). **(A)** Flow cytometry dot-plot with selected gates for OT-I CD8 T cell sorting (left panel) and quality control of sorted cells from vasculature (Red gate, middle-left panel), interstitium (Grey gate, middle right panel) and airways (Blue gate, right panel) **(B)** Heatmap and table illustrating fold change in gene expression between BAS and interstitium (Left column), BAS and vasculature (Middle column) and interstitium and vasculature (Right column) of influenza-specific OT-I CD8 T cells. Only genes with statistically significant differences are shown. **(C)** Expression of chemokines, cytokines and transcription factors as measured by multiplexed single-cell RT-PCR array. Shown are results from one experiment with 3 mice. For B, Two-tailed unpaired Student's t-test was used to compare groups. For C a contingency Fisher's exact test was performed. \*,  $P < 0.05$ ; \*\*,  $P < 0.01$ ; \*\*\*,  $P < 0.001$ .

#### **5.1.4. Influenza-specific CTLs show similar killing capacity regardless of their location**

After finding only small differences in gene expression between influenza-specific CTLs in the interstitium and BAS of infected mice, I next investigated whether there are functional differences based on location. A main function of CTLs is the antigen-specific killing of infected cells following TCR engagement of MHC-I/peptide complexes. Thus, I investigated whether the ability to lyse target cells differed between CTLs located in different compartments of the influenza-infected lung.

First, I performed an *in vivo* kill assay directed against 2 MHC-I ligands from WSN-S8L to assess whether CTLs in the lung are indeed able to lyse target cells. For this, I used naïve splenocytes as target cells that were loaded with either SIINFEKL (H-2K<sup>b</sup> ligand) or NP366-374 (H-2D<sup>b</sup> ligand), or with an irrelevant peptide (KAVYNFATM). Target cells were either labelled with different concentration of CFSE or cell tracker eFluor670 to distinguish them and mixed at an equal ratio (Figure 6A). A total of  $1 \times 10^7$  cells were transferred i.v. and a total of  $6 \times 10^6$  cells were transferred i.t. into mice that had been infected with WSN-S8L 7 days earlier (Figure 6A). After 4h, the remaining target cells in mLN, spleen and BAL were quantified by flow cytometry (Figure 6C and D). Transfer of target cells i.v. allows for quantification of antigen-specific kill in those organs, whereas i.t. transfer, allows for quantification of lysis by cells in the BAS. Of note, this assay does not permit quantification of killing activity by interstitial cells because target cells do not infiltrate the lung. Killing in mediastinal Lymph node and spleen was highly efficient, with over 50% of the target cells being lysed within 4h (Figure 6C and D). As expected, control non-infected mice showed no detectable kill activity (Figure 6D). Cytotoxicity in the BAS under the conditions tested was less efficient since only 10 to

20% of target cells were killed within 4h. I observed no differences between the killing of SIINFEKL or NP366-374 -loaded targets (Figure 6D). These results demonstrate that CTLs in the airways were able to kill target cells in an antigen-specific manner, although with lower efficiency as those in secondary lymphoid organs. Reduced killing capacity in the airways may reflect a biological difference or may be due to the fact that target cells are artificially administered i.t. not efficiently becoming into contact with CTLs across the airways.

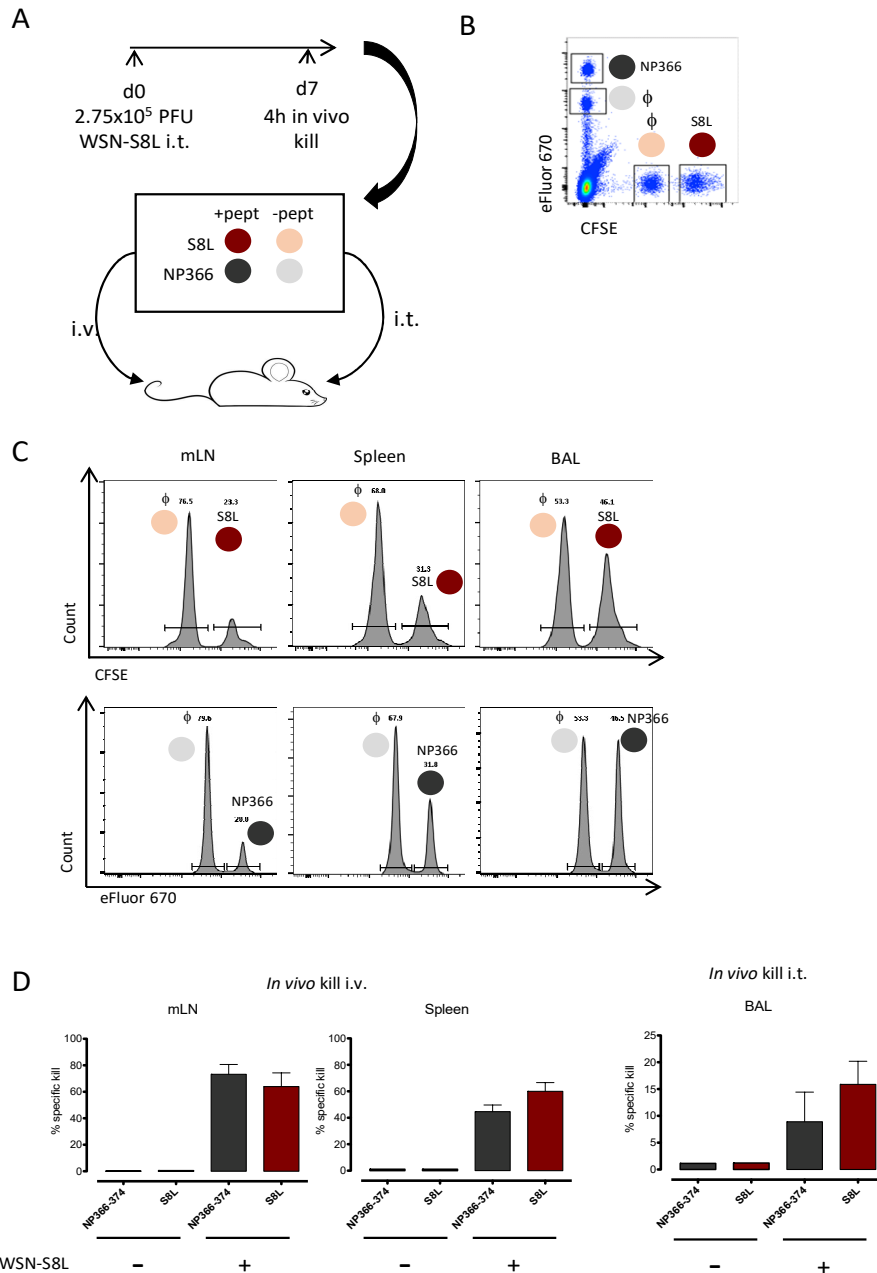


**Figure 6. CTLs show good killing capacity in BAS and high capacity in mLN and spleen.** (A) 7 days after infection mice were injected i.v. or i.t. with splenocyte targets loaded with either S8L or NP366-374 peptides. As a negative control, unloaded splenocytes were used in the same numbers. To differentiate between targets, S8L loaded splenocytes were stained with high dilution of CFSE while their respective controls were stained with a low dilution of CFSE. On the other hand, NP366-374 loaded splenocytes were stained with high dilution of eFluor670 while their respective controls were stained with a low dilution of eFluor 670. (B) Representative flow cytometry dot-plot of splenocyte targets loaded with either, NP366-374 on the y axis and S8L on the x axis. (C) Representative flow cytometry histograms of killing in mLN, spleen and BAS for both peptides. (D) percentage of specific kill for each peptide in mLN (left graph), spleen (middle graph) and BAS (right graph). Shown are results from a representative of at least 2 independent experiments with 3 mice per group.

Having established that pulmonary CTLs can kill targets, I next quantified differences in the killing ability between CTLs located in different lung compartments in an *in vitro* killing assay. For this, I transferred naïve CD45.1 OT-I CD8 T cells into CD45.2 recipients and infected them 1 day later with  $2.75 \times 10^5$  PFU WSN-S8L (Figure 7A). 7 days post infection, I performed an *in vitro* antigen-specific cytotoxicity assay using sorted OT-I cells from the three different pulmonary compartments identified by IDEAL as effector CTLs. Different numbers of CTLs were co-incubated with a constant number of target cells consisting of an equal mixture of splenocytes loaded with S8L and  $1 \mu\text{M}$  CFSE, and splenocytes loaded with an irrelevant peptide (KAVYNFATM) and  $0.1 \mu\text{M}$  CFSE. Specific kill of S8L-loded targets was measured by flow cytometry 5h later (Figure 7C). No differences in killing capacity were found between interstitial and airway CTLs. On the other hand, CTLs collected from the vasculature showed higher killing capacity at 0,5 and 2 E:T when compared to airway CTLs. In addition, CTLs present on the lung (vascular lumen, interstitium or airway lumen) had higher killing capacity compared to that of the mLN on the higher E:T. Taken together, these data shows that CTLs acquire higher activation and killing capacity when reaching the lung microenvironment compared to CTLs in the draining LNs. However, there were no differences in the cytotoxic capacity between CTLs in the interstitium and in the BAS.

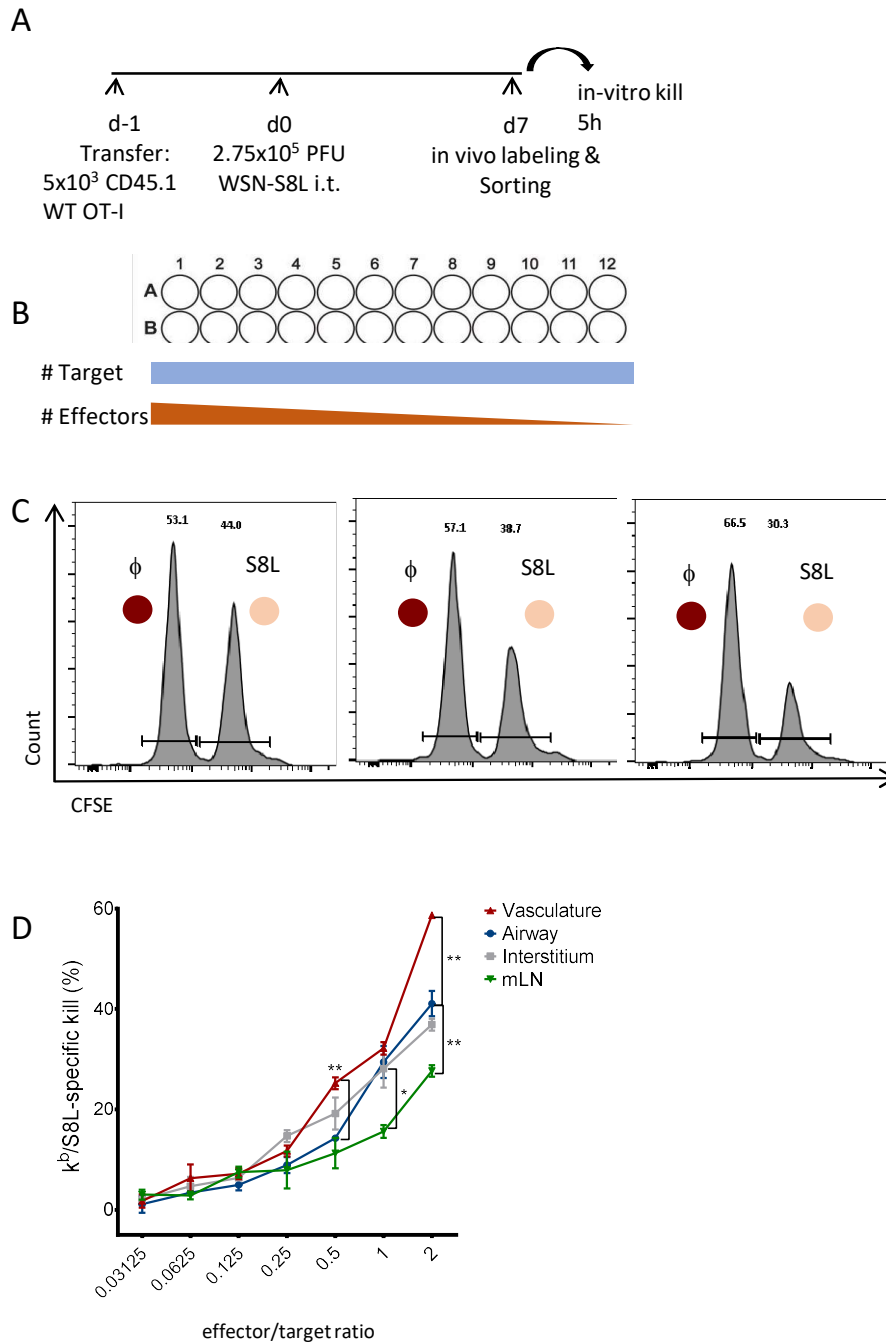


**Figure 7. Cytotoxic activity of CD8 T cells is similar across lung compartments. (A)** Cartoon depicting experimental of *in vitro* kill setup. 5x10<sup>3</sup> CD45.1 OT-I T cells were transferred into B6 mice 1-day prior i.t. 2.75x10<sup>5</sup> PFU WSN-S8L. Mice were sampled at day 7 post infection by differential labelling and CD45.1 OT-I cells sorted with FACS ARIA III. **(B)** Splenocyte targets were loaded with S8L peptide. As a negative control, unloaded splenocytes were used in a 1:1 ratio to peptide targets. To differentiate between targets, S8L loaded splenocytes were stained with high dilution of CFSE while their respective controls were stained with a low dilution of CFSE. Sorted cells were cultured with decreasing of effector to target ratios for 5h prior measurement of *in vitro* kill. **(C)** Representative flow cytometry histograms of target kill by vascular (Left panel), interstitial (middle panel) or airway (right panel) OT-I CTLs at a E:T ratio of 0.25 **(D)** K<sup>b</sup>/S8L specific kill by OT-I T cells shown as %. Shown are results from a representative of at least 2 independent experiments with 3 mice per group. \*, P < 0.05; \*\*, P < 0.01 (One-way ANOVA)



The development of a new method to analyze the lungs provided me with the opportunity to accurately study T cell positioning and its implications during influenza infection. Despite finding slight differences on their transcriptomics profiles, BAS and interstitial CTLs showed very similar behavior *in vivo* as they seem to be able to migrate to any lung compartment and their killing capacity is similar regardless of which compartment they were isolated from. Taken together these results suggest activated CD8 T cells are ready to protect as early as they reach the lung environment.

## **5.2. CD8 T cell protection during primary and secondary viral infection**

Upon influenza infection, a strong innate response will be the prelude of the adaptive response which leads to viral clearance. Within the adaptive immune response against influenza, we can distinguish between antibody producing B cells and T cell responses with CD8 and CD4 T cells<sup>208,211,212</sup>. Although CD8 T cells are thought to be an important player in viral clearance, it has been shown that in some cases CTLs might not be necessary because CD4 T cells and B cells synergize to provide protection<sup>96,98</sup>. It is thus important to determine the extent to which CD8 T cells confer protection and when they are relevant during a primary or secondary infection.

### **5.2.1. CTLs do not alter the course of disease in primary influenza infection**

During primary influenza infection, CD8 T cells differentiate into effector CTLs that then migrate into the infected lung via the blood using CXCR3<sup>209</sup>. I then aimed to assess the degree of protection provided by CD8 T cells *in vivo* as the microenvironment and easier access to infected cells could play a role in their protective capacity.

To investigate that, naïve mice were infected i.t with  $5 \times 10^3$  PFU influenza virus PR8 on day 0. In addition, CD8 T cells were depleted at day -1, 4, 9 and 14 after infection by i.p. administration of 300 µg of α-CD8α antibody (Figure 8A). Mice in control group (or control mice) were treated equally but with an isotype-matched irrelevant antibody against TNP. Efficient CD8 T cell depletion was confirmed by a virtual lack of those cells in the blood as monitored during the first 14 days after infection (Figure 8B). CD8 T cell-depleted mice were not more susceptible to infection than their isotype control counterparts as demonstrated by similar weight loss kinetics (Figure 8C), indicating that CD8 T cells were not essential in providing protection against a primary influenza infection.

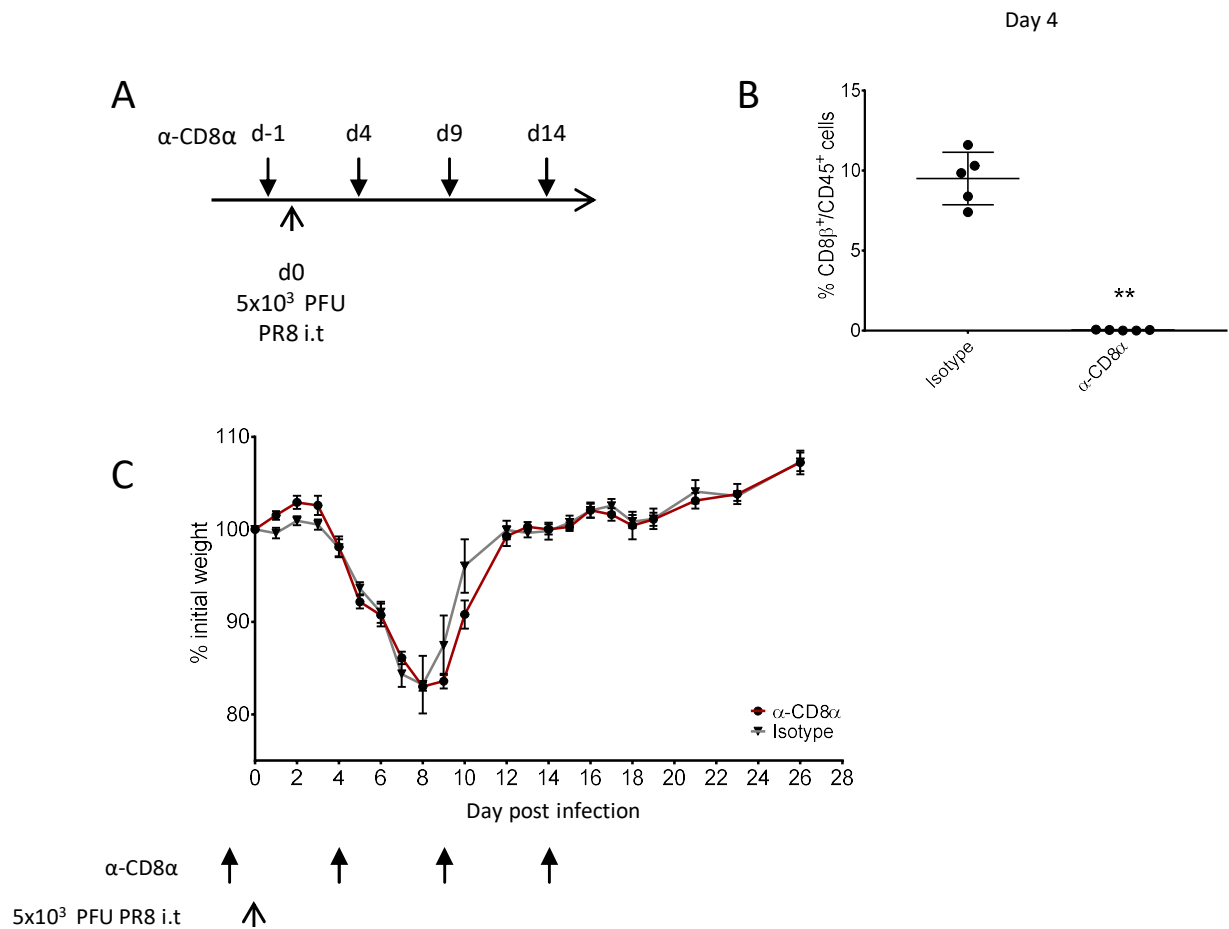


**Figure 8. Endogenous CD8 T cells are dispensable during acute influenza infection. (A)** Cartoon depicting experimental protocol. CD8 T cells were depleted by administration of 300 $\mu$ g of depleting  $\alpha$ -CD8 $\alpha$  i.p. every 5 days, starting at day -1 and finishing at day 14 post infection (bold arrows). Control mice received isotype matching antibodies. Mice were infected at day 0 with  $5 \times 10^3$  PFUs of PR8 influenza virus i.t. (line arrow). **(B)** Control of CD8 T cell depletion was performed before administration of the next depletion dose at day 4, 9 and 14. Quantification of CD8 $\beta^+$  cells within the CD45 $^+$  compartment in control and depleted mice. **(C)** Weight loss was quantified as an indicator of disease severity, represented as % of weight respective to day 0. Shown are results from a representative of at least 2 independent experiments with 5 mice per group. \*,  $P < 0.05$ ; \*\*,  $P < 0.01$  (unpaired Student's t-test)

Since depletion of CD8 T cells resulted in no change on disease outcome, I hypothesized that perhaps the delay of the CD8 T cell response in respect to viral clearance could be the reason why depleting CD8 T cells had no effect. To investigate if the timing of generation and migration of antigen-specific CD8 T cells into the lung was indeed the responsible for that result, I activated OT-I T cells in donor mice and transferred them into recipient mice either 1 day before or 1 day after infection with  $2.75 \times 10^5$  PFU WSN-S8L i.t..

Depletion of CD8 T cells during primary influenza infection showed they are not required to efficiently eliminate influenza virus, confirming previous results<sup>213,214</sup>. However, this does not mean that they cannot help eliminate and control influenza infection if present in sufficient numbers early during infection since IFV is typically cleared within the first 5 days, when virus-specific CTL numbers are intrinsically low. To investigate whether CTLs are protective in earlier stages of infection, I *in vivo* activated OT-I CTLs (Figure 9A left cartoon) and isolated them from infected lungs at day 6 post infection. I then adoptively transferred  $1 \times 10^6$  activated OT-I T cells into recipient mice that were subsequently infected with WSN-S8L influenza 1 day later (Figure 9). Infected mice without OT-I cell transfer served as a control group. Transferred OT-I CTLs engrafted into influenza-infected mice as demonstrated by their presence in peripheral blood 16 days after infection (17 days after transfer) (Figure 9B and C), even though the CTL compartment has typically undergone strong contraction at this time point. To our surprise, transfer of relatively large numbers of activated influenza-specific CTLs did not affect disease outcome because mice lost weight with similar kinetics to control mice that had received no T cell transfer (Figure 9D).

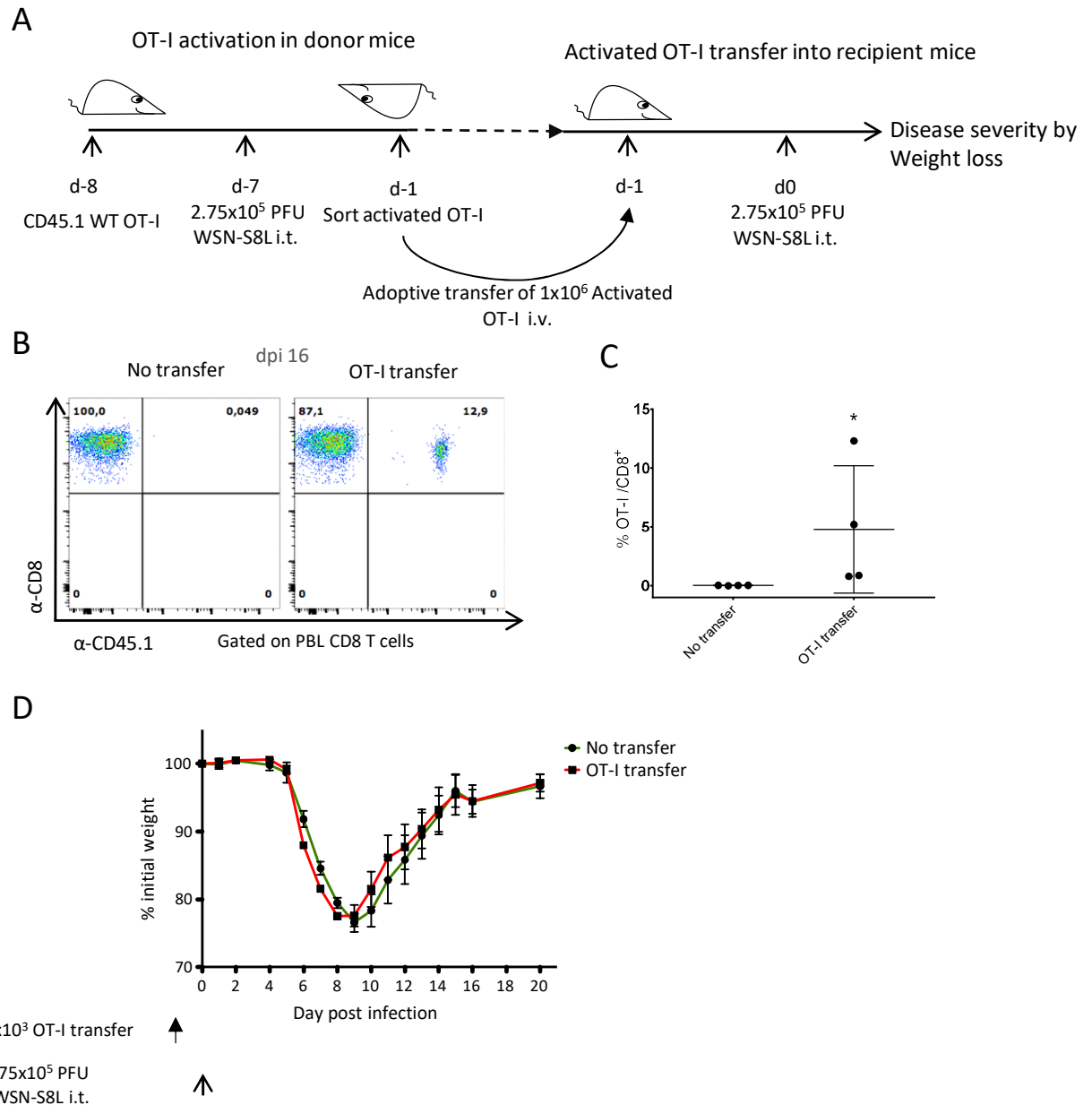


**Figure 9. Transfer of activated influenza-specific effector CTLs prior to infection does not confer protection against primary influenza infection. (A)** Cartoon depicting experimental setup. OT-I T cells were transferred into B6 mice 1-day prior i.t. WSN-S8L infection. Mice were sampled at day 6 post infection by differential labelling and CD45.1 OT-I cells sorted with FACS ARIA III. Sorted *in vivo* activated CD45.1 OT-I T cells were then transferred into naïve B6 mice and 1 day later infected by i.t administration of  $2.75 \times 10^5$  PFU WSN-S8L. **(B)** Representative dot plots of OT-I presence in blood of non-transferred control mice (left) and OT-I transferred mice (right) **(C)** Percentage of CD45.1<sup>+</sup> OT-I within the CD8 T cell compartment in PBL 16 days after infection. **(D)** Weight loss was monitored as an indicator of disease severity, represented as % of weight respective to day 0. Shown are results from a representative of at least 2 independent experiments with 5 mice per group. \*,  $P < 0.05$  (unpaired Student's t-test)

In order to exclude a putative impairment on T cell function following adoptive transfer into non-infected mice for 24h prior to flu infection (Figure 9A) as a putative causative factor for the lack of protection, I next performed a similar experiment as that depicted in Figure 9A with the exception that the influenza-specific OT-I effector CTLs were adoptively transferred 1 day after infection of recipient mice with influenza WSN-S8L (Figure 10A). Recipient mice received OT-I CTLs derived from either the lung or its draining mediastinal lymph nodes (mLNs). Control mice were also infected but received no adoptive cell transfer. Regardless of whether mice received OT-I CTLs or not, they showed identical weight loss until day 7 after infection (Figure 10B), when experiment was stopped to confirm presence of OT-I CTLs in the lung. At this time point, influenza has already been cleared from the lungs<sup>215</sup>, indicating that transfer of activated influenza-specific CD8 T cells conferred no protection. Lack of protection by transferred OT-I T cells cannot be merely explained by reduced numbers of transferred cells reaching the infected lung because an average of 53% and 38% of pulmonary CD8 T cells were the transferred OT-I CD8 T cells originally derived from the mLN or lung, respectively (Figure 10C and D). These results demonstrate that despite engrafting into infected recipient mice at high frequency, transfer of activated influenza-specific CTLs is not protective against primary influenza infection.

Taken together, these results suggest that CD8 T cells do not play a key role in overcoming primary acute influenza infections. This may be explained by the fact that during primary infection, influenza virus expansion has faster kinetics than that of the CD8 T cell response. Virus expansion reaches peak viral load around day 3 post infection while peak CTL response occurs around day 7 post infection. However, during secondary infections, memory CD8 T cells react faster and provide quick responses against viral antigens, thus, providing early protection against secondary infections.

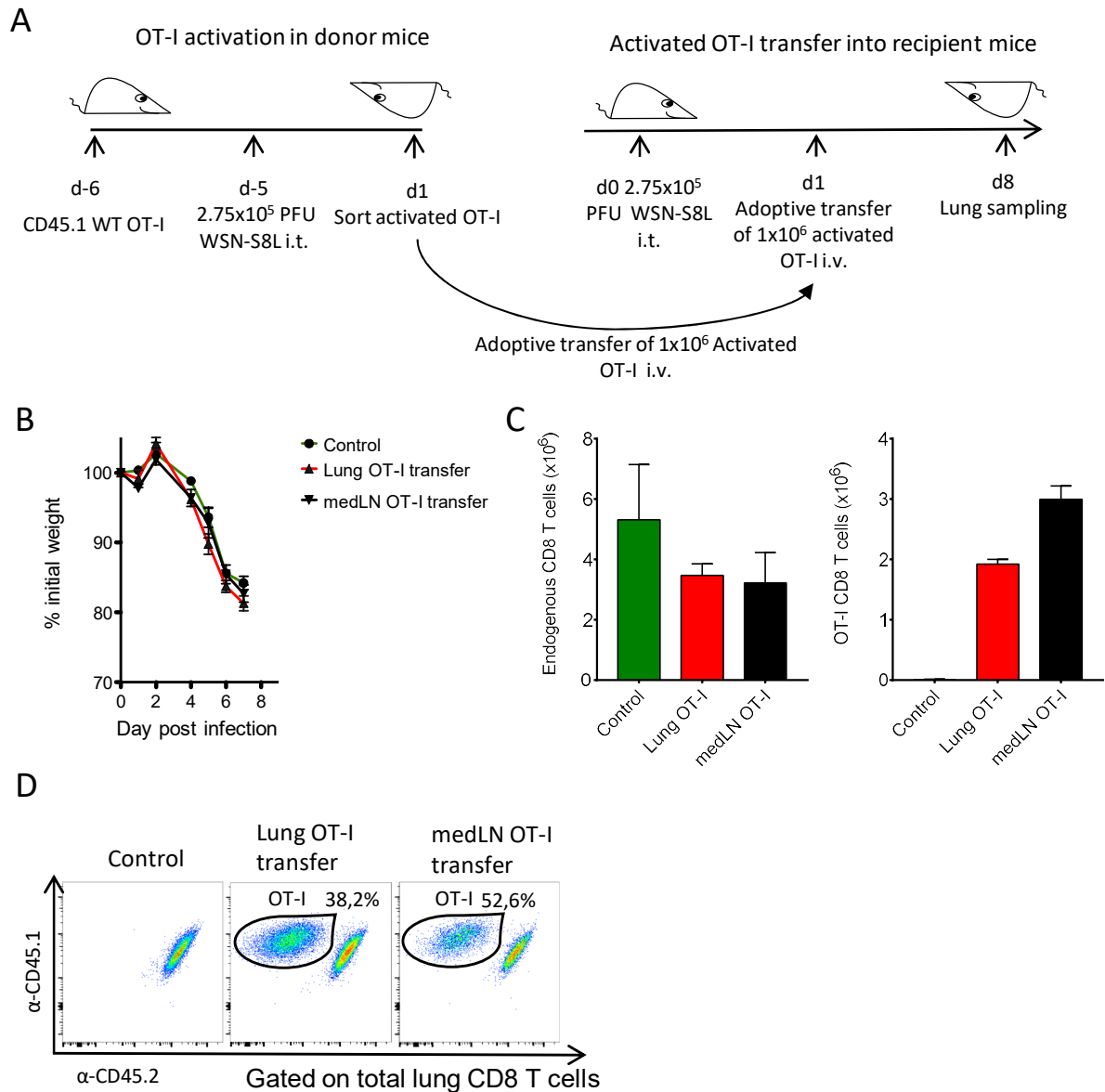


**Figure 10. Activated antigen-specific CTLs do not confer protection even when transferred early after primary infection.** (A) Cartoon depicting experimental setup. Pulmonary interstitial and mLN OT-I cells were identified by IDEAL and FACS sorted. OT-I CTLs were transferred i.v. into recipient mice that were infected 1 day earlier with  $2.75 \times 10^5$  PFU WSN-S8L i.t.. Lungs were then sampled 6 days later for analysis. (B) weight loss kinetics in WSN-S8L-infected mice transferred with the indicated  $K^b/S8L$ -specific CTLs. (C) Endogenous CD8 T cells (left panel) and OT-I T cells (right panel) present in the lungs of mice treated as indicated. (D) Representative flow cytometry dot-plots of total CD8 T cells in the lungs from infected recipient mice treated as indicated. Gates indicate transferred OT-I CTLs. Shown are results from one experiment with 5 mice per group.

### **5.2.2. Memory CD8 T cells are protective during secondary influenza infection**

The results so far indicate that effector CTLs are not essential to protect mice against influenza infection. This may be because IFV infection is typically cleared within the first 4-5 days after infection, when the number of influenza-specific CTLs in the lung is still residual<sup>215</sup>. During a secondary infection, however, tissue-resident and circulating memory CTLs may provide a rapid protection during the initial stages of IFV infection. Indeed, the generation of memory CD8 T cells during a primary influenza infection are believed to partially protect against secondary heterologous IFV infections<sup>146,216</sup>. However, the distribution of memory CTLs across the lung as well as the cellular interactions required for protection remain unresolved.

I firstly aimed at determining the extent to which memory influenza-specific CD8 T cells protect against a secondary infection. Influenza-specific memory CD8 T cells were generated by infecting mice with influenza X31 (H3N2) on day -48 (Figure 11A). on day 0 mice were re-infected with IFV using the heterologous strain PR8 (H1N1) to minimize antibody cross-reactivity (Figure 11A). To determine the role of memory CD8 T cells during the secondary infection, a group of mice received depleting  $\alpha$ -CD8a antibody on day -1 and every 5 days thereafter until the end of the experiment (Figure 11A). Control group received isotype-matched irrelevant antibody against TNP. Efficient CD8 T cell depletion in blood was confirmed by flow cytometry (Figure 11B) as well as in the lung at day 16 (Figure 11C). Mice with an untouched CD8 T cell compartment lost up to 13.4% (9.2% on average) of the initial weight and quickly recovered by day 6 after 2ry infection (Figure 11D). However, mice depleted of CD8 T cells showed significantly higher weight loss from day 3 after 2ry infection (up to 19.5%, average 13.5%) (Figure 11D) and only recovered the pre-infection weight between day 9 and 14 (Figure 11D). Therefore, these results indicate that, in contrast to primary PR8 influenza infection, memory CD8 T cell responses are protective during a secondary PR8 infection.

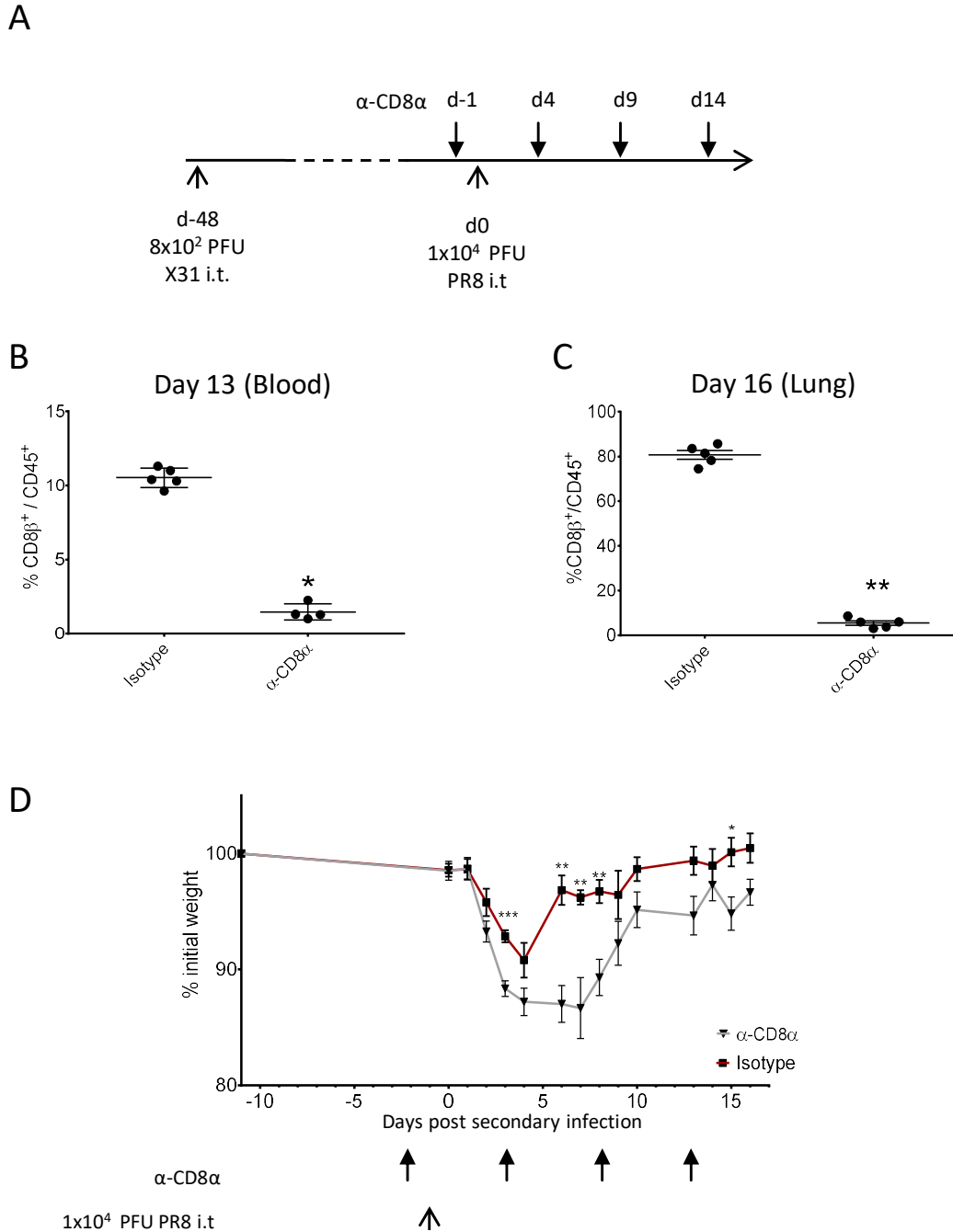


**Figure 11. CD8 T cell depletion during secondary influenza challenge results in delayed recovery.** (A) Cartoon depicting experimental protocol. B6 mice were infected i.t. with  $8 \times 10^2$  PFUs of influenza X31 (H3N2) at day -48. CD8 T cells were depleted by administration of  $300 \mu\text{g}$  of depleting  $\alpha$ -CD8 $\alpha$  i.p. every 5 days starting at day -1 before secondary infection. Control mice received isotype-matched irrelevant antibodies. Mice received a secondary infection at day 0 by i.t. administration of  $1 \times 10^4$  PFUs of PR8 (H1N1) influenza virus. (B) Control of CD8 T cell depletion was performed before administration of the next depletion dose at day 4, 9 and 14. Representative graph of CD8 $\beta^+$  cells within the CD45 $^+$  compartment in the blood of control and depleted mice. (C) Percentage of CD8 $\beta^+$  cells within the CD45 $^+$  compartment in the lung of control and depleted mice on day 16 post-secondary infection. (D) Weight loss was monitored as an indicator of disease severity. Shown are results from a representative of at least 2 independent experiments with 4 mice per group. \*,  $P < 0.05$ ; \*\*,  $P < 0.01$ ; \*\*\*,  $P < 0.001$  (unpaired Student's t-test)



### **5.2.3. Memory CTLs quickly upregulate CD69 and migrate into the BAS upon secondary challenge**

Tissue resident memory T cells ( $T_{RM}$ ) reside in the lung after primary infection and respond quickly to a secondary challenge. It is then of interest to know the early memory T cell response. It remains unclear whether  $T_{RM}$  primarily reside in one specific lung compartment and how does memory CTL location affect early T cell activation. To investigate this, I determined the level of activation and distribution of CD8 memory T cells within the different lung compartments before and shortly after secondary challenge. Mice received a primary challenge i.t. of WSN-S8L. To elicit a secondary antigen specific T cell response, mice were challenged with S8L peptide i.t. 48 days after primary WSN-S8L infection and sampled 1 day later (Figure 12A). To determine the location and activation levels of memory CTLs without secondary challenge mice were sampled at day 47. Mice were sampled using IDEAL and stained with  $\alpha$ -CD44 and  $\alpha$ -CD69 to assess early activation of memory CTLs. I divided memory CTLs in 6 groups based on their CD69 expression, from low expression on gate 1 to high expression on gate 6 (Figure 12B and C left panel). I then investigated compartment distribution of memory CTLs within each CD69 expression group (Figure 12B, C, D and E). Steady state memory CD8 T cells express low levels of CD69 (Figure 12B) and distribute mainly through the lung interstitium with a smaller population in the airway and vasculature (Figure 12D). Upon secondary challenge, memory CTLs quickly upregulate CD69 expression and migrate into the BAS (Figure 12C and E). At the same time, circulating memory CTLs increase in the vasculature showing low expression of CD69 (Figure 12B and D). These results indicate memory CD8 T mainly reside in the lung interstitium and upon secondary challenge quickly upregulate CD69 and migrate into the BAS.

Despite mostly residing in the interstitium during steady state, highly activated memory cells quickly migrate into the lung airways. It is then possible that memory T cell protection is mainly conferred by memory CTLs in the BAS. On the other hand, the mechanisms by which memory CD8 T cells confer protection remain unresolved, thus, I investigated whether or not direct killing of infected epithelial cells by virus-specific memory CTLs was required for early protection during a secondary influenza infection.

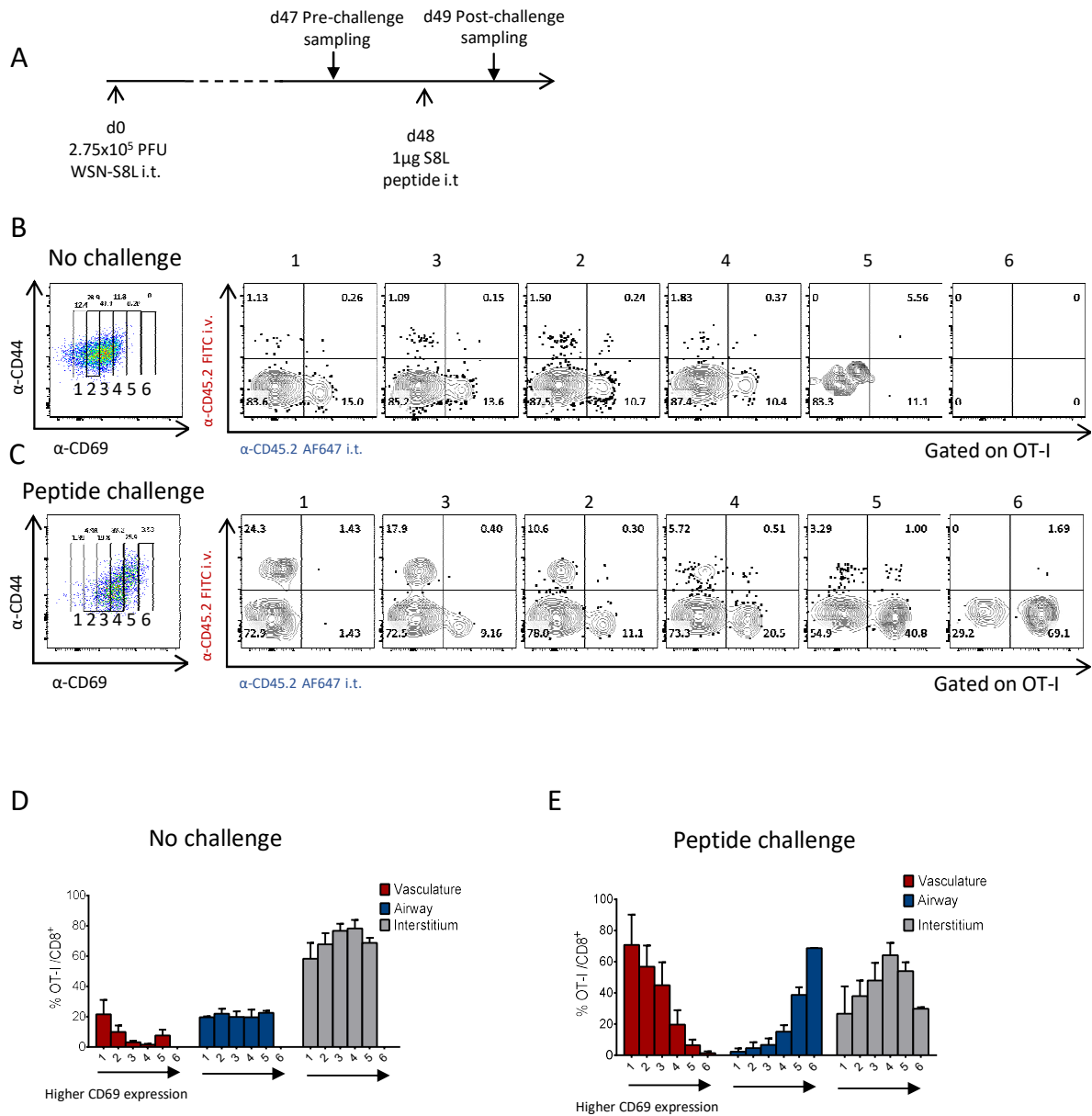


**Figure 12. Influenza-specific memory CD8 T cells become activated upon TCR engagement and rapidly migrate into the BAS. (A)** Illustration depicting experimental setup. **(B)** Representative flow cytometry dot-plots of OT-I CD8 T cells measuring CD44 and CD69 expression in non-challenged mice (left). OT-I CD8 T cell distribution within the different lung compartments according to their CD69 expression from low (Panel 1) to high (Panel 6) **(C)** Representative flow cytometry dot-plots of OT-I CD8 T cells measuring CD44 and CD69 expression in secondary peptide challenge mice (left). OT-I CD8 T cell distribution within the different lung compartments according to their CD69 expression from low (Panel 1) to high (Panel 6) **(D)** Quantification of OT-I CD8 T cell distribution in the infected lung according to CD69 expression, from low (columns 1) to high (columns 6) expression in non-challenged mice. **(E)** Quantification of OT-I CD8 T cell distribution in the infected lung according to CD69 expression, from low (columns 1) to high (columns 6) expression in secondary peptide challenged mice. Shown are results from one experiment with 3 mice per group.

#### 5.2.4. Lack of MHC-I in non-immune cells promotes CD8 T cell-mediated protection during secondary influenza infection

Consistent with previous reports<sup>129,217</sup>, I found that memory CD8 T cells play an important role on protection against secondary influenza infection (Figure 11C). However, the mechanisms that lead to CTL-mediated protection are uncharacterized. CD8 T cells can confer protection either via killing of infected epithelium or production of extracellular molecules upon activation. MHC-I is a key player during CD8 T cell responses as viral antigen presentation by MHC-I from immune cells such as DCs provides an activation signal to CD8 T cells<sup>116</sup>. Furthermore, CD8 T cells recognize infected cells via MHC-I, rendering MHC-I expression in epithelial cells crucial for CD8 T cells to detect influenza infected epithelium<sup>111</sup>. In addition, antigen-specific activation of virus-specific T cells by cells that are not directly infected may result in cytokine production, such as IFN $\gamma$  that promotes also protection against infections<sup>218</sup>. In order to investigate whether direct recognition of infected epithelial cells by memory virus-specific CTLs is key for protection during secondary flu infection, I generated bone marrow (BM) chimeric mice in which MHC-I expression was restricted to the immune compartment (WT- $\rightarrow$  $\beta_2m^{-/-}$ ) and thus absent from non-immune cells such as pulmonary epithelial cells (Figure 13A). Complete lack of MHC-I expression results in impaired positive CD8 T cell selection in the thymus basically leading to absence of peripheral CD8 T cells<sup>219</sup>. However, MHC-I expression by BM-derived cells is sufficient to warrant thymic positive selection and priming of naive T cells in the periphery<sup>220</sup>.

To determine the level of chimerism, H-2K<sup>b</sup> (K<sup>b</sup>) expression was analyzed on peripheral blood CD19<sup>-</sup>CD8<sup>+</sup> T cells, CD19<sup>+</sup>CD8<sup>-</sup> B cells and other CD19<sup>-</sup>CD8<sup>-</sup> immune cells 90 days after reconstitution (Figure 13A and B). As expected,  $\beta_2m^{-/-}$  $\rightarrow$  $\beta_2m^{-/-}$  BM chimeric mice showed residual K<sup>b</sup> expression (Figure 13C, D and E). Similarly, all B cells and CD19<sup>-</sup>CD8<sup>-</sup> immune cells in WT $\rightarrow$ WT and WT $\rightarrow$  $\beta_2m^{-/-}$  BM chimeric mice showed normal K<sup>b</sup> expression, similar to that of WT mice (Figure 13E), demonstrating efficient chimerism. As expected, CD8 T cell chimerism in WT $\rightarrow$  $\beta_2m^{-/-}$  BM chimeric mice was between 78 and 95% (Figure 14 C and E), in line with previous reports indicating a lower degree of chimerism in the T cell compartment compared to that in B cells and myeloid cells<sup>221</sup>. Since CD8 T cells may show different activation levels in the different chimeras, I quantified the expression levels of the activation marker CD44. In contrast to their WT counterparts, most CD8 T cells in WT $\rightarrow$ WT and WT $\rightarrow$  $\beta_2m^{-/-}$  chimeras

showed high CD44 expression (Figure 14E), indicating similar lymphopenia-induced proliferation during chimerism and activation status independently of  $\beta_2m$  chimerism. Both CD19<sup>+</sup> and CD19<sup>-</sup>CD8<sup>-</sup> cells showed similar levels of expression of CD44 across groups (Figure 14F and G). Taken together, these results demonstrate a high chimerism and CD8 T cell engraftment in the WT->WT and WT->  $\beta_2m^{-/-}$  chimeras.

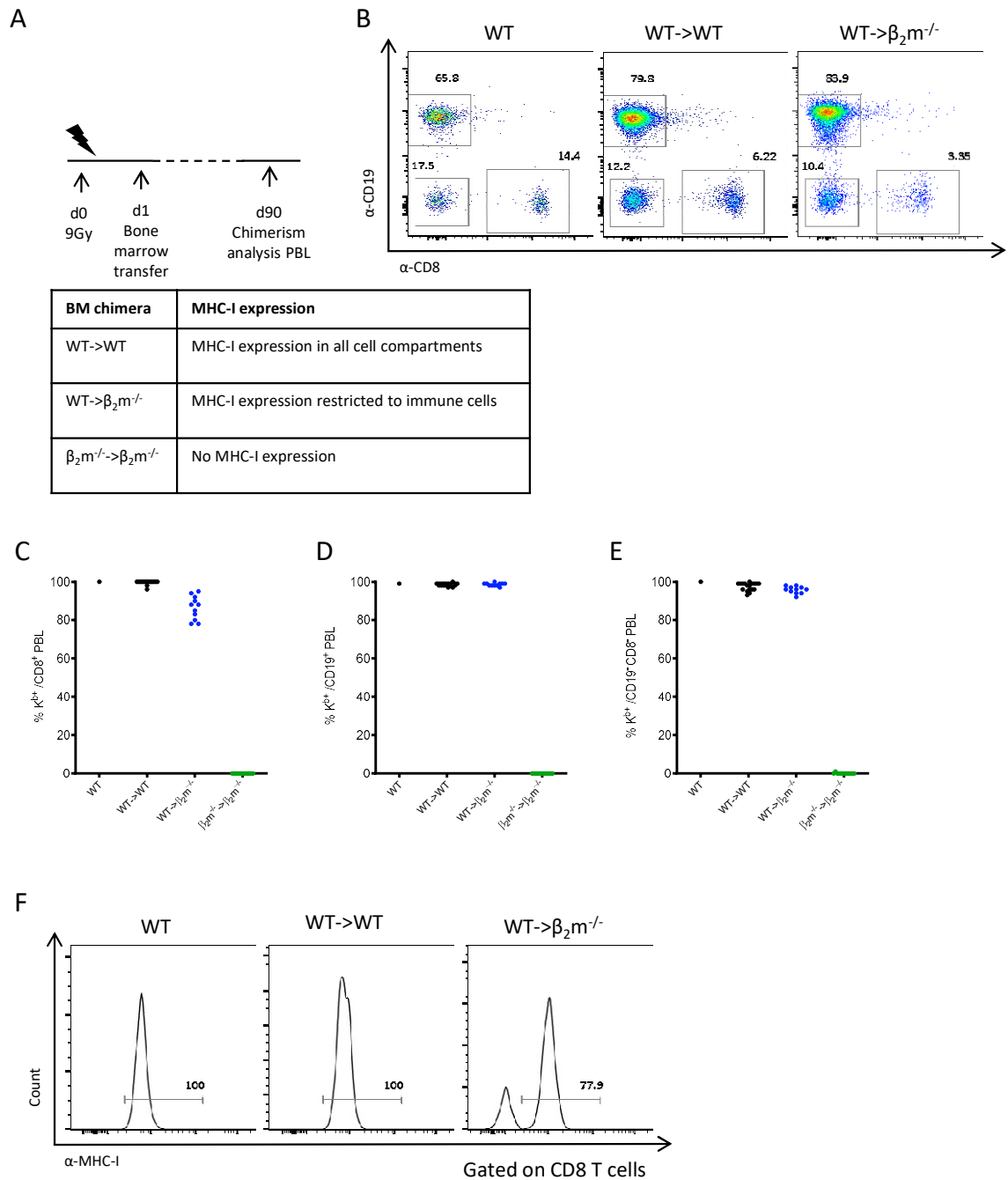


**Figure 13. Successful chimerism as measured by  $K^b$  expression level in immune cells.** (A) Illustration depicting experimental setup. (B) Representative flow cytometry dot-plots of the gating strategy for the analysis of CD8<sup>+</sup>, CD19<sup>+</sup> and CD8<sup>+</sup>/CD19<sup>-</sup> cells in all different BMx, WT->WT, WT-> $\beta_2m^{-/-}$  and  $\beta_2m^{-/-}$ -> $\beta_2m^{-/-}$ . (C-E) Percentage of CD8<sup>+</sup> T cells (C), CD19<sup>+</sup> B cells (D), and other immune cells (E). (F) Representative flow cytometry histograms of  $K^b$  expression on CD8 T cells in naïve WT mice (Left panel), WT->WT (Middle panel) and WT-> $\beta_2m^{-/-}$  (Right panel) BM chimeric mice. Shown are results from one experiment with 11 mice per group.

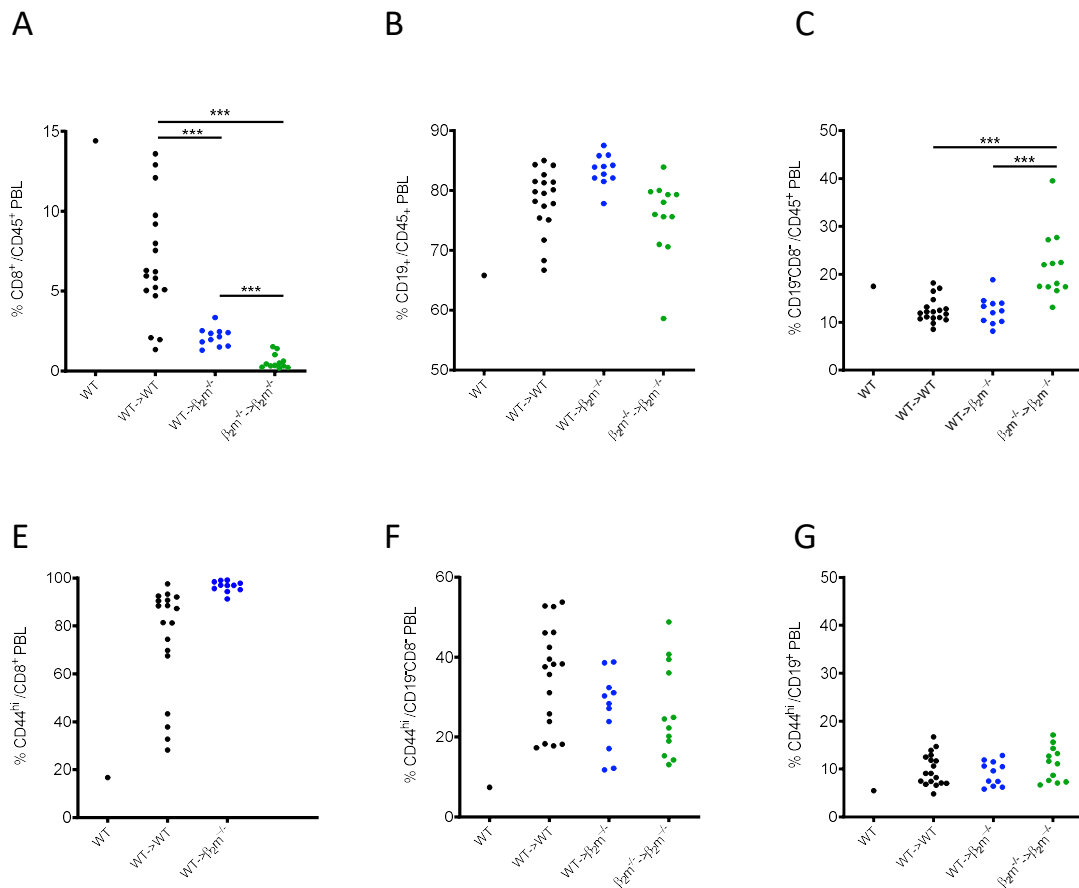


**Figure 14. CD8 T cell engraftment and CD44 expression in BMx. (A)** Percentage of CD8<sup>+</sup> T cells within the CD45<sup>+</sup> compartment in peripheral blood. **(B)** Percentage of CD19<sup>+</sup> cells within the CD45<sup>+</sup> compartment in peripheral blood. **(C)** Percentage of CD8<sup>+</sup>/CD19<sup>-</sup> cells within the CD45<sup>+</sup> compartment in peripheral blood. **(D)** Percentage of CD8<sup>+</sup> T cells expressing CD44 in peripheral blood. **(E)** Percentage of CD19<sup>+</sup> cells expressing CD44 in peripheral blood. **(F)** Percentage of CD8<sup>-</sup>/CD19<sup>-</sup> cells expressing CD44 in peripheral blood. Each dot represents results from an independent mouse. Shown are results from 1 experiment with at least 11 mice per group. \*, P < 0.05; \*\*, P < 0.01; \*\*\*, P < 0.001 (One-way ANOVA)

I then investigated if memory CD8 T cells require interaction with MHC-I on epithelial cells to confer protection. To induce the formation of influenza-specific memory CD8 T cell pool I performed a heterologous flu infection by infecting chimeric mice with IFV X31 (H2N3) (Figure 15A) and, 4 months later when mice had fully recovered, by infecting with an otherwise lethal dose of IFV PR8 (H1N1) (Figure 15A). To focus on CD8 T cell memory, CD4 T cells were depleted using depleting  $\alpha$ -CD4 mAb administered i.p. during 2<sup>o</sup> infection (Figure 15A). I first analyzed whether the absence of  $\beta$ 2m in non-immune cells had a significant impact on the influenza-specific CTL cell repertoire by performing a TCR affinity assay. For this, splenic and mLN T cells from 3-8 mice were pooled 4 days after 2ry infection. Cells were then incubated in

decreasing concentrations of either influenza dextramer (NP366-374) to determine their TCR binding affinity. Both, WT->WT and WT-> $\beta_2m^{-/-}$  showed influenza-specific CTLs that bound NP366-374 dextramer in a dose-dependent manner (Figure 15B). Independently of the NP366-374 dextramer concentration used, there were about twice as much specific CTLs from WT->WT BM chimeras than their WT-> $\beta_2m^{-/-}$  counterparts (Figure 15C). However, the polyclonal TCR affinity was apparently similar since as revealed once data was normalized because both groups showed near identical dextramer binding intensity with decreasing dextramer concentrations (Figure 15D). These results indicate that although a lower percentage of activated CD8 T cells are specific for NP366-374 in WT-> $\beta_2m^{-/-}$  mice, those who are have similar binding affinity to the dextramer as their WT->WT counterparts.

I next investigate the functional affinity of those memory CTLs by analyzing the IFN $\gamma$  response to a decreasing concentration of the immunodominant NP366-374 peptide *in vitro* (Figure 16A). Consistently with dextramer staining (Figure 15B), WT-> $\beta_2m^{-/-}$  contained about half of the IFN $\gamma$ -responding NP366-374-specific CTLs. However, IFN $\gamma$  production in a per-cell basis was similar between CTLs from WT->WT and WT->  $\beta_2m^{-/-}$  mice as measured by IFN $\gamma$  MFI in the highest peptide concentration (Figure 16B). In addition, both groups showed similar decrease of on-rate in IFN $\gamma$  producing memory T cells (Figure 16C) as well as IFN $\gamma$  production in a per cell basis (Figure 16D). Similar assays with other influenza-derived peptides (PA224-233, NPPB1-F2 62-70 and MP M1 128-135) yielded no reliable IFN $\gamma$  response. Taken together, these results show that, although the NP366-374-specific CD8 T cell repertoire during a secondary influenza infection is somewhat reduced, its reactivity to antigen is similar in terms of TCR binding and IFN $\gamma$  production.

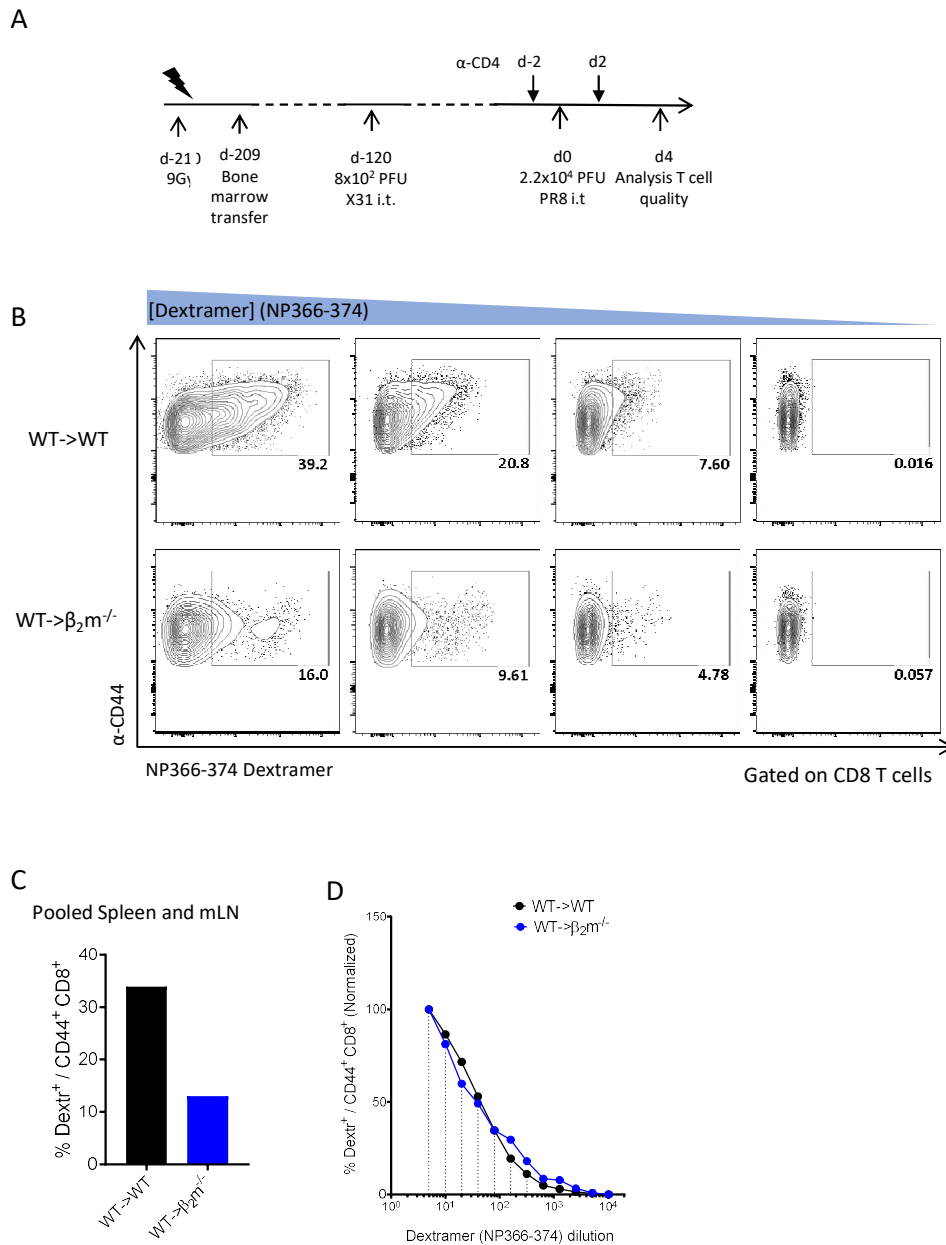


**Figure 15. Comparable TCR affinity in CD8 T cells between WT->WT and WT-> $\beta_2m^{-/-}$  BMx.** (A) Illustration depicting experimental setup. Host WT and  $\beta_2m^{-/-}$  mice were irradiated at 9Gy at day -210 and received bone marrow transfer i.v. at day 1 post irradiation. Mice were then infected i.t. with  $8 \times 10^2$  PFUs influenza X31 (H3N2) at day -120 and left to fully recover. Prior secondary challenge, mice were depleted of CD4 T cells by i.p. administration of depleting  $\alpha$ -CD4 at day -2 and once more after secondary challenge at day 2. Mice were then infected with a lethal dose for 1ry of  $2.2 \times 10^4$  PFUs influenza PR8 (H1N1) at day 0 and sampled 4 days later. (B) Representative flow cytometry dot-plots of NP366-374 dextramer binding intensity in WT->WT (Upper panels) and WT-> $\beta_2m^{-/-}$  (Lower panels) BMx. (C) Percentage of NP366-374 dextramer<sup>+</sup> CD8<sup>+</sup>/CD44<sup>+</sup> T cells in pooled spleen and mLN. (D) TCR affinity assay shown as normalized percentage of dextramer<sup>+</sup> CD8<sup>+</sup>/CD44<sup>+</sup> T cells in pooled spleen and mLN across different dextramer concentrations. Shown are results from 1 experiment with cells pooled from at least 3 mice per group.



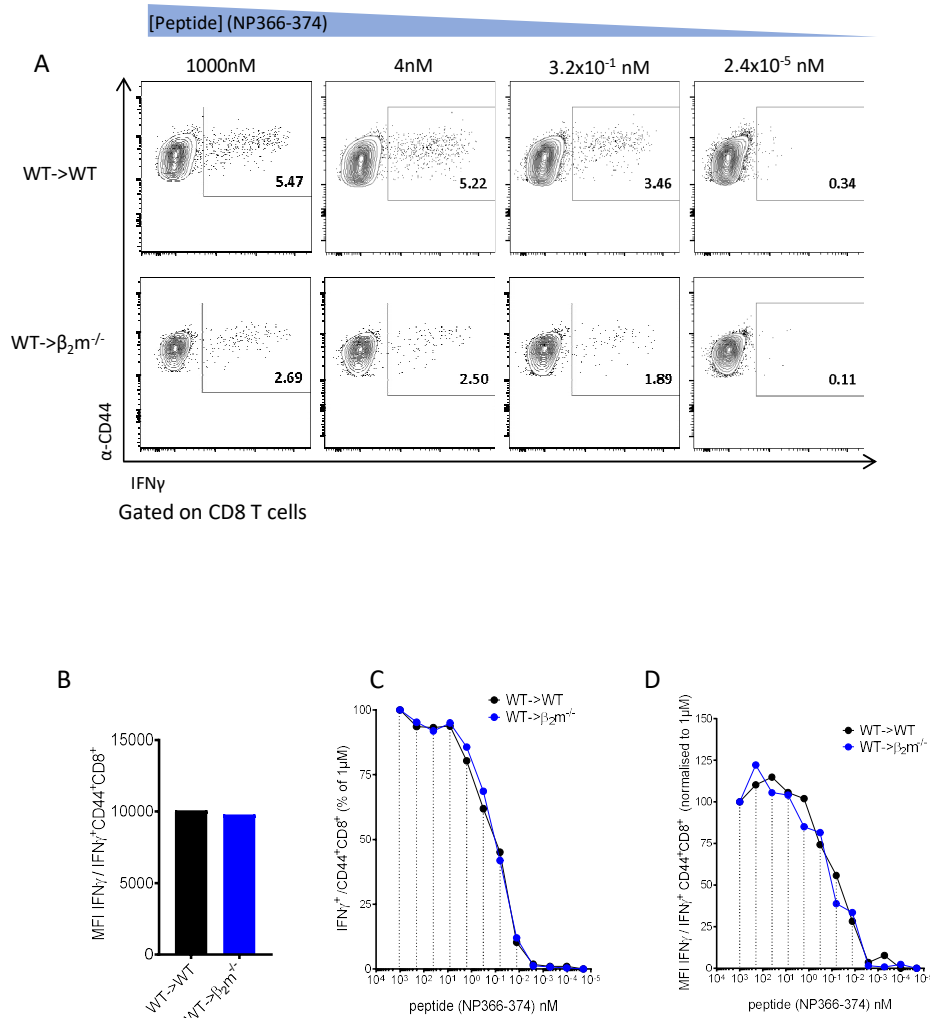


**Figure 16. Comparable CTL TCR on-rate between WT->WT and WT->β<sub>2</sub>m<sup>-/-</sup> BMx (A)** Representative flow cytometry dot-plots of IFNγ expression decay from high peptide (NP366-374) restimulation (Left panels) to low peptide restimulation (Right panels) in WT->WT (Upper panels) and WT->β<sub>2</sub>m<sup>-/-</sup> (Lower panels) BMx. **(B)** Mean fluorescence intensity of IFNγ expression in CD8<sup>+</sup>/CD44<sup>+</sup> T cells in pooled spleen and mLN at highest peptide concentration. **(C)** TCR on-rate assay as normalized percentage of CD8<sup>+</sup>/CD44<sup>+</sup> cells expressing IFNγ. **(D)** TCR on-rate assay as normalized percentage of IFNγ MFI in CD8<sup>+</sup>/CD44<sup>+</sup> cells expressing IFNγ. Shown are results from 1 experiment with at least 3 mice per group.

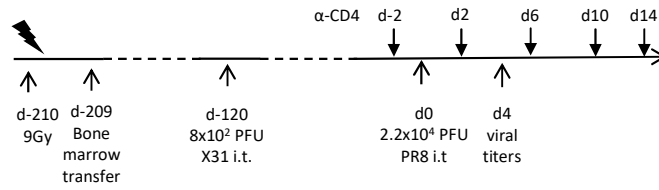
Once I established that T cell responses were comparable between groups, I continued to investigate the role of MHC-I expression on epithelial cells for protection against influenza virus by following disease activity with weight loss as viral load as read outs. Mice were initially infected with X31 i.t. (Figure 17A) and weight loss was measured until day 35 post primary infection. Consistent with my previous results (Figure 11), although β<sub>2</sub>m expression was required for optimal recovery of flu-induced weight loss during the 1ry infection, it was not essential (Figure 17B), showing that CD8 T cells are dispensable during acute infection. However, CD8 T cells were indispensable for

protection during a 2ry flu infection because all  $\beta_2m$ -deficient mice lacking CD8 T cells died while none of the mice expressing  $\beta_2m$  did (Figure 17C, D). Interestingly, during secondary challenge with an otherwise lethal dose, lack of  $\beta_2m$  expression on non-immune cells, such as infected epithelial cells, resulted in protection from early and absolute weight loss as well as in faster recovery (Figure 17C). WT- $\rightarrow\beta_2m^{-/-}$  mice showed a significantly lower weight loss compared to their chimera counterparts during the peak of the infection between days 0 and 7 (Figure 17C). In addition, WT- $\rightarrow\beta_2m^{-/-}$  mice recovered quicker and had a significantly higher weight gain during the recovery phase starting on day 7 (Figure 17C). WT- $\rightarrow$ WT mice lost weight as soon as day 1 after 2ry infection, and started to recover at a similar date as  $\beta_2m^{-/-}\rightarrow\beta_2m^{-/-}$ . However, a significantly higher weight loss by WT- $\rightarrow$ WT compared to their WT- $\rightarrow\beta_2m^{-/-}$  counterparts, resulted in a slower recovery. Despite both groups reaching 100% survival WT- $\rightarrow$ WT did not recover to the same extent as WT- $\rightarrow\beta_2m^{-/-}$ .

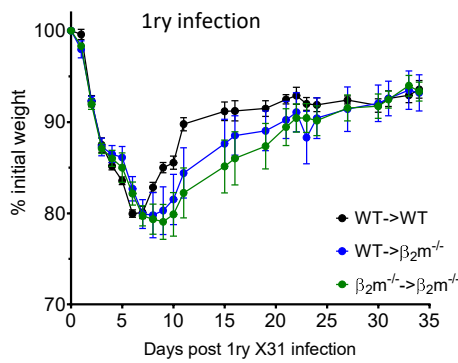
Increased susceptibility to weight loss was likely a reflection of higher viral load as mice lacking  $\beta_2m$  expression had the highest influenza load in the lung (Figure 17E). However, despite a clear difference in weight loss, we did not observe differences in viral load (Figure 17E) or neutrophils (Figure 17F) in mice with normal  $\beta_2m$  expression or those lacking it on non-immune cells such as infected epithelial cells. This result may be explained by the inability of CD8 T cells to directly kill infected epithelial cells as they lack MHC-I, and would be in line with a reduced pathology as measured by weight loss.

In conclusion, these results show memory CD8 T cells confer protection beyond killing of infected epithelial cells via direct TCR-MHC-I/peptide interaction. Furthermore, these data indicate that killing of infected epithelial cells might result in more severe disease development. However, it remains unclear how memory CD8 T cells get quickly activated and can react in such a prompt fashion.

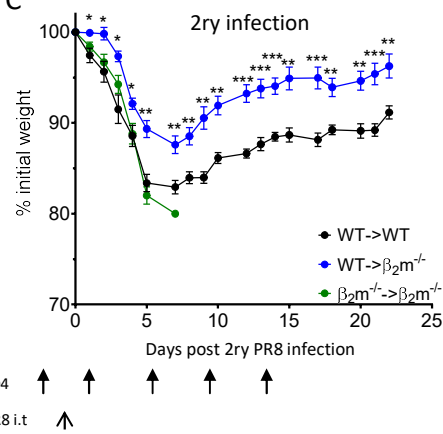
A



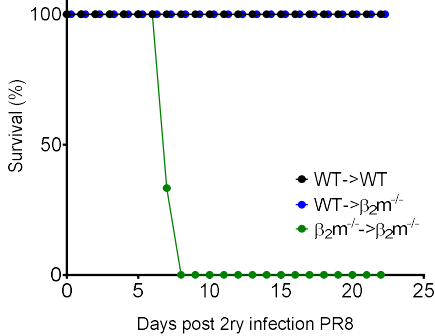
B



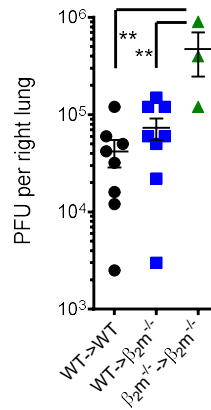
C



D



E



F

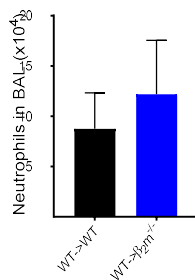


**Figure 17. Lack of MHC-I on the epithelium confers protection during secondary challenge.** (A) Illustration depicting experimental setup. Host WT and  $\beta_2m^{-/-}$  mice were irradiated at 9Gy at day -210 and received bone marrow transfer i.v. at day 1 post irradiation. Mice were then infected i.t. with  $8 \times 10^2$  PFUs influenza X31 at day -120 and weight loss was followed until full recovery. Prior secondary challenge, mice were depleted of CD4 T cells by i.p. administration of depleting  $\alpha$ -CD4 at day -2 and continued to receive ab every 4 days until day 14. Mice were then infected with a lethal dose of  $2.2 \times 10^4$  PFUs influenza PR8 at day 0 and weight loss was followed to assess disease severity. (B) Weight loss was followed as an indicator of disease severity, represented as % of weight respective to day 0. (C) Weight loss was followed as an indicator of disease severity. (D) % of surviving mice during secondary

challenge. **(E)** Viral titers as measured by plaque assay. **(F)** Number of neutrophils in BAL of WT->WT and WT-> $\beta_2m^{-/-}$  at day 4 post-secondary infection. Shown are results from a representative of 2 (B, C, D, F) or 1 (E) independent experiments with 8 (WT->WT, WT-> $\beta_2m^{-/-}$ ) and 3 ( $\beta_2m^{-/-}$ -> $\beta_2m^{-/-}$ ) mice per group. \*, P< 0.05; \*\*, P< 0.01; \*\*\*, P< 0.001 (One-way ANOVA).

### **5.2.5. Dendritic cells are key for memory CD8 T cell-mediated protection against influenza.**

After showing that memory CTLs are required for protection against influenza infection and that MHC-I expression on non-immune cells is detrimental for the infection outcome, I next sought to investigate whether and which accessory cells promotes CD8 T cell-mediated protection.

To investigate this, I used the  $\beta_2m^{-/-}$  bone marrow chimera model to ensure the non-immune cells do not express MHC-I. To reconstitute the immune repertoire, I made use of bone marrow from DOG mice, which allow for DC depletion through diphtheria toxin (DT) administration. Using this system, I can study the role of DC-T cell interactions in an environment without MHC-I on the non-immune cells. Lack of MHC-I on non-immune cells provides a suitable environment to specifically study the interaction between DCs and T cells in the context of MHC-I. To generate BMx, mice were irradiated at 9Gy and DOG bone marrow transferred 1 day later (Figure 18A). WT->WT BM chimeras served as control as both, immune and non-immune cells express MHC-I and show a normal response against infection.

Chimerism was analyzed in PBL at day 90 post irradiation on CD8<sup>+</sup> and CD19<sup>+</sup> cells (Figure 18B) and measured by percentage of H-2Kb (K<sup>b</sup>) expression where all mice showed near 100% K<sup>b</sup> expression in both CD8 (Figure 18C left panel) and CD19 cells (Figure 18C right panel), demonstrating efficient chimerism. Moreover, CD8 T cells made up to 13% of CD45 cells but with high variability between mice (Figure 18D left panel). Most of the mice showed high CD44 expression (Figure 18D right panel), as expected in these chimeras and as we observed in our previous WT->  $\beta_2m^{-/-}$  (Figure 14E). Finally, CD19 cells comprised ca. 80% of CD45 cells in PBL (Figure 18E left panel). Furthermore, consistent with our previous BMx, less than 20% of CD19 cells expressed high levels of CD44 (Figure 18E right panel). Taken together, DOG->  $\beta_2m^{-/-}$  chimerized well and presented a good opportunity to study the relevance of DC-T cell interactions during secondary viral challenge.

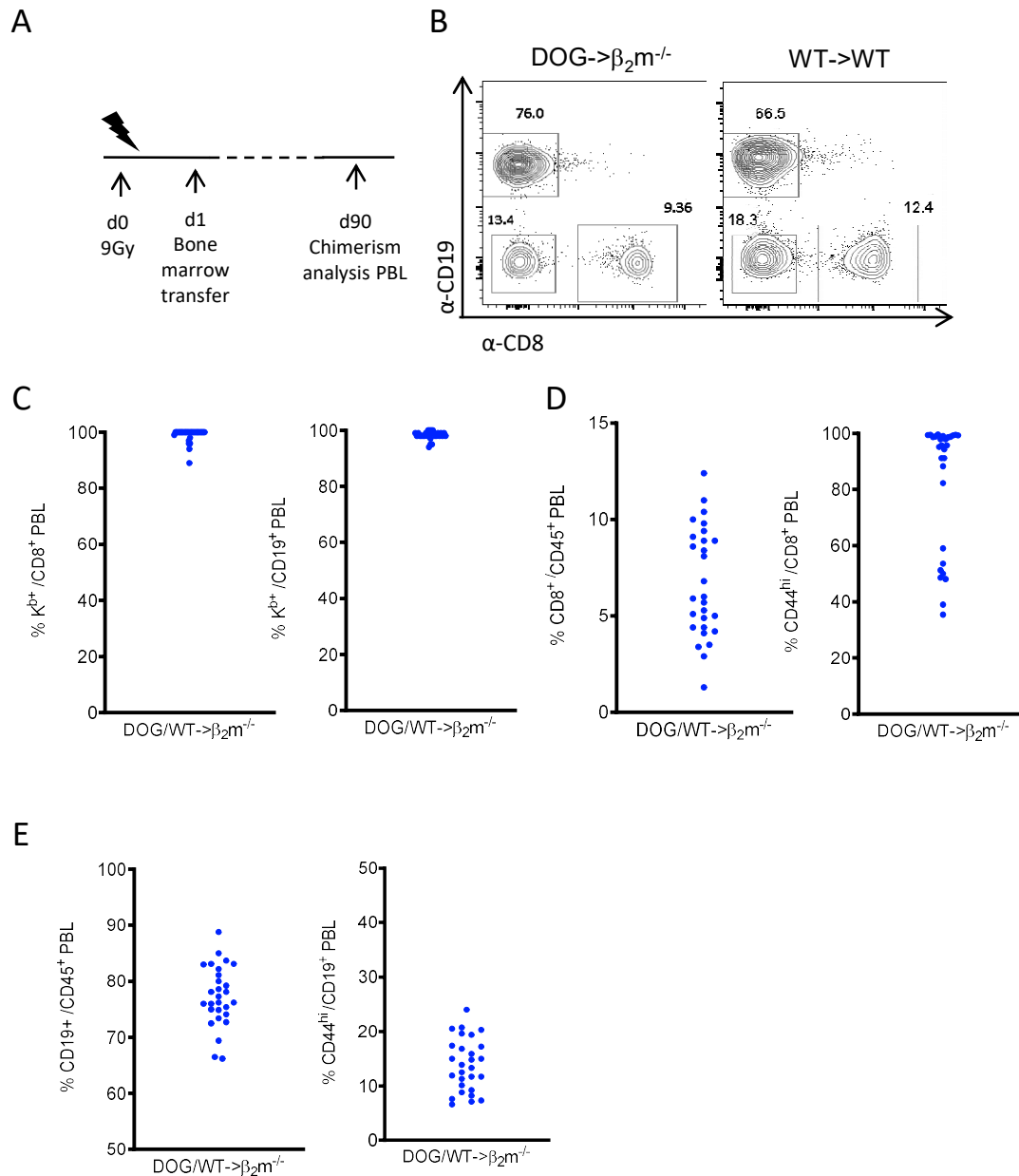


**Figure 18. Chimerism in DOG/WT-> $\beta_2m^{-/-}$  as measured by  $K^b$  expression (A)** Illustration depicting experimental setup. **(B)** Representative flow cytometry dot-plots of gating strategy for the analysis of CD8<sup>+</sup>, CD19<sup>+</sup> and CD8<sup>+</sup>/CD19<sup>-</sup> cells. **(C)** Percentage of CD8 (Left) and CD19 (Right) cells expressing  $K^b$  in peripheral blood. **(D)** Percentage of CD8 (Left) cells within the CD45<sup>+</sup> compartment (Left) and percentage of CD8<sup>+</sup> T cells expressing CD44 (Right) in peripheral blood. **(E)** Percentage of CD19<sup>+</sup> cells within the CD45<sup>+</sup> compartment (Left) and percentage of CD19<sup>+</sup> cells expressing CD44 (Right) in peripheral blood. Shown are results from 1 experiment with 29 mice.

Chimeric mice were initially infected with  $8 \times 10^2$  PFU IFV X31 (H3N2) i.t. and then infected with a heterologous  $2.2 \times 10^4$  PFU IFV PR8 (H1N1) 120 days later. To focus on CD8 T cell memory, CD4 T cells were depleted using depleting  $\alpha$ -CD4 mAb administered i.p. on days -2 and 2 post 2ry infection. On days -2 and -1 after 2ry

infection, half of the mice received DT at to deplete DC (DC- group), while the other half was untreated with DT and, thus, contained normal DC numbers (DC+ group) (Figure 19A and B). All mice were infected with a lethal influenza PR8 dose for 1ry of  $2.2 \times 10^4$  PFU on day 0 and sampled 4 days later to assess the CTL response quality and viral titers (Figure 19A). To measure the quality of the T cell response, the TCR on-rate was investigated by peptide restimulation and IFN $\gamma$  production. I then pooled mLN and spleen CTLs and restimulated these cells in decreasing concentration of NP366-37 peptide (Figure 19B). At high peptide concentrations of 40-1.6 nM, TCR on-rate as measured by IFN $\gamma$  producing CTLs was comparable across groups (Figure 19C). However, DOG- $\beta_2m^{-/-}$ , DC- mice showed a reduction in IFN $\gamma$ -producing CTLs at concentrations lower than 0.32 nM peptide when compared to the other chimeras. I then normalized the results to the highest peptide concentration to compare the loss of IFN $\gamma$  response with decreasing peptide concentrations across all groups. IFN $\gamma$  production in a per cell basis was similar across all groups and peptide concentrations (Figure 19D). These results show CD8 T cells have lower affinity when they are restricted of MHC-I interactions with epithelium and dendritic cells as shown in IFN $\gamma$  producing CTLs and viral titers (Figure 19C, D and G).

DCs have been proposed to promote T cell recall responses by inducing memory T cell proliferation<sup>222</sup>. To rule out the possibility that DC depletion resulted in reduced CTL numbers in the lung, I collected the BAL and quantified total and influenza-specific CD8 T cell numbers. Both, the number of total (Figure 19E) and NP366-374-specific (Figure 19F) CTLs were comparable between groups. Finally, to determine the extent to which lack of DCs has an effect on protective CD8 T cell responses against a secondary challenge, I analyzed viral titers in the lung 4 days after 2ry influenza infection. There were higher viral titers in DOG- $\beta_2m^{-/-}$ , DC- mice compared to DOG- $\beta_2m^{-/-}$ , DC+ and WT- $\beta_2m^{-/-}$  (Figure 19G), indicating that CD8 T cells likely require DC interaction to provide protection against a 2ry challenge.

In conclusion, these results show that DCs are not required to increase the number of influenza-specific memory CTLs, but they are required in the absence of MHC-I on epithelium to increase the affinity of memory CTLs towards a given influenza antigen. As a result, memory CTL response is impaired and results in increased viral burden.

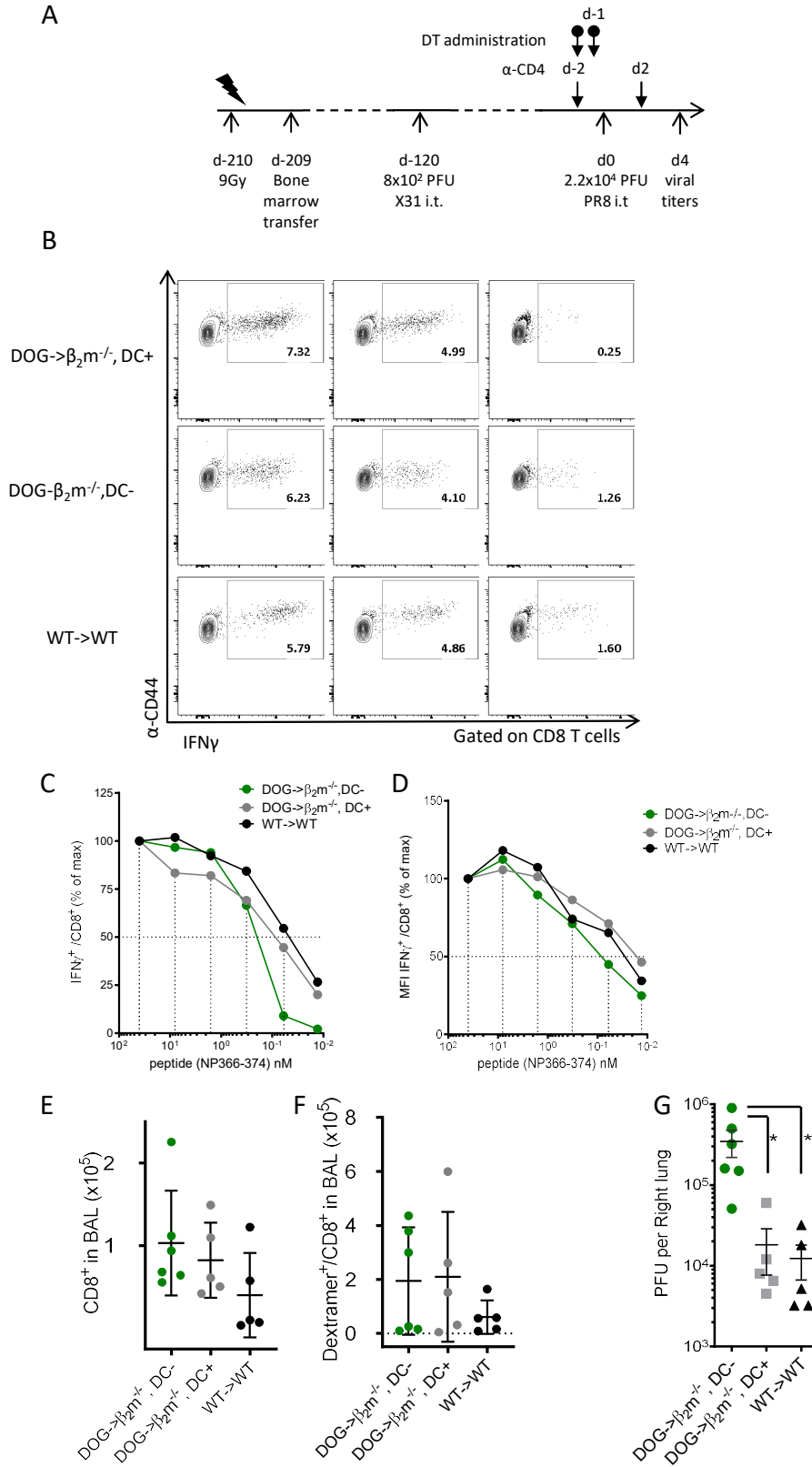


**Figure 19. Lack of DC-CTL interaction results in impaired memory CTL protection (A)** Illustration depicting experimental setup. Host WT and  $\beta_2m^{-/-}$  mice were irradiated at 9Gy at day -210 and received bone marrow transfer i.v. at day 1 post irradiation. Mice were then infected i.t. with  $8 \times 10^2$  PFUs influenza X31 at day -120 and left to fully recover. Prior secondary challenge, mice were depleted of CD4 T cells by i.p. administration of depleting  $\alpha$ -CD4 at day -2 and once more after secondary challenge at day 2. In addition, DC- group received

administration of DT i.p. at days -2 and -1 to deplete DCs. Mice were then infected with a lethal dose of  $2.2 \times 10^4$  PFUs influenza PR8 at day 0 and finally sampled 4 days after secondary challenge. **(B)** Representative flow cytometry dot-plots of IFN $\gamma$  expression decay from high peptide (NP366-374) restimulation (Left panels) to low peptide restimulation (Right panels) in DOG- $\beta_2m^{-/-}$ , DC- (upper panels), DOG- $\beta_2m^{-/-}$ , DC+ (Middle line panels) and WT- $\beta_2m^{-/-}$  (Lower panels). **(C)** TCR affinity assay as normalized percentage of CD8 $^+$ /CD44 $^+$  cells expressing IFN $\gamma$ . **(D)** TCR affinity assay as normalized percentage of IFN $\gamma$  MFI in CD8 $^+$ /CD44 $^+$  cells expressing IFN $\gamma$ . **(E)** Total number of CD8 $^+$  T cells in BAL at day 4 post-secondary challenge. **(F)** Total number of dextramer $^+$  CD8 $^+$  T cells in BAL at day 4 post-secondary challenge. **(G)** Viral titers as measured by plaque assay. Results shown as PFU per right lung. Shown are results from 1 experiment with 5 to 6 mice per group. \*, P < 0.05; \*\*, P < 0.01; \*\*\*, P < 0.001 (One-way ANOVA).



## 6. Discussion

During influenza infection in the lung, there is controversy whether CD8 T cell responses are important for efficient recovery<sup>100,115,223</sup>. Furthermore, the exact mechanisms of CD8 T cell migration into the lung as well as the putative mechanisms of protection are still unresolved. In this study, I aimed to elucidate whether and how CD8 T cells confer protection in both acute and memory infections as well as delineate the mechanisms that regulate CD8 T cell entry into the lung environment after infection.

By implementing IDEAL, a novel *in vivo* differential labelling that allows for identification of the precise cellular location in the lung, I circumvented the limitations of classical protocols for analyzing T cells at different anatomical compartments of the lung -i.e., intravascular, interstitial and within the airway lumen. Using this method, I could accurately identify the positioning of CTLs during primary and secondary flu infections, and perform compartment-specific analysis of influenza-specific CTLs. While genomics analysis shed interesting differences in gene expression of *Gzmb* (Granzyme B) and *Prf1* (Perforin), those were not carried out to a biological effect when measuring their killing capacity<sup>224</sup>. In fact, I found once CTLs locate in the lung environment, they can migrate into any of the mentioned lung compartments without apparent imprinting in their transcriptomic profile of functional cytotoxicity.

Importantly, influenza-specific CD8 T cells showed to be dispensable in our model of acute influenza infection as neither depletion nor transfer of effector influenza-specific CD8 T cells had any impact on disease outcome. However, depletion of CD8 T cells prior secondary challenge with a heterotypic influenza strain proved CD8 T cells to be key to a prompt recovery. To further understand how memory CD8 T cells confer protection during secondary challenges I used a model of BMx where only immune cells express MHC-I (WT- $\rightarrow\beta 2m^{-/-}$ ), hence, rendering CD8 T cells incapable of killing infected epithelium. My results indicate that killing of infected lung epithelium via MHC-I interactions with memory CTLs is detrimental to the host. In fact, lack of EpC-CTL MHC-I/TCR interactions did not have any detrimental effect on viral load but resulted in a significantly improved disease outcome. Since there are no EpC-CTL MHC-I/TCR interactions in WT- $\rightarrow\beta 2m^{-/-}$  BMx, I then investigated DC-CTL interactions on that mouse model to assess the role of DCs in memory T cell activation. Finally, lack of MHC-I/TCR interactions with EpCs and DCs resulted in significantly higher viral load

and worsened disease outcome, highlighting the role of DCs in driving CD8 T cell-mediated protection during a 2ry flu challenge. Taken together, my results prove CD8 T cells need MHC-I interactions with DCs and are key to a prompt recovery upon secondary infection. In addition, I showed how killing of infected epithelium is detrimental for the host, possibly due to immunopathology from an excessive killing of a vital cellular component of the lung structure and gas exchange.

Despite extensive research on T cell migration<sup>149,225,226</sup> during inflammation into a variety of organs, the exact mechanisms employed by CTLs to infiltrate the infected lung remain unresolved<sup>227</sup>. Activated T cells enter the lung<sup>153,208</sup> through adhesion and chemokine dependent mechanisms. CTLs bind ICAM-1 and 2 on endothelial cells lining alveolar capillaries, resulting in increased T cell retention inside capillaries. Increased retention times are thought to be of high importance to chemotactic T cell extravasation<sup>226</sup>. In addition, CXCL12 trails left by neutrophils have been shown to pave the path for activated CTL migration into the infected lung<sup>83</sup>. CXCR6 and CCR5 have also been postulated as key players for CTL extravasation<sup>228</sup>. I have shown how CXCR3 is also a key mediator for CTL translocation from the lung vasculature into the interstitial compartment during acute influenza infection<sup>209</sup> while Slütter et al.<sup>129</sup> have shown it during secondary challenge. By identifying the cues that lead activated CTLs into the infected lung, T cell trafficking into the lung may be modulated to either reduce immune pathology or increase T cell infiltration to combat an active infection.

Although the mechanisms of T cell egression from the vasculature have already been partially identified<sup>225</sup>, the precise location of T cells within the lung has been unresolved. Anderson et al.<sup>153</sup> have shown how perfusion protocols are often not efficient enough to eliminate all cells present in the vasculature. It is possible that CD44<sup>hi</sup> CTLs are closely associated to the luminal side of the endothelium whereas CD44<sup>lo</sup> CTLs comprise the pool of circulating naïve T cells that were not efficiently perfused. Currently, it is not clear whether the CD44<sup>hi</sup> CTLs found in the circulation after perfusion are in circulation or whether a fraction of them are attached to the endothelial luminal side. In the latter, it would be interesting to unveil whether they are in transit to the infected lung, or whether they are positioned at that location for immune surveillance, or both.

It has been postulated that CTLs in the lung interstitium can reenter circulation, however, once in the BAS they lose the capacity to do so<sup>229,230</sup>. In addition, it is believed

that only terminally activated T cells migrate into the BAS and Flügel et al.<sup>231</sup> have observed CD4 T cell recirculation between the interstitial and the bronchoalveolar compartments. In accordance with these results, I could show how CTLs can also migrate between lung compartments during acute infection regardless of the compartment they were isolated from. Finally, CTLs isolated from the BAS showed similar migration to that of their interstitial and vascular counterparts. Taken together, these results suggest CTLs do not have preferential migration into a specific lung compartment and their impairment to rejoin circulation is likely due to lack of direct contact with endothelium.

Although CTLs show no preference in migration to either interstitium or BAS, it remains unclear if location plays a role in their transcriptomic profile and function. Since influenza infects pulmonary epithelial cells<sup>113</sup>, influenza-specific CTLs are left with only 2 options to directly interact with and directly eliminate infected cells: squeeze throughout the interstitium between the basal membrane and epithelium, or migrate to the broncho-alveolar space and scan epithelial cells from the luminal side. I hypothesized that the later may be advantageous since CTLs may be able to scan a higher number of epithelial cells from the luminal side. Here, I have demonstrated using a novel *in vivo* cytotoxicity assay that CTLs present in the airway lumen are able to kill target cells in an antigen-specific manner. This suggests that CTLs present in the BAS could possess more efficient cytotoxic properties. To test this, I followed two different approaches. First, I analyzed gene expression by influenza specific CTLs located at the interstitium or BAS 7 days after influenza infection. Secondly, I studied compartment-specific cytotoxic activity using an *in vitro* cytotoxicity assay that allows to use the same number of effector cells. Interestingly, while some cytotoxicity associated genes such as *Gzmb* and *Prf1* were upregulated in the BAS compared to the interstitium those differences did not have an impact on their actual antigen-specific killing activity as the killing capacity of CTLs from different compartments showed comparable killing rates. Besides *Gzmb* and *Prf1* gene analysis of CTLs in the airways showed some other genes expressed significantly higher than in the interstitium. These genes were involved in immune regulation (*Nt5e* -coding for CD73 -, *Ctla4* and *Tigit* - T Cell Immunoreceptor With Ig And ITIM Domains -), cellular adhesion (*Itgb2*), signals for persistence of memory precursor effector cells (*Hvem* - *TNFRSF14* -) and cell migration (*Ccl3* and *Ccl4*). Upregulation of cell migration chemokines such as *Ccl3* could indicate a positive feedback loop by CTLs in aims to retain CTLs in the lung

environment and promote further CTL migration into the infected area. In addition, CTLs on the vasculature had a significantly different gene expression profile, likely showing how CD8 T cells become terminally differentiated once in the infected tissue<sup>116,225</sup>. Considering those results, it is feasible that despite significant differences between airway and interstitium in the expression of some genes, those do not result in a biological effect. Lack of direct correlation between gene and protein expression is common and can be as low as a 40% due to protein stability, degradation of mRNA or a low rate of mRNA transcription compared to protein translation<sup>232</sup>.

It has been reported that CD8 T cells confer protection during acute influenza infection. However, contradictory reports show mice can recover less effectively from influenza infection when lacking CD8 T cells<sup>96,233</sup> while others reported CD8 T cell-deficient mice suffered from delayed clearance and high mortality<sup>97</sup>. Consequently, the whether and how CD8 T cell responses are beneficial or detrimental during influenza remain controversial. In addition, the interplay between B cell, CD4 and CD8 T cells is key to an efficient immune response against influenza virus. CD8 T cells alone cannot effectively clear an influenza infection<sup>223,234</sup>, and neither can CD4<sup>98,235</sup> and B cells<sup>95,236</sup>. In the experiments presented here, depletion of CD8 T cells during acute influenza PR8 infection in B6 mice proved CD8 to be dispensable in this infectious model. In addition, preventive transfers of activated influenza-specific CD8 T cells before or shortly after infection did not result in any enhanced protection to infected mice, although cells reached the lungs in significant numbers. Taken together, my results are consistent with previous reports showing CD8 T cells to be dispensable during influenza primary infection. Discrepancies between different studies and my own results may be due to a diversity of factors: a) environmental factors such as housing, food, microbiota, handling, b) use of different strains of mice (BALBc vs B6), c) use of different strains of virus and/or concentrations and d) the approach to study T cell deficiency, either depletion or the use of knockout mice.

Although CD8 T cells might be dispensable during acute infection, some studies have identified a protective role during secondary challenge<sup>146,154,216</sup>. I confirmed those studies by depleting CD8 T cells during secondary challenge and observed a delayed recovery when compared to their control counterparts. Several studies have shown the importance of T<sub>RM</sub> in recovery of secondary challenges<sup>129,171,172</sup>. However, despite the extensive research on T<sub>RM</sub> in the past years, there is little known on how tissue resident

memory CTLs confer protection against secondary infections. I have observed how, upon infection, quick activation of memory CTLs leads to transmigration into the BAS. However, the limited number of memory cells and the fact that  $T_{RM}$  do not migrate<sup>46,171,216</sup> rendered the possibility of sorting and transferring memory cells from different compartments not feasible, hence, I could not study compartment specific  $T_{RM}$  responses.

Activation of  $T_{RM}$  following infection is thought to be antigen dependent<sup>216</sup>, however, the possibility of innate-like activation of  $T_{RM}$  has yet to be explored. On the other hand, it has been postulated that circulating memory T cells can be activated in an innate-like fashion by recognizing activating cytokines such as IL-12, IL-18, IL-15 and type I IFN<sup>237</sup>. Using a model of BMx lacking MHC-I on epithelium and expressing DTR on CD11c cells I could determine the extent to which DCs are key to the memory CD8 T cell response, showing how antigen specific activation through DCs is key to a prompt memory response. However, in this study I could not differentiate between  $T_{RM}$ ,  $T_{CM}$  and  $T_{EM}$  cells. Nevertheless, under that environment, memory T cell response showed diminished affinity and significantly higher viral titers, suggesting DC-T cell interaction is pivotal. Despite the prompt response of memory CD8 T cells, my results show that DC-T cell interaction is still a key step into the T cell memory response.

Memory T cell protection can occur by either direct interactions<sup>238</sup> with infected epithelium or indirectly by secreting cytokines and chemokines such as IFN $\gamma$ <sup>218</sup>. However, it is still unclear if one or both methods provide protection or lead to immunopathology. Although the goal is to eliminate the virus from the system, direct targeting and killing of all infected epithelial cells often leads to immunopathology<sup>60,183</sup>. Indeed, I found how mice lacking MHC-I in their epithelium (hence, rendering killing of epithelial cells impossible) showed marginally higher viral titers and a better disease outcome as measured by weight loss, as WT mice showed significantly higher weight loss and slower recovery compared to their knock-out counterparts. To note, both memory groups WT and KO were significantly more protected to a secondary lethal influenza infection compared to a naive mouse. These results show that memory T cells provide significant protection to secondary influenza infections, however, a full-fledged T cell response and quick elimination of the virus results in an immunopathology that could be avoided by switching their protective mechanisms to secretion of cytokines and chemokines or modulating their cytotoxicity. These results

provide further clarity in the importance of chemokine and cytokine production as a key signal during recall responses, not only containing the infection but orchestrating the whole response by attracting other cell types to the site of infection. Finally, it has been recently shown how cytotoxic T cells can only kill at a rate of 2-16 virus-infected cells per day<sup>239</sup> and given the limited number of memory T cells in the system, these results further strengthen the necessity of a strong secretory function by memory T cells.

The model I used to study memory T cell response against influenza has some caveats. Mice deficient in  $\beta_2m$  lack surface MHC-I expression and thus the CD8 T cell compartment fails to undergo positive selection in the thymus<sup>196</sup>. Thymic epithelial cells are key in inducing negative selection and participate also in positive selection<sup>240</sup>. However, MHC-expression by bone marrow-derived cells has been shown to be sufficient to mediate positive selection<sup>241</sup>. Although I have seen lower peripheral CD8 T cell numbers in WT- $\rightarrow\beta_2m^{-/-}$  BMx mice, their antigen-specific response to an influenza challenge was comparable to their WT- $\rightarrow$ WT BMx counterparts in terms of T cell expansion, TCR affinity and function, indicating that positive selection of flu-specific T cells took place in WT- $\rightarrow\beta_2m^{-/-}$  BMx mice. Taken together, these results show how WT- $\rightarrow\beta_2m^{-/-}$  chimeras can mount a robust influenza-specific T cell repertoire with similar TCR affinities compared to that of their WT- $\rightarrow$ WT BMx counterparts.

Understanding the dynamics of memory T cell responses and the interplay between their protective functions can be key to not only have a better control of secondary infections in patients but pivotal to the generation of novel vaccines based on memory T cell generation within the lung environment to protect against further influenza infections. Although memory T cells will already be protective, modulating their cytolytic capacity could add significant value to those vaccines that are targeted specially to the most vulnerable, where that extra protection could be key to survival.

My research has provided with a brand new and unparalleled method of lung analysis, allowing for enough precision to successfully determine how activated CD8 T cells can freely migrate to any lung compartment during acute influenza infections, as well as perform similarly on the cytotoxic tests. Finally, I could prove how DC-T cell interactions are key to an efficient control of viral titers in secondary lethal infections and how memory T cell protection is enhanced when T cells cannot directly kill infected targets, thus, potentially reducing immunopathology.

## 7. Bibliography

1. Adams, W. C. Measurement of breathing rate and volume in routinely performed daily activities : final report, contract no. A033-205 /. (The Division, 1993).
2. Sue Walker, Maryann Wood, Jenny Nicol. Mastering Medical Terminology - 2nd Edition. (Elsevier, 2016).
3. Ochs, M. et al. The Number of Alveoli in the Human Lung. *Am. J. Respir. Crit. Care Med.* **169**, 120–124 (2004).
4. Suki, B., Stamenovic, D. & Hubmayr, R. Lung Parenchymal Mechanics. *Compr. Physiol.* **1**, 1317–1351 (2011).
5. Lloyd, C. M. & Marsland, B. J. Lung Homeostasis: Influence of Age, Microbes, and the Immune System. *Immunity* **46**, 549–561 (2017).
6. Weibel, E. R. Lung Cell Biology. in *Comprehensive Physiology* (John Wiley & Sons, Inc., 2011). doi:10.1002/cphy.cp030102.
7. Salgado, C. D., Farr, B. M., Hall, K. K. & Hayden, F. G. Influenza in the acute hospital setting. *Lancet Infect. Dis.* **2**, 145–155 (2002).
8. Bouvier, N. M. & Palese, P. THE BIOLOGY OF INFLUENZA VIRUSES. *Vaccine* **26**, D49–D53 (2008).
9. Petrova, V. N. & Russell, C. A. The evolution of seasonal influenza viruses. *Nat. Rev. Microbiol.* **16**, 47 (2018).
10. McKean, D. et al. Generation of antibody diversity in the immune response of BALB/c mice to influenza virus hemagglutinin. *Proc. Natl. Acad. Sci. U. S. A.* **81**, 3180–3184 (1984).
11. Qi, L. et al. Role of Sialic Acid Binding Specificity of the 1918 Influenza Virus Hemagglutinin Protein in Virulence and Pathogenesis for Mice. *J. Virol.* **83**, 3754–3761 (2009).

12. Wu, W. & Air, G. M. Binding of influenza viruses to sialic acids: reassortant viruses with A/NWS/33 hemagglutinin bind to  $\alpha$ 2,8-linked sialic acid. *Virology* **325**, 340–350 (2004).
13. Samji, T. Influenza A: Understanding the Viral Life Cycle. *Yale J. Biol. Med.* **82**, 153–159 (2009).
14. Skehel, J. J. & Wiley, D. C. Receptor binding and membrane fusion in virus entry: the influenza hemagglutinin. *Annu. Rev. Biochem.* **69**, 531–569 (2000).
15. Baum, L. G. & Paulson, J. C. Sialyloligosaccharides of the respiratory epithelium in the selection of human influenza virus receptor specificity. *Acta Histochem. Suppl.* **40**, 35–38 (1990).
16. Ito, T. et al. Molecular basis for the generation in pigs of influenza A viruses with pandemic potential. *J. Virol.* **72**, 7367–7373 (1998).
17. Lh, P. & Ra, L. The M2 proton channels of influenza A and B viruses. *J. Biol. Chem.* **281**, 8997–9000 (2005).
18. In vitro dissection of the membrane and RNP binding activities of influenza virus M1 protein. - Abstract - Europe PMC.  
<http://europepmc.org/article/MED/11222100>.
19. H, A. et al. Crystal structure of the M1 protein-binding domain of the influenza A virus nuclear export protein (NEP/NS2). *Embo J.* **22**, 4646–4655 (2003).
20. S, B., H, A., Rw, R. & F, B. Nuclear traffic of influenza virus proteins and ribonucleoprotein complexes. *Virus Res.* **124**, 12–21 (2006).
21. Chen, R. & Holmes, E. C. Avian Influenza Virus Exhibits Rapid Evolutionary Dynamics. *Mol. Biol. Evol.* **23**, 2336–2341 (2006).
22. Lamb, R. A. & Krug, R. M. *Orthomyxoviridae: The viruses and their replication.* Fields Virol. (1996).



23. Treanor, J. Influenza vaccine--outmaneuvering antigenic shift and drift. *N. Engl. J. Med.* **350**, 218–220 (2004).
24. Carrat, F. & Flahault, A. Influenza vaccine: the challenge of antigenic drift. *Vaccine* **25**, 6852–6862 (2007).
25. Stambas, J. et al. Killer T cells in influenza. *Pharmacol. Ther.* **120**, 186–196 (2008).
26. Koutsakos, M. et al. Human CD8 + T cell cross-reactivity across influenza A, B and C viruses. *Nat. Immunol.* **20**, 613 (2019).
27. Turley, C. B. et al. Safety and immunogenicity of a recombinant M2e-flagellin influenza vaccine (STF2.4xM2e) in healthy adults. *Vaccine* **29**, 5145–5152 (2011).
28. De Filette, M. et al. Universal influenza A M2e-HBc vaccine protects against disease even in the presence of pre-existing anti-HBc antibodies. *Vaccine* **26**, 6503–6507 (2008).
29. Corti, D. et al. A neutralizing antibody selected from plasma cells that binds to group 1 and group 2 influenza A hemagglutinins. *Science* **333**, 850–856 (2011).
30. Berlanda Scorza, F., Tsvetnitsky, V. & Donnelly, J. J. Universal influenza vaccines: Shifting to better vaccines. *Vaccine* **34**, 2926–2933 (2016).
31. Effros, R. M. Anatomy, development, and physiology of the lungs. *GI Motil.* Online (2006) doi:10.1038/gimo73.
32. Goss, V., Hunt, A. N. & Postle, A. D. Regulation of lung surfactant phospholipid synthesis and metabolism. *Biochim. Biophys. Acta BBA - Mol. Cell Biol. Lipids* **1831**, 448–458 (2013).
33. Benne, C. A. et al. Interactions of Surfactant Protein a with Influenza A Viruses: Binding and Neutralization. *J. Infect. Dis.* **171**, 335–341 (1995).

34. Hartshorn, K. L. et al. Evidence for a protective role of pulmonary surfactant protein D (SP-D) against influenza A viruses. *J. Clin. Invest.* **94**, 311–319 (1994).
35. Hartshorn, K. L. et al. Mechanisms of anti-influenza activity of surfactant proteins A and D: comparison with serum collectins. *Am. J. Physiol.-Lung Cell. Mol. Physiol.* **273**, L1156–L1166 (1997).
36. Hartshorn, K. L. et al. Neutrophil deactivation by influenza A viruses: mechanisms of protection after viral opsonization with collectins and hemagglutination-inhibiting antibodies. *Blood* **87**, 3450–3461 (1996).
37. Ehre, C. et al. Overexpressing mouse model demonstrates the protective role of Muc5ac in the lungs. *Proc. Natl. Acad. Sci. U. S. A.* **109**, 16528–16533 (2012).
38. Hamilton, J. R. et al. Club cells surviving influenza A virus infection induce temporary nonspecific antiviral immunity. *Proc. Natl. Acad. Sci.* **113**, 3861–3866 (2016).
39. Goffic, R. L. et al. Cutting Edge: Influenza A Virus Activates TLR3-Dependent Inflammatory and RIG-I-Dependent Antiviral Responses in Human Lung Epithelial Cells. *J. Immunol.* **178**, 3368–3372 (2007).
40. Slater, L. et al. Co-ordinated Role of TLR3, RIG-I and MDA5 in the Innate Response to Rhinovirus in Bronchial Epithelium. *PLOS Pathog.* **6**, e1001178 (2010).
41. Rintahaka, J., Wiik, D., Kovanen, P. E., Alenius, H. & Matikainen, S. Cytosolic Antiviral RNA Recognition Pathway Activates Caspases 1 and 3. *J. Immunol.* **180**, 1749–1757 (2008).
42. Poeck, H. et al. Recognition of RNA virus by RIG-I results in activation of CARD9 and inflammasome signaling for interleukin 1 $\beta$  production. *Nat. Immunol.* **11**, 63–69 (2010).

43. Yoneyama, M. & Fujita, T. RNA recognition and signal transduction by RIG-I-like receptors. *Immunol. Rev.* **227**, 54–65 (2009).
44. Davis, B. K., Wen, H. & Ting, J. P.-Y. The inflammasome NLRs in immunity, inflammation, and associated diseases. *Annu. Rev. Immunol.* **29**, 707–735 (2011).
45. Lamkanfi, M. Emerging inflammasome effector mechanisms. *Nat. Rev. Immunol.* **11**, 213–220 (2011).
46. Iwasaki, A. & Pillai, P. S. Innate immunity to influenza virus infection. *Nat. Rev. Immunol.* **14**, 315–328 (2014).
47. García-Sastre, A. & Biron, C. A. Type 1 Interferons and the Virus-Host Relationship: A Lesson in Détente. *Science* **312**, 879–882 (2006).
48. McNab, F., Mayer-Barber, K., Sher, A., Wack, A. & O’Garra, A. Type I interferons in infectious disease. *Nat. Rev. Immunol.* **15**, 87–103 (2015).
49. Kim, H. J. et al. Reactive Oxygen Species Induce Antiviral Innate Immune Response through IFN- $\lambda$  Regulation in Human Nasal Epithelial Cells. *Am. J. Respir. Cell Mol. Biol.* **49**, 855–865 (2013).
50. Galani, I. E. et al. Interferon- $\lambda$  Mediates Non-redundant Front-Line Antiviral Protection against Influenza Virus Infection without Compromising Host Fitness. *Immunity* **46**, 875-890.e6 (2017).
51. Wack, A., Terczyńska-Dyla, E. & Hartmann, R. Guarding the frontiers: the biology of type III interferons. *Nat. Immunol.* **16**, 802–809 (2015).
52. Yan, N. & Chen, Z. J. Intrinsic antiviral immunity. *Nat. Immunol.* **13**, 214–222 (2012).
53. Salomon, R. et al. Mx1 gene protects mice against the highly lethal human H5N1 influenza virus. *Cell Cycle Georget. Tex* **6**, 2417–2421 (2007).

54. Pavlovic, J., Haller, O. & Staeheli, P. Human and mouse Mx proteins inhibit different steps of the influenza virus multiplication cycle. *J. Virol.* **66**, 2564–2569 (1992).
55. Brass, A. L. et al. The IFITM proteins mediate cellular resistance to influenza A H1N1 virus, West Nile virus, and dengue virus. *Cell* **139**, 1243–1254 (2009).
56. Feeley, E. M. et al. IFITM3 inhibits influenza A virus infection by preventing cytosolic entry. *PLoS Pathog.* **7**, e1002337 (2011).
57. Pichlmair, A. et al. IFIT1 is an antiviral protein that recognizes 5'-triphosphate RNA. *Nat. Immunol.* **12**, 624–630 (2011).
58. Daffis, S. et al. 2'-O methylation of the viral mRNA cap evades host restriction by IFIT family members. *Nature* **468**, 452–456 (2010).
59. Davidson, S., Crotta, S., McCabe, T. M. & Wack, A. Pathogenic potential of interferon  $\alpha\beta$  in acute influenza infection. *Nat. Commun.* **5**, 3864 (2014).
60. Damjanovic et al. Immunopathology in influenza virus infection: uncoupling the friend from foe.  
<http://www.sciencedirect.com/science/article/pii/S1521661612001416>.
61. Chan, M. C. W. et al. Tropism and Innate Host Responses of the 2009 Pandemic H1N1 Influenza Virus in ex Vivo and in Vitro Cultures of Human Conjunctiva and Respiratory Tract. *Am. J. Pathol.* **176**, 1828–1840 (2010).
62. Lam, W., Yeung, A. C., Chu, I. M. & Chan, P. K. Profiles of cytokine and chemokine gene expression in human pulmonary epithelial cells induced by human and avian influenza viruses. *Virol. J.* **7**, 344 (2010).
63. Epithelial-derived TGF- $\beta$ 1 acts as a pro-viral factor in the lung during influenza A infection | *Mucosal Immunology*. <https://www.nature.com/articles/mi201777>.
64. Dinarello, C. A. Immunological and Inflammatory Functions of the Interleukin-1 Family. *Annu. Rev. Immunol.* **27**, 519–550 (2009).

65. Tamaru Masahiro et al. Interleukin-1 $\beta$  Induces Tissue- and Cell Type–Specific Expression of Adhesion Molecules In Vivo. *Arterioscler. Thromb. Vasc. Biol.* **18**, 1292–1303 (1998).
66. Barlow, P. G. et al. Antiviral Activity and Increased Host Defense against Influenza Infection Elicited by the Human Cathelicidin LL-37. *PLOS ONE* **6**, e25333 (2011).
67. Tripathi, S. et al. The human cathelicidin LL-37 inhibits influenza A viruses through a mechanism distinct from that of surfactant protein D or defensins. *J. Gen. Virol.* **94**, 40–49 (2013).
68. Hussell, T. & Bell, T. J. Alveolar macrophages: plasticity in a tissue-specific context. *Nat. Rev. Immunol.* **14**, 81–93 (2014).
69. Joshi, N., Walter, J. M. & Misharin, A. V. Alveolar Macrophages. *Cell. Immunol.* **330**, 86–90 (2018).
70. Pérez-Arellano, J. L., Alcázar-Montero, M. C. & Jiménez-López, A. Alveolar macrophage: origin, kinetics and relationship with cells of the alveolo-interstitial region. *Allergol. Immunopathol. (Madr.)* **18**, 175–183 (1990).
71. Jayasekera, J. P., Vinuesa, C. G., Karupiah, G. & King, N. J. C. Enhanced antiviral antibody secretion and attenuated immunopathology during influenza virus infection in nitric oxide synthase-2-deficient mice. *J. Gen. Virol.* **87**, 3361–3371 (2006).
72. Jong, M. D. de et al. Fatal outcome of human influenza A (H5N1) is associated with high viral load and hypercytokinemia. *Nat. Med.* **12**, 1203 (2006).
73. He, W. et al. Alveolar macrophages are critical for broadly-reactive antibody-mediated protection against influenza A virus in mice. *Nat. Commun.* **8**, 846 (2017).

74. Schwab, A. J., Salamand, A., Merhi, Y., Simard, A. & Dupuis, J. Kinetic analysis of pulmonary neutrophil retention in vivo using the multiple-indicator-dilution technique. *J. Appl. Physiol. Bethesda Md* 1985 **95**, 279–291 (2003).
75. Hogg, J. C., Doerschuk, C. M., Wiggs, B. & Minshall, D. Neutrophil retention during a single transit through the pulmonary circulation. *J. Appl. Physiol. Bethesda Md* 1985 **73**, 1683–1685 (1992).
76. Dimasi, D., Sun, W. Y. & Bonder, C. S. Neutrophil interactions with the vascular endothelium. *Int. Immunopharmacol.* **17**, 1167–1175 (2013).
77. Downey, G. P. & Worthen, G. S. Neutrophil retention in model capillaries: deformability, geometry, and hydrodynamic forces. *J. Appl. Physiol.* **65**, 1861–1871 (1988).
78. Lien, D. C. et al. Physiological neutrophil sequestration in the lung: visual evidence for localization in capillaries. *J. Appl. Physiol. Bethesda Md* 1985 **62**, 1236–1243 (1987).
79. Yoder, M. C. et al. Pulmonary microcirculatory kinetics of neutrophils deficient in leukocyte adhesion-promoting glycoproteins. *J. Appl. Physiol. Bethesda Md* 1985 **69**, 207–213 (1990).
80. Doyle, N. A. et al. Neutrophil margination, sequestration, and emigration in the lungs of L-selectin-deficient mice. *J. Clin. Invest.* **99**, 526–533 (1997).
81. Tate, M. D. et al. The Role of Neutrophils during Mild and Severe Influenza Virus Infections of Mice. *PLOS ONE* **6**, e17618 (2011).
82. Camp, J. V. & Jonsson, C. B. A Role for Neutrophils in Viral Respiratory Disease. *Front. Immunol.* **8**, 550 (2017).
83. Lim, K. et al. Neutrophil trails guide influenza-specific CD8<sup>+</sup> T cells in the airways. *Science* **349**, aaa4352 (2015).

84. Tate, M. D. et al. Neutrophils Ameliorate Lung Injury and the Development of Severe Disease during Influenza Infection. *J. Immunol.* **183**, 7441–7450 (2009).
85. Narasaraju, T. et al. Excessive Neutrophils and Neutrophil Extracellular Traps Contribute to Acute Lung Injury of Influenza Pneumonitis. *Am. J. Pathol.* **179**, 199–210 (2011).
86. Hartshorn, K. L., Daigneault, D. E., White, M. R. & Tauber, A. I. Anomalous features of human neutrophil activation by influenza A virus are shared by related viruses and sialic acid-binding lectins. *J. Leukoc. Biol.* **51**, 230–236 (1992).
87. Saffarzadeh, M. et al. Neutrophil Extracellular Traps Directly Induce Epithelial and Endothelial Cell Death: A Predominant Role of Histones. *PLOS ONE* **7**, e32366 (2012).
88. Banchereau, J. et al. Immunobiology of dendritic cells. *Annu Rev Immunol* **18**, 767–811 (2000).
89. Lauvau, G. & Soudja, S. M. MECHANISMS OF MEMORY T CELL ACTIVATION AND EFFECTIVE IMMUNITY. *Adv. Exp. Med. Biol.* **850**, 73–80 (2015).
90. Stockwin, L. H., McGonagle, D., Martin, I. G. & Blair, G. E. Dendritic cells: immunological sentinels with a central role in health and disease. *Immunol. Cell Biol.* **78**, 91–102 (2000).
91. Marsland, B. J. et al. CCL19 and CCL21 induce a potent proinflammatory differentiation program in licensed dendritic cells. *Immunity* **22**, 493–505 (2005).
92. Förster, R. et al. CCR7 coordinates the primary immune response by establishing functional microenvironments in secondary lymphoid organs. *Cell* **99**, 23–33 (1999).

93. Brown, F. D. & Turley, S. J. Fibroblastic Reticular Cells: Organization and Regulation of the T Lymphocyte Life Cycle. *J. Immunol. Baltim. Md* 1950 **194**, 1389–1394 (2015).
94. Fletcher, A. L., Acton, S. E. & Knoblich, K. Lymph node fibroblastic reticular cells in health and disease. *Nat. Rev. Immunol.* **15**, 350–361 (2015).
95. Brown, D. M., Román, E. & Swain, S. L. CD4 T cell responses to influenza infection. *Semin. Immunol.* **16**, 171–177 (2004).
96. Eichelberger, M., Allan, W., Zijlstra, M., Jaenisch, R. & Doherty, P. C. Clearance of influenza virus respiratory infection in mice lacking class I major histocompatibility complex-restricted CD8+ T cells. *J. Exp. Med.* **174**, (1991).
97. Bender, B. S., Croghan, T., Zhang, L. & Small, P. A. Transgenic mice lacking class I major histocompatibility complex-restricted T cells have delayed viral clearance and increased mortality after influenza virus challenge. *J. Exp. Med.* (1992).
98. Topham, D. J. & Doherty, P. C. Clearance of an Influenza A Virus by CD4+ T Cells Is Inefficient in the Absence of B Cells. *J. Virol.* **72**, 882–885 (1998).
99. Topham, D. J., Tripp, R. A., Hamilton-Easton, A. M., Sarawar, S. R. & Doherty, P. C. Quantitative analysis of the influenza virus-specific CD4+ T cell memory in the absence of B cells and Ig. *J. Immunol. Baltim. Md* 1950 **157**, 2947–2952 (1996).
100. Topham, D. J., Tripp, R. A. & Doherty, P. C. CD8+ T cells clear influenza virus by perforin or Fas-dependent processes. *J. Immunol. Baltim. Md* 1950 **159**, 5197–5200 (1997).
101. Wells, M. A., Albrecht, P. & Ennis, F. A. Recovery from a viral respiratory infection. I. Influenza pneumonia in normal and T-deficient mice. *J. Immunol. Baltim. Md* 1950 **126**, 1036–1041 (1981).



102. Qi, Q. et al. Diversity and clonal selection in the human T-cell repertoire. *Proc. Natl. Acad. Sci. U. S. A.* **111**, 13139–13144 (2014).
103. Huang, J. et al. Detection, phenotyping, and quantification of antigen-specific T cells using a peptide-MHC dodecamer. *Proc. Natl. Acad. Sci. U. S. A.* **113**, E1890–E1897 (2016).
104. Bousso, P. & Robey, E. Dynamics of CD8+ T cell priming by dendritic cells in intact lymph nodes. *Nat. Immunol.* **4**, 579–585 (2003).
105. Mandl, J. N. et al. Quantification of lymph node transit times reveals differences in antigen surveillance strategies of naïve CD4+ and CD8+ T cells. *Proc. Natl. Acad. Sci.* **109**, 18036–18041 (2012).
106. van Montfoort, N., van der Aa, E. & Woltman, A. M. Understanding MHC class I presentation of viral antigens by human dendritic cells as a basis for rational design of therapeutic vaccines. *Front. Immunol.* **5**, 182 (2014).
107. Rinaldo, C. R. & Piazza, P. Virus infection of dendritic cells: portal for host invasion and host defense. *Trends Microbiol.* **12**, 337–345 (2004).
108. Gutiérrez-Martínez, E. et al. Cross-Presentation of Cell-Associated Antigens by MHC Class I in Dendritic Cell Subsets. *Front. Immunol.* **6**, 363 (2015).
109. Joffre, O. P., Segura, E., Savina, A. & Amigorena, S. Cross-presentation by dendritic cells. *Nat Rev Immunol* **12**, 557–69 (2012).
110. Burgdorf, S., Schölz, C., Kautz, A., Tampé, R. & Kurts, C. Spatial and mechanistic separation of cross-presentation and endogenous antigen presentation. *Nat. Immunol.* **9**, 558–566 (2008).
111. Cresswell, P., Ackerman, A. L., Giodini, A., Peaper, D. R. & Wearsch, P. A. Mechanisms of MHC class I-restricted antigen processing and cross-presentation. *Immunol Rev* **207**, 145–57 (2005).

112. Helft, J. et al. Cross-presenting CD103+ dendritic cells are protected from influenza virus infection. *J. Clin. Invest.* **122**, 4037–4047 (2012).
113. Wu, N.-H. et al. The differentiated airway epithelium infected by influenza viruses maintains the barrier function despite a dramatic loss of ciliated cells. *Sci. Rep.* **6**, 39668 (2016).
114. Rocha, N. & Neefjes, J. MHC class II molecules on the move for successful antigen presentation. *EMBO J.* **27**, 1–5 (2008).
115. Flynn, K. J. et al. Virus-Specific CD8+ T Cells in Primary and Secondary Influenza Pneumonia. *Immunity* **8**, 683–691 (1998).
116. Wiesel, M., Walton, S., Richter, K. & Oxenius, A. Virus-specific CD8 T cells: activation, differentiation and memory formation. *APMIS Acta Pathol. Microbiol. Immunol. Scand.* **117**, 356–381 (2009).
117. Chambers, C. A. & Allison, J. P. Costimulatory regulation of T cell function. *Curr. Opin. Cell Biol.* **11**, 203–210 (1999).
118. Doyle, A. M. et al. Induction of cytotoxic T lymphocyte antigen 4 (CTLA-4) restricts clonal expansion of helper T cells. *J Exp Med* **194**, 893–902 (2001).
119. Tivol, E. A. et al. Loss of CTLA-4 leads to massive lymphoproliferation and fatal multiorgan tissue destruction, revealing a critical negative regulatory role of CTLA-4. *Immunity* **3**, 541–547 (1995).
120. Roifman, C. M. & Grunebaum, E. 35 - Primary T-cell immunodeficiencies. in *Clinical Immunology (Fourth Edition)* (eds. Rich, R. R. et al.) 437–453 (Content Repository Only!, 2013). doi:10.1016/B978-0-7234-3691-1.00052-0.
121. Henry, C. J., Ornelles, D. A., Mitchell, L. M., Brzoza-Lewis, K. L. & Hiltbold, E. M. IL-12 produced by dendritic cells augments CD8+ T cell activation through the production of the chemokines CCL1 and CCL17. *J. Immunol. Baltim. Md 1950* **181**, 8576–8584 (2008).

122. Schroder, K., Hertzog, P. J., Ravasi, T. & Hume, D. A. Interferon- $\gamma$ : an overview of signals, mechanisms and functions. *J. Leukoc. Biol.* **75**, 163–189 (2004).
123. Luckheeram, R. V., Zhou, R., Verma, A. D. & Xia, B. CD4(+)T cells: differentiation and functions. *Clin Dev Immunol* **2012**, 925135 (2012).
124. Yoo, J.-K., Kim, T. S., Hufford, M. M. & Braciale, T. J. Viral infection of the lung: Host response and sequelae. *J. Allergy Clin. Immunol.* **132**, 1263–1276 (2013).
125. Benechet, A. P. et al. T cell-intrinsic S1PR1 regulates endogenous effector T-cell egress dynamics from lymph nodes during infection. *Proc. Natl. Acad. Sci. U. S. A.* **113**, 2182–2187 (2016).
126. Kang, B. H., Manderschied, B. D., Huang, Y. C., Crapo, J. D. & Chang, L. Y. Contrasting response of lung parenchymal cells to instilled TNF alpha and IFN gamma: the inducibility of specific cell ICAM-1 in vivo. *Am. J. Respir. Cell Mol. Biol.* **15**, 540–550 (1996).
127. Pober, J. S. et al. Two distinct monokines, interleukin 1 and tumor necrosis factor, each independently induce biosynthesis and transient expression of the same antigen on the surface of cultured human vascular endothelial cells. *J. Immunol. Baltim. Md 1950* **136**, 1680–1687 (1986).
128. Dustin, M. L., Rothlein, R., Bhan, A. K., Dinarello, C. A. & Springer, T. A. Induction by IL 1 and interferon-gamma: tissue distribution, biochemistry, and function of a natural adherence molecule (ICAM-1). *J. Immunol. Baltim. Md 1950* **137**, 245–254 (1986).
129. Slütter, B., Pewe, L. L., Kaech, S. M. & Harty, J. T. Lung Airway-Surveilling CXCR3hi Memory CD8+ T Cells Are Critical for Protection against Influenza A Virus. *Immunity* **39**, 939–948 (2013).

130. Mikhak, Z., Strassner, J. P. & Luster, A. D. Lung dendritic cells imprint T cell lung homing and promote lung immunity through the chemokine receptor CCR4. *J. Exp. Med.* **210**, 1855–1869 (2013).
131. Barry, M. & Bleackley, R. C. Cytotoxic T lymphocytes: all roads lead to death. *Nat. Rev. Immunol.* **2**, 401–409 (2002).
132. Lopez, J. A. et al. Perforin forms transient pores on the target cell plasma membrane to facilitate rapid access of granzymes during killer cell attack. *Blood* **121**, 2659–2668 (2013).
133. Brincks, E. L., Katewa, A., Kucaba, T. A., Griffith, T. S. & Legge, K. L. CD8 T cells utilize TNF-related apoptosis-inducing ligand (TRAIL) to control influenza virus infection. *J. Immunol. Baltim. Md 1950* **181**, 4918–4925 (2008).
134. Hassin, D., Garber, O. G., Meiraz, A., Schiffenbauer, Y. S. & Berke, G. Cytotoxic T lymphocyte perforin and Fas ligand working in concert even when Fas ligand lytic action is still not detectable. *Immunology* **133**, 190–6 (2011).
135. Trapani, J. A. & Smyth, M. J. Functional significance of the perforin/granzyme cell death pathway. *Nat. Rev. Immunol.* **2**, 735–747 (2002).
136. Metkar, S. S. et al. Granzyme B activates procaspase-3 which signals a mitochondrial amplification loop for maximal apoptosis. *J. Cell Biol.* **160**, 875–885 (2003).
137. Sutton, V. R. et al. Initiation of apoptosis by granzyme B requires direct cleavage of bid, but not direct granzyme B-mediated caspase activation. *J. Exp. Med.* **192**, 1403–1414 (2000).
138. Falschlehner, C., Schaefer, U. & Walczak, H. Following TRAIL's path in the immune system. *Immunology* **127**, 145–154 (2009).

139. Dockrell, D. H. The multiple roles of Fas ligand in the pathogenesis of infectious diseases. *Clin. Microbiol. Infect. Off. Publ. Eur. Soc. Clin. Microbiol. Infect. Dis.* **9**, 766–779 (2003).
140. Lowin, B., Hahne, M., Mattmann, C. & Tschopp, J. Cytolytic T-cell cytotoxicity is mediated through perforin and Fas lytic pathways. *Nature* **370**, 650–652 (1994).
141. Kaech, S. M., Wherry, E. J. & Ahmed, R. Effector and memory T-cell differentiation: implications for vaccine development. *Nat. Rev. Immunol.* **2**, 251–262 (2002).
142. Badovinac, V. P., Porter, B. B. & Harty, J. T. Programmed contraction of CD8(+) T cells after infection. *Nat. Immunol.* **3**, 619–626 (2002).
143. Hamann, D. et al. Phenotypic and functional separation of memory and effector human CD8+ T cells. *J. Exp. Med.* **186**, 1407–1418 (1997).
144. Chen, Y., Zander, R., Khatun, A., Schauder, D. M. & Cui, W. Transcriptional and Epigenetic Regulation of Effector and Memory CD8 T Cell Differentiation. *Front. Immunol.* **9**, (2018).
145. Laidlaw, B. J., Craft, J. E. & Kaech, S. M. The multifaceted role of CD4(+) T cells in CD8(+) T cell memory. *Nat. Rev. Immunol.* **16**, 102–111 (2016).
146. Gebhardt, T. & Mackay, L. K. Local immunity by tissue-resident CD8(+) memory T cells. *Front. Immunol.* **3**, 340 (2012).
147. Sallusto, F., Geginat, J. & Lanzavecchia, A. Central Memory and Effector Memory T Cell Subsets: Function, Generation, and Maintenance. *Annu. Rev. Immunol.* **22**, 745–763 (2004).
148. Das, A. et al. Effector/memory CD4 T cells making either Th1 or Th2 cytokines commonly co-express T-bet and GATA-3. *PLoS ONE* **12**, (2017).

149. Mueller, S. N., Gebhardt, T., Carbone, F. R. & Heath, W. R. Memory T cell subsets, migration patterns, and tissue residence. *Annu. Rev. Immunol.* **31**, 137–161 (2013).
150. Liu, L. et al. Epidermal injury and infection during poxvirus immunization is crucial for the generation of highly protective T cell-mediated immunity. *Nat. Med.* **16**, 224–227 (2010).
151. Clark, R. A. et al. Skin effector memory T cells do not recirculate and provide immune protection in alemtuzumab-treated CTCL patients. *Sci. Transl. Med.* **4**, 117ra7 (2012).
152. Turner, D. L. et al. Lung niches for the generation and maintenance of tissue-resident memory T cells. *Mucosal Immunol.* **7**, 501–510 (2014).
153. Anderson, K. G. et al. Cutting edge: intravascular staining redefines lung CD8 T cell responses. *J. Immunol. Baltim. Md 1950* **189**, 2702–2706 (2012).
154. Takamura, S. et al. Specific niches for lung-resident memory CD8<sup>+</sup> T cells at the site of tissue regeneration enable CD69-independent maintenance. *J. Exp. Med.* [jem.20160938](https://doi.org/10.1084/jem.20160938) (2016) doi:10.1084/jem.20160938.
155. Mackay, L. K. et al. Long-lived epithelial immunity by tissue-resident memory T (TRM) cells in the absence of persisting local antigen presentation. *Proc. Natl. Acad. Sci. U. S. A.* **109**, 7037–7042 (2012).
156. Shin, H. & Iwasaki, A. A vaccine strategy that protects against genital herpes by establishing local memory T cells. *Nature* **491**, 463–467 (2012).
157. Wakim, L. M., Woodward-Davis, A. & Bevan, M. J. Memory T cells persisting within the brain after local infection show functional adaptations to their tissue of residence. *Proc. Natl. Acad. Sci. U. S. A.* **107**, 17872–17879 (2010).

158. Masopust, D., Vezys, V., Wherry, E. J., Barber, D. L. & Ahmed, R. Cutting edge: gut microenvironment promotes differentiation of a unique memory CD8 T cell population. *J. Immunol. Baltim. Md 1950* **176**, 2079–2083 (2006).
159. Masopust, D. et al. Dynamic T cell migration program provides resident memory within intestinal epithelium. *J. Exp. Med.* **207**, 553–564 (2010).
160. Hadley, G. A., Bartlett, S. T., Via, C. S., Rostapshova, E. A. & Moainie, S. The epithelial cell-specific integrin, CD103 (alpha E integrin), defines a novel subset of alloreactive CD8+ CTL. *J. Immunol.* **159**, 3748–3756 (1997).
161. Skon, C. N. et al. Transcriptional downregulation of S1pr1 is required for the establishment of resident memory CD8+ T cells. *Nat. Immunol.* **14**, 1285–1293 (2013).
162. Fonseca, R. et al. Developmental plasticity allows outside-in immune responses by resident memory T cells. *Nat. Immunol.* **21**, 412–421 (2020).
163. Buchholz, V. R., Schumacher, T. N. M. & Busch, D. H. T Cell Fate at the Single-Cell Level. *Annu. Rev. Immunol.* **34**, null (2016).
164. Barber, D. L., Wherry, E. J. & Ahmed, R. Cutting edge: rapid in vivo killing by memory CD8 T cells. *J. Immunol. Baltim. Md 1950* **171**, 27–31 (2003).
165. Kersh, E. N. et al. Rapid demethylation of the IFN-gamma gene occurs in memory but not naive CD8 T cells. *J. Immunol. Baltim. Md 1950* **176**, 4083–4093 (2006).
166. Chang, J. T. et al. Asymmetric T Lymphocyte Division in the Initiation of Adaptive Immune Responses. *Science* **315**, 1687–1691 (2007).
167. King, C. G. et al. T Cell Affinity Regulates Asymmetric Division, Effector Cell Differentiation, and Tissue Pathology. *Immunity* **37**, 709–720 (2012).

168. Tan, J. T. et al. Interleukin (IL)-15 and IL-7 jointly regulate homeostatic proliferation of memory phenotype CD8<sup>+</sup> cells but are not required for memory phenotype CD4<sup>+</sup> cells. *J. Exp. Med.* **195**, 1523–1532 (2002).
169. Lau, L. L., Jamieson, B. D., Somasundaram, T. & Ahmed, R. Cytotoxic T-cell memory without antigen. *Nature* **369**, 648–652 (1994).
170. Macallan, D. C., Borghans, J. A. M. & Asquith, B. Human T Cell Memory: A Dynamic View. *Vaccines* **5**, 5 (2017).
171. Schenkel, J. M. & Masopust, D. Tissue-resident memory T cells. *Immunity* **41**, 886–897 (2014).
172. Mueller, S. N. & Mackay, L. K. Tissue-resident memory T cells: local specialists in immune defence. *Nat. Rev. Immunol.* **16**, 79–89 (2016).
173. Park, S. L. et al. Local proliferation maintains a stable pool of tissue-resident memory T cells after antiviral recall responses. *Nat. Immunol.* **19**, 183 (2018).
174. Park, S. L. et al. Tissue-resident memory CD8<sup>+</sup> T cells promote melanoma-immune equilibrium in skin. *Nature* **565**, 366–371 (2019).
175. Qi, H., Egen, J. G., Huang, A. Y. C. & Germain, R. N. Extrafollicular activation of lymph node B cells by antigen-bearing dendritic cells. *Science* **312**, 1672–1676 (2006).
176. Boyden, A. W., Legge, K. L. & Waldschmidt, T. J. Pulmonary infection with influenza A virus induces site-specific germinal center and T follicular helper cell responses. *PloS One* **7**, e40733 (2012).
177. Nutt, S. L. & Tarlinton, D. M. Germinal center B and follicular helper T cells: siblings, cousins or just good friends? *Nat. Immunol.* **12**, 472–477 (2011).
178. McHeyzer-Williams, M., Okitsu, S., Wang, N. & McHeyzer-Williams, L. Molecular programming of B cell memory. *Nat. Rev. Immunol.* **12**, 24–34 (2011).



179. Cerutti, A. The regulation of IgA class switching. *Nat. Rev. Immunol.* **8**, 421–434 (2008).
180. Krammer, F. The human antibody response to influenza A virus infection and vaccination. *Nat. Rev. Immunol.* **19**, 383–397 (2019).
181. Perrone, L. A., Plowden, J. K., García-Sastre, A., Katz, J. M. & Tumpey, T. M. H5N1 and 1918 Pandemic Influenza Virus Infection Results in Early and Excessive Infiltration of Macrophages and Neutrophils in the Lungs of Mice. *PLoS Pathog.* **4**, (2008).
182. Duan, S. & Thomas, P. G. Balancing Immune Protection and Immune Pathology by CD8(+) T-Cell Responses to Influenza Infection. *Front. Immunol.* **7**, 25 (2016).
183. Xu, L. et al. Cutting edge: pulmonary immunopathology mediated by antigen-specific expression of TNF-alpha by antiviral CD8+ T cells. *J. Immunol. Baltim. Md 1950* **173**, 721–725 (2004).
184. Barré-Sinoussi, F. & Montagutelli, X. Animal models are essential to biological research: issues and perspectives. *Future Sci. OA* **1**, (2015).
185. Bouvier, N. M. & Lowen, A. C. Animal Models for Influenza Virus Pathogenesis and Transmission. *Viruses* **2**, 1530–1563 (2010).
186. Maher, J. A. & DeStefano, J. The Ferret: An Animal Model to Study Influenza Virus. *Lab Anim.* **33**, 50–53.
187. Rodriguez, L., Nogales, A. & Martínez-Sobrido, L. Influenza A Virus Studies in a Mouse Model of Infection. *J. Vis. Exp. JoVE* (2017) doi:10.3791/55898.
188. Perlman, R. L. Mouse models of human disease. *Evol. Med. Public Health* **2016**, 170–176 (2016).
189. Blazejewska, P. et al. Pathogenicity of different PR8 influenza A virus variants in mice is determined by both viral and host factors. *Virology* **412**, 36–45 (2011).

190. Garulli, B., Di Mario, G., Sciaraffia, E., Kawaoka, Y. & Castrucci, M. R. Immunogenicity of a Recombinant Influenza Virus Bearing Both the CD4+ and CD8+ T Cell Epitopes of Ovalbumin. *J. Biomed. Biotechnol.* **2011**, (2011).
191. Kilbourne, E. D. Future influenza vaccines and the use of genetic recombinants. *Bull. World Health Organ.* **41**, 643–645 (1969).
192. Mardiney, M. & Malech, H. L. Enhanced engraftment of hematopoietic progenitor cells in mice treated with granulocyte colony-stimulating factor before low-dose irradiation: implications for gene therapy. *Blood* **87**, 4049–4056 (1996).
193. Hogquist, K. A. et al. T cell receptor antagonist peptides induce positive selection. *Cell* **76**, 17–27 (1994).
194. Hancock, W. W. et al. Requirement of the Chemokine Receptor CXCR3 for Acute Allograft Rejection. *J. Exp. Med.* **192**, 1515–1520 (2000).
195. Trowbridge, I. S. & Mazauskas, C. Immunological properties of murine thymus-dependent lymphocyte surface glycoproteins. *Eur J Immunol* **6**, 557–62 (1976).
196. Zijlstra, M. et al. Beta 2-microglobulin deficient mice lack CD4-8+ cytolytic T cells. *Nature* **344**, 742–746 (1990).
197. Hochweller, K., Striegler, J., Hämmerling, G. J. & Garbi, N. A novel CD11c.DTR transgenic mouse for depletion of dendritic cells reveals their requirement for homeostatic proliferation of natural killer cells. *Eur. J. Immunol.* **38**, 2776–2783 (2008).
198. Kastenmüller, W. et al. Peripheral pre-positioning and local CXCL9 chemokine-mediated guidance orchestrate rapid memory CD8+ T cell responses in the lymph node. *Immunity* **38**, 502–513 (2013).
199. Holland, T. et al. Rescue of T-cell function during persistent pulmonary adenoviral infection by Toll-like receptor 9 activation. *J. Allergy Clin. Immunol.* (2017) doi:<https://doi.org/10.1016/j.jaci.2017.06.048>.

200. Ewart, S. L., Gavett, S. H., Margolick, J. & Wills-Karp, M. Cyclosporin A attenuates genetic airway hyperresponsiveness in mice but not through inhibition of CD4+ or CD8+ T cells. *Am. J. Respir. Cell Mol. Biol.* **14**, 627–634 (1996).
201. Höglund, P. et al. Recognition of beta 2-microglobulin-negative (beta 2m-) T-cell blasts by natural killer cells from normal but not from beta 2m- mice: nonresponsiveness controlled by beta 2m- bone marrow in chimeric mice. *Proc. Natl. Acad. Sci.* **88**, 10332–10336 (1991).
202. Anderson, K. G. et al. Intravascular staining for discrimination of vascular and tissue leukocytes. *Nat. Protoc.* **9**, 209–222 (2014).
203. Miloud, T., Fiegler, N., Suffner, J., Hämmerling, G. J. & Garbi, N. Organ-specific cellular requirements for in vivo dendritic cell generation. *J. Immunol. Baltim. Md* 1950 **188**, 1125–1135 (2012).
204. Kedzierska, K. et al. Quantification of Repertoire Diversity of Influenza-Specific Epitopes with Predominant Public or Private TCR Usage. *J. Immunol.* **177**, 6705–6712 (2006).
205. Feuerer, M. et al. Bone marrow as a priming site for T-cell responses to blood-borne antigen. *Nat. Med.* **9**, 1151–1157 (2003).
206. Einfeld, A. J., Neumann, G. & Kawaoka, Y. Influenza A Virus Isolation, Culture and Identification. *Nat. Protoc.* **9**, 2663–2681 (2014).
207. Brandes, M., Klauschen, F., Kuchen, S. & Germain, R. N. A Systems Analysis Identifies a Feed-forward Inflammatory Circuit Leading to Lethal Influenza Infection. *Cell* **154**, 197–212 (2013).
208. Topham, D. J., Castrucci, M. R., Wingo, F. S., Belz, G. T. & Doherty, P. C. The Role of Antigen in the Localization of Naive, Acutely Activated, and Memory

- CD8+ T Cells to the Lung During Influenza Pneumonia. *J. Immunol.* **167**, 6983–6990 (2001).
209. Vento-Asturias, S. Differential in vivo labelling for precise analysis of immune cell trafficking during viral infection in the lung- MS.C thesis.
210. Hufford, M. M., Kim, T. S., Sun, J. & Braciale, T. J. The Effector T Cell Response to Influenza Infection. *Curr. Top. Microbiol. Immunol.* **386**, 423–455 (2015).
211. Butz, E. A. & Bevan, M. J. Massive Expansion of Antigen-Specific CD8+ T Cells during an Acute Virus Infection. *Immunity* **8**, 167–175 (1998).
212. Chiu, C. & Openshaw, P. J. Antiviral B cell and T cell immunity in the lungs. *Nat. Immunol.* **16**, 18–26 (2015).
213. Brown, D. M., Dilzer, A. M., Meents, D. L. & Swain, S. L. CD4 T Cell-Mediated Protection from Lethal Influenza: Perforin and Antibody-Mediated Mechanisms Give a One-Two Punch. *J. Immunol.* **177**, 2888–2898 (2006).
214. Brown, D. M., Lampe, A. T. & Workman, A. M. The Differentiation and Protective Function of Cytolytic CD4 T Cells in Influenza Infection. *Front. Immunol.* **7**, (2016).
215. Baccam, P., Beauchemin, C., Macken, C. A., Hayden, F. G. & Perelson, A. S. Kinetics of Influenza A Virus Infection in Humans. *J. Virol.* **80**, 7590–7599 (2006).
216. Schenkel, J. M. et al. Resident memory CD8 T cells trigger protective innate and adaptive immune responses. *Science* **346**, 98–101 (2014).
217. Sckisel, G. D. et al. Influenza infection results in local expansion of memory CD8 +T cells with antigen non-specific phenotype and function. *Clin. Exp. Immunol.* **175**, 79–91 (2013).
218. McMaster, S. R., Wilson, J. J., Wang, H. & Kohlmeier, J. E. Airway-Resident Memory CD8 T Cells Provide Antigen-Specific Protection against Respiratory

- Virus Challenge through Rapid IFN- $\gamma$  Production. *J. Immunol.* **195**, 203–209 (2015).
219. Urdahl, K. B., Sun, J. C. & Bevan, M. J. Positive selection of MHC class Ib–restricted CD8<sup>+</sup> T cells on hematopoietic cells. *Nat. Immunol.* **3**, 772 (2002).
220. Zerrahn, J. et al. Class I MHC molecules on hematopoietic cells can support intrathymic positive selection of T cell receptor transgenic T cells. *Proc. Natl. Acad. Sci.* **96**, 11470–11475 (1999).
221. Holl, E. K. Generation of Bone Marrow and Fetal Liver Chimeric Mice. *Methods Mol. Biol. Clifton NJ* **1032**, 315–321 (2013).
222. Zammit, D. J., Cauley, L. S., Pham, Q.-M. & Lefrançois, L. Dendritic Cells Maximize the Memory CD8 T Cell Response to Infection. *Immunity* **22**, 561–570 (2005).
223. Mozdzanowska, K., Maiese, K. & Gerhard, W. Th Cell-Deficient Mice Control Influenza Virus Infection More Effectively Than Th- and B Cell-Deficient Mice: Evidence for a Th-Independent Contribution by B Cells to Virus Clearance. *J. Immunol.* **164**, 2635–2643 (2000).
224. Regner, M. et al. Cutting Edge: Rapid and Efficient In Vivo Cytotoxicity by Cytotoxic T Cells Is Independent of Granzymes A and B. *J. Immunol.* **183**, 37–40 (2009).
225. Weninger, W., Manjunath, N. & von Andrian, U. H. Migration and differentiation of CD8<sup>+</sup> T cells. *Immunol. Rev.* **186**, 221–233 (2002).
226. Galkina, E. Preferential migration of effector CD8<sup>+</sup> T cells into the interstitium of the normal lung. *J. Clin. Invest.* **115**, 3473–3483 (2005).
227. Ronen Alon et al. Leukocyte trafficking to the lungs and beyond: lessons from influenza for COVID-19. *Nat Rev Immunol* (In Press).

228. Griffith, J. W., Sokol, C. L. & Luster, A. D. Chemokines and Chemokine Receptors: Positioning Cells for Host Defense and Immunity. [Httpdxdoiorg101146annurev-Immunol-032713-120145](http://dx.doi.org/10.1146/annurev-immunol-032713-120145).
229. Harris, N. L., Watt, V., Ronchese, F. & Le Gros, G. Differential T cell function and fate in lymph node and nonlymphoid tissues. *J. Exp. Med.* **195**, 317–326 (2002).
230. Hogan, R. J. et al. Long-term maintenance of virus-specific effector memory CD8<sup>+</sup> T cells in the lung airways depends on proliferation. *J. Immunol. Baltim. Md 1950* **169**, 4976–4981 (2002).
231. Odoardi, F. et al. T cells become licensed in the lung to enter the central nervous system. *Nature* **488**, 675–679 (2012).
232. Vogel, C. & Marcotte, E. M. Insights into the regulation of protein abundance from proteomic and transcriptomic analyses. *Nat. Rev. Genet.* **13**, 227–232 (2012).
233. Scherle, P. A., Palladino, G. & Gerhard, W. Mice can recover from pulmonary influenza virus infection in the absence of class I-restricted cytotoxic T cells. *J. Immunol.* **148**, 212–217 (1992).
234. McCormick, S. et al. Control of Pathogenic CD4 T Cells and Lethal Immunopathology by Signaling Immuno adaptor DAP12 during Influenza Infection. *J. Immunol.* **187**, 4280–4292 (2011).
235. Mozdzanowska, K., Furchner, M., Maiese, K. & Gerhard, W. CD4<sup>+</sup>T Cells Are Ineffective in Clearing a Pulmonary Infection with Influenza Type A Virus in the Absence of B Cells. *Virology* **239**, 217–225 (1997).
236. Graham, M. B. & Braciale, T. J. Resistance to and Recovery from Lethal Influenza Virus Infection in B Lymphocyte-deficient Mice. *J. Exp. Med.* **186**, 2063–2068 (1997).

237. Berg, R. E., Crossley, E., Murray, S. & Forman, J. Memory CD8<sup>+</sup> T cells provide innate immune protection against *Listeria monocytogenes* in the absence of cognate antigen. *J. Exp. Med.* **198**, 1583–1593 (2003).
238. Harty, J. T., Tvinnereim, A. R. & White, D. W. CD8<sup>+</sup> T cell effector mechanisms in resistance to infection. *Annu Rev Immunol* **18**, 275–308 (2000).
239. Halle, S. et al. In Vivo Killing Capacity of Cytotoxic T Cells Is Limited and Involves Dynamic Interactions and T Cell Cooperativity. *Immunity* **44**, 233–245 (2016).
240. Klein, L., Hinterberger, M., Wirnsberger, G. & Kyewski, B. Antigen presentation in the thymus for positive selection and central tolerance induction. *Nat Rev Immunol* **9**, 833–44 (2009).
241. Zinkernagel, R. M. & Althage, A. On the role of thymic epithelium vs. bone marrow-derived cells in repertoire selection of T cells. *Proc. Natl. Acad. Sci. U. S. A.* **96**, 8092–8097 (1999).

## 8. Abbreviations

<b>AlvM</b>	Alveolar Macrophage
<b>ab</b>	Antibody
<b>APC</b>	Antigen presenting cell
<b>AF</b>	Autofluorescence
<b>BAL</b>	Bronchoalveolar Lavage
<b>BAS</b>	Bronchoalveolar Space
<b>BMx</b>	Bone Marrow Chimera
<b>CCL</b>	C-C chemokine ligand
<b>CCR</b>	C-C chemokine receptor
<b>CD</b>	Cluster of differentiation
<b>CFSE</b>	Carboxyfluorescein succinimidyl ester
<b>CXCR</b>	C-X.C chemokine receptor
<b>CTL</b>	Cytotoxic T Lymphocytes
<b>d</b>	Day
<b>DC</b>	Dendritic Cell
<b>DC-</b>	Dendritic cell deficient
<b>DC+</b>	Dendritic cell proficient
<b>DNA</b>	Desoxyribonucleic Acid
<b>DN</b>	Double Negative
<b>DT</b>	Diphtheria Toxin
<b>EpC</b>	Epithelial Cell
<b>HA</b>	hemagglutinin
<b>H&amp;E</b>	Hematoxylin and Eosin staining
<b>MHC</b>	Histocompatibility complex
<b>ic</b>	ice cold
<b>IgG</b>	immunoglobulin
<b>ILC</b>	Innate lymphoid cell
<b>IFN</b>	Interferon
<b>IP</b>	interferon-gamma induced protein
<b>IL</b>	Interleukin
<b>ICAM</b>	Intracellular adhesion molecule
<b>i.t.</b>	Intratracheal
<b>i.v.</b>	Intravenous
<b>i.p.</b>	Intraperitoneal
<b>LFA</b>	Lymphocyte function-associated antigen
<b>MCP</b>	monocyte chemoattractant 1
<b>NK</b>	natural killer cell
<b>NA</b>	Neuraminidase
<b>NP</b>	Nucleoprotein
<b>PBL</b>	Peripheral Blood leukocytes
<b>PBS</b>	Phosphate-buffered solution
<b>PFU</b>	Plaque forming units
<b>PMN</b>	Polymorphonuclear neutrophils
<b>r.p.m</b>	revolutions per minute
<b>RNA</b>	Ribonucleic Acid
<b>T<sub>CM</sub></b>	Central Memory T cell



<b>TCR</b>	T cell receptor
<b>T<sub>EM</sub></b>	Effector Memory T cell
<b>TNF</b>	Tumor necrosis factor
<b>T<sub>RM</sub></b>	Resident Memory T cell
<b>Th1</b>	Type 1 T helper cell
<b>wt</b>	wild type

## 9. Appendix

List of genes analyzed by Nanostring:

AP-1	Bst1	Casp8	Ccrl2	Cd44	Cebpb	Ctsg	Defb1
AQP 9	Bst2	Ccbp2	Cd109	Cd46	Cfb	Ctss	Defb1 4
Abcb1 0	Btk	Ccl11	Cd14	Cd48	Cfd	Cul9	Dpp4
Abcb1 a	Btla	Ccl12	Cd160	Cd5	Cfh	Cx3cl 1	Ebi3
Abcf1	Btnl1	Ccl19	Cd163	Cd53	Cfi	Cx3cr 1	Emr1
Abl1	Btnl2	Ccl2	Cd164	Cd55	Cfp		Entpd 1
Adal	C1qa	Ccl20	Cd19	Cd59b	Chuk	Cxcl1	
Ahr	C1qb	Ccl22	Cd1d1	Cd6	Ciita	Cxcl1 0	Eome s
Aicda	C1qbp	Ccl24	Cd2	Cd69	Cish		
Aire	C1ra	Ccl25	Cd209 g	Cd7	Clec4 a4	Cxcl1 1	Ets1
App	C1s	Ccl26	Cd22	Cd74			Fadd
Arhgd1 b	C2	Ccl3	Cd226	Cd79a	Clec4 e	Cxcl1 2	Fas
Atg16l 1	C3	Ccl4	Cd244	Cd79b	Clec5 a	Cxcl1 3	Fasl
Atm	C4a	Ccl5	Cd247	Cd80			Fcamr
B2m	C4bp	Ccl6	Cd24a	Cd81	Clu	Cxcl1 5	Fcer1 a
BAD	C6	Ccl7	Cd27	Cd82	Cmklr 1	Cxcl3	Fcer1 g
Batf	C7	Ccl8	Cd274	Cd83	Cr2	Cxcl9	Fcgr1
Batf3	C8a	Ccl9	Cd28	Cd86	Cradd	Cxcr1	Fcgr2 b
Bax	C8b	Ccr10	Cd34	Cd8a	Crlf2	Cxcr2	Fcgr3
Bcap3 1	C8g	Ccr2	Cd36	Cd8b1	Csf1	Cxcr3	Fcgr4
Bcl2	C9	Ccr3	Cd3d	Cd9	Csf1r	Cxcr4	Fcgrt
Bcl3	CD10 3	Ccr4	Cd3e	Cd96	Csf2	Cxcr5	Fkbp5
Bcl6	Camp	Ccr5	Cd3ea p	Cd97	Csf2rb	Cxcr6	Fn1
Bid	Card9	Ccr6	Cd4	Cd99	Csf3r	Cybb	Folr4
Blnk	Casp1	Ccr7	Cd40	Cdhn1 a	Ctla4	DGAT 1	Foxp3
	Casp2	Ccr8	Cd40l g	Ceaca m1	Ctnnb 1	DIVA	Frmpd 4
	Casp3	Ccr9			Ctsc	Ddx58	
		Ccrl1					

Fyn	Hc	Ikzf3	Il1r2	Il9	Klra1	Ly86	Ms4a1
Galectin-1	Hcst	Ikzf4	Il1rap	Ilf3	Klra21	Ly96	Msr1
Gata3	Hfe	Il10	Il1rl1	Irak1	Klra4	MCL-1	Muc1
Gfi1	Hif1a	Il10ra	Il1rl2	Irak2	Klra5	Maf	Mx1
Gm1099	Hlx	Il10rb	Il1rn	Irak3	Klra6	Map4k1	Myd88
Gp1bb	Icam1	Il11ra1	Il2	Irak4	Klra7	Map4k1	Ncam1
Gpi1	Icam2	Il12a	Il20	Irf1	Klra8	Map4k2	Ncf4
Gpr183	Icam4	Il12b	Il21	Irf3	Klrb1	Map4k4	Neuropilin-1
Gpr44	Icam5	Il12rb1	Il21r	Irf4	Klrc1	Mapk1	Nfatc1
Gyk	Icos	Il12rb1	Il22	Irf5	Klrc2	Mapk1	Nfatc2
Gzma	Icosl	Il12rb2	Il22ra2	Irf7	Klrc3	Mapk1	Nfatc3
Gzmb	Ifi204	Il13	Il23a	Irf8	Klrd1	Mapk1	Nfil3
H2-Aa	Ifi35	Il13ra1	Il23r	Irgm1	Klrk1	Mapk4	Nfil3
H2-Ab1	Ifih1	Il15	Il25	Itga2b	Lag3	Mapk2	Nfkb1
H2-DMa	Ifit2	Il15ra	Il27	Itga4	Lair1	Marco	Nfkb2
H2-DMb2	Ifitm1	Il16	Il27ra	Itga5	Lck	Masp1	Nfkbiz
H2-Ea-ps	Ifna1	Il17a	Il28a	Itga6	Lcp2	Masp2	Nod2
H2-Eb1	Ifna2	Il17b	Il2ra	Itgal	Lef1	Mbl2	Nos2
H2-K1	Ifnar1	Il17f	Il2rb	Itgam	Lif	Mbp	Notch1
H2-Ob	Ifnar2	Il17g	Il2rg	Itgax	Lilra5	Mif	Notch2
H2-Q10	Ifnb1	Il17ra	Il3	Itgb1	Lilra6	Mme	Nox1
H60a	Ifnb2	Il17rb	Il33	Itgb2	Lilrb3	Mmp10	Nox3
Hamp	Ifnf	Il17re	Il4	Itln1	Lilrb4	Mmp11	Nox4
Havcr1	Ifngr1	Il18	Il4ra	Jak1	Litaf	Mmp14	Npc1
	Ifngr2	Il18r1	Il5	Jak2	Lrrc32	Mmp2	Nr4a1
	Igf2r	Il18ra	Il6	Jak3	Lta	Mmp3	Nt5e
	Ikbkap	Il18rb	Il6ra	Kir3dl1	Ltb	Mmp7	PUMA
	Ikbkb	Il19	Il6st	Kir3dl2	Ltb4r1	Mr1	Pax5
	Ikbke	Il1a	Il7	Kit	Ltb4r2		
	Ikbkg	Il1b	Il7r		Ltbr		
	Ikzf1	Il1r1			Ltf		
	Ikzf2						

Pdcd1	Prkcd	Rela	Sigirr	Tap1	Tmem	Tnfsf1	Vcam
Pdcd1	Psemb	Relb	Ski	Tapbp	173	2	1
Ig2	10	Rorc	Slamf	Tbk1	Tnf	Tnfsf1	Vtn
Pdcd2	Psemb	Runx1	1	Tbx21	Tnfaip	3b	Xbp1
Pdgfb	11	Runx3	Slamf	Tcf4	3	Tnfsf1	Xcl1
Pdgfrb	Psemb	Runx3	7	Tcf7	Tnfaip	4	Xcr1
Pecam1	5	S100a	Smad	Tcf7	6	Tnfsf1	Zap70
	7	8	3	Tfrc	Tnfrsf	5	Zap70
	9	S100a	Smad	Tgfb1	11a	Tnfsf1	Zbtb7
Phlpp1	Psemb	9	5	Tgfb2	Tnfrsf	8	b
Phlpp2	Psmc	S1PR	Socs1	Tgfb3	13b	Tnfsf8	Zeb1
	2	1	Socs3	Tgfb3	Tnfrsf	Tollip	ptger2
Pigr	Psmc	SAMD	Spn	Tgfb3	13c	Traf1	Alas1
	7	3	Src	Tgfb3	Tnfrsf	Traf2	Eef1g
Pla2g2a	Ptafr	SLC2	Stat1	Tgfb2	14	Traf2	Eef1g
		A1	Stat1	Tgfb2	Tnfrsf	Traf3	G6pdx
Pla2g2e	Ptger4	SLC3	Stat2	Thy1	17	Traf4	Gapdh
		3A1	Stat2	Tigit	Tnfrsf	Traf5	Gusb
Plau	Ptgs2	SLC3	Stat3	Timd2	1b	Traf6	Hprt
		A2	Stat4	Tirap	Tnfrsf	Traf6	Hprt
Plaur	Ptk2	A2	Stat4	Tirap	4	Trem1	Oaz1
Pml	Ptpn2	SLC7	Stat5a	Tlr1	4	Trem2	Oaz1
		A5	Stat5a	Tlr1	Tnfrsf	Trem2	Polr1b
Pou2f2	Ptpn2	Sele	Stat5b	Tlr2	8	Trp53	Polr2a
	2	Sele	Stat6	Tlr2	8	Trp53	Polr2a
Pparg	Ptpn6	Sell	Syk	Tlr3	Tnfrsf	Tslp	Ppia
		Sell	Syk	Tlr3	9	Tslp	Ppia
Ppbb	Ptpnc	Selplg	TNRS	Tlr4	Tnfsf1	Tyk2	Rpl19
		Selplg	F25	Tlr4	0	Tyk2	Rpl19
Prdm1	Rae1	Serpin	F25	Tlr5	Tnfsf1	Tyrob	Sdha
		g1	Tagap	Tlr5	0	p	Sdha
Prf1	Rag1	Sh2d1	Tagap	Tlr8	Tnfsf1	Ube2l	Tbp
		a	Tal1	Tlr8	1	3	Tbp
Prim1	Rag2	a	Tal1	Tlr9	1	3	Tubb5

## 10. Publications

Cossarizza, A., Chang, H.-D., Radbruch, A., Acs, A., Adam, D., Adam-Klages, S., Agace, W.W., Aghaeepour, N., Akdis, M., Allez, M., Garbi, N., **Vento-Asturias, S.**, Holland, T., et al. (2019). **Guidelines for the use of flow cytometry and cell sorting in immunological studies (second edition)**. *Eur J Immunol* 49, 1457–1973. DOI: 10.1002/eji.201970107

Cossarizza, A., Chang, H.-D., Radbruch, A., Akdis, M., Andrä, I., Annunziato, F., Bacher, P., Barnaba, V., Battistini, L., Bauer, W.M., Garbi, N., **Vento-Asturias, S.**, Holland, T., et al. (2017). **Guidelines for the use of flow cytometry and cell sorting in immunological studies**. *Eur J Immunol* 47, 1584–1797. DOI: 10.1002/eji.201646632

Holland, T., Wohlleber, D., Marx, S., Kreuzberg, T., **Vento-Asturias, S.**, Schmitt-Mbamunyo, C., Welz, M., Janas, M., Komander, K., Eickhoff, S., et al. (2017). **Rescue of T-cell function during persistent pulmonary adenoviral infection by Toll-like receptor 9 activation**. *Journal of Allergy and Clinical Immunology*. DOI: 10.1016/j.jaci.2017.06.048

Kronsteiner, B., Bassaganya-Riera, J., Philipson, C., Viladomiu, M., Carbo, A., Pedragosa, M., **Vento, S.**, and Hontecillas, R. (2013). **Helicobacter pylori Infection in a Pig Model Is Dominated by Th1 and Cytotoxic CD8+ T Cell Responses**. *Infect Immun* 81, 3803–3813. DOI: 10.1128/IAI.00660-13

## 11. Acknowledgments

I would like to start by thanking Prof. Dr. Natalio Garbi for giving me the opportunity to conduct my PhD project and providing great supervision during my time in his group.

I am grateful to have had Christine by my side during my PhD, we spent countless hours together in the lab and this work would have not been possible without her.

Special thanks for their help, both scientifically and non-scientifically, from Tristan and Thomas, great colleagues and friends. In addition, I cannot forget the help and great discussions provided by Philipp, Teresa, Charlie, Christoph and Sarah. Thanks for the great moments and experiences we shared.

I would also like to thank the members of my committee Prof. Dr. Joachim L. Schultze, Prof. Dr. Irmgard Förster and Prof. Dr. Jochen Dingfelder.

Finally, I could not have done this without the constant support and encouragement provided by Clarissa and my family who have never left my side during this long journey.